A SEARCH FOR A SCREENING EFFECT DUE TO ATOMIC ELECTRONS IN ELECTRON NUCLEAR SCATTERING

Thesis

Submitted by

RICHARD C. DOUGAL, B.Sc. (Edinburgh)

for the degree of

DOCTOR OF PHILOSOPHY

University of Edinburgh

August, 1963.

C O N T E N T S

C O N T E N T S (Contd.)

C O N T E N T S (Contd.)

CHAPTER I

INTRODUCTION: THE SCREENING EFFECT IN ELECTRON-NUCLEAR SCATTERING

In general, electron scattering experiments are carried out either to check the theoretical values of the electron scattering cross sections or, assuming the scattering theory to be valid, to measure some property of the incident electron beam or of the target material. Since the proposals by Lee and Yang of parity non-conservation in weak interactions (Lee and Yang, 1956) and of the consequent polarisation of electrons emitted in beta decay (Lee and Yang, 1957), most electron scattering experiments have been of the second type - at least for electrons with energies in the range 100 - 1,000 keV, approximately. Such experiments are usually designed to provide a value for the polarisation of the incident electron beam, i.e. the extent to which the spins of the electrons in the beam are aligned in some particular direction. This polarisation is deduced from the degree to which electrons are scattered asymmetrically in passing through thin foils. The type of scattering investigated depends broadly on the energy of the incident electrons. For energies up to about 400 keV, electron-nuclear (or Mott) scattering is usually used (Mott, 1929 and 1932) while for higher energies electron-

electron (or Møller) scattering proves more suitable (Møller, 1932). For many years before the polarisation of electrons from β-decay was proposed and demonstrated, polarisation-dependent scattering asymmetries were investigated in "double scattering" work (Dymond, 1934; Richter, 1937; Shull, 1942; Ryu, Hashimoto and Nonaka, 1953; Nelson and Pidd, 1959). Polarised electron beams were obtained by the nuclear scattering of assumed unpolarised electron beams through an angle of about 90° by material of high atomic number (Mott, 1929 and 1932). The polarisation was then investigated by means of a second scattering process. Several review papers are available in which descriptions and discussion of the relevant theoretical and experimental work may be found (Tolhoek, 1956; Grodzins, 1959; Page, 1959, 1962; Sternheimer, 1959). It is probably reasonable to state briefly that at the moment there is quite good agreement between the experimental results and the theories of beta decay and electron scattering which were assumed. The position regarding the first type of experiment - the measurement of scattering cross-sections for electrons with energies in the range 100 keV to a few MeV - was well summarised in a group of three papers published in 1959 (Spiegel et al., 1959; Spiegel, Miller and Waldman, 1959; Kepes, Waldman and Miller, 1959). The earlier experiments discussed there tended to indicate agreement between theory and experiment.

However, the new measurements also reported in these three papers indicated agreement for the relatively few Møller scattering cross-sections investigated, but general disagreement for the large range of Mott scattering cross-sections, even after all the possible corrections had, apparently, been made.

From the results of both types of scattering experiment mentioned above, it seems that the theories assumed might not allow for all the processes involved in beta decay and electron scattering. In particular, when Mott scattering is involved in an experiment, a consideration of "screening" as a source of error is almost invariably made. These considerations are, however, little more than qualitative, because very few theoretical or experimental investigations of screening have been undertaken. The so-called screening effect is attributed to the part played by the atomic electrons in making the electric potential distribution actually involved in the Mott scattering process different from that of a "point nucleus". The simplest way of visualising this is to assume that the effective nuclear charge for the scattering process is equal to the actual nuclear charge only if the electron being scattered approaches close to the nucleus. For larger distances, the presence of the negatively charged atomic electrons results in the effective nuclear charge being less than the actual nuclear charge.

In the theoretical studies of this effect, it was customary to use approximations to the self-consistent fields for the scattering atom considered (Massey and Mohr, 1941; Mohr, 1943; Mohr and Tassie, 1954). The main object of these theoretical studies was to find out whether or not screening could account for discrepancies between the theoretical and the experimental scattering asymmetries found in double scattering work. The conclusion reached in the third paper (Mohr and Tassie, 1954) was "that screening has a relatively small effect on the scattering above 33 keV and on the polarisation above 121 keV."

In the two earlier papers, however, a way was suggested in which scattering theory could be amended to agree with the experimental measurements. This was to replace the atomic potential $Z_p e^2/r$ with $(Z_p e^2/r)\{1 - \exp(-\lambda r)\}$. Here Z_p is the effective nuclear charge for the potential according to the self-consistent field theory, e is the electron charge, r is the radial distance from the centre of the atom and λ is a quantity with dimensions length^{-1}. It seemed that for electrons with energy $\sim$100 keV, a value of $\lambda a_o \sim 100$ would be necessary for agreement between theory and experiment. a_o is the first Bohr orbit radius (5.29×10^{-9} cm.). The additional factor $\{1 - \exp(-\lambda r)\}$ would therefore be important at radial distances $r \sim 1/\lambda \sim a_o/100 \sim 5 \times 10^{-11}$ cm. The idea was

rejected. In the first paper (Massey and Mohr, 1941) it was pointed out that "the departure from the Coulomb form would affect the orbits of K electrons [which have radii $\sim 5 \times 10^{-11}$ cm.] and would be apparent in various ways. It can therefore be regarded as out of the question." In the second paper (Mohr, 1943) it was pointed out that the large value of λ would "involve modifications of the atomic field at distances which seem impossibly large." It appears that no consideration was given to the possibility that the effective field for electron-nuclear scattering might well be different from the effective field for other phenomena (K-shell orbits, etc.). This was stressed in a later theoretical treatment of screening by van der Spuy (van der Spuy, 1959) who stressed that in considering the electron scattering process, the importance of the Pauli exclusion principle must not be underestimated. He obtained an expression for an additional correction to the scattering potential which could be greater than the screening correction of Mohr and others, but which at the same time would not affect other atomic properties, so overcoming the difficulties mentioned by Massey and Mohr. His treatment "starts from the notion that for scattering on a heavy atom the lower orders (at least) of the incident electron partial waves each find a region in space round the nucleus which is already fully occupied in the sense of the exclusion principle, and which would in effect be

repulsive to the corresponding partial component. In this sense the scattering is a many-body problem in which the operation of the exclusion principle must be fully recognised." Van der Spuy simplified his treatment by considering the effects of the K-shell electrons only and making the calculations non-relativistic except for the explicit allowance for electron spins. He concluded that "the modified overall Coulomb potential for the s partial wave

$$= -\frac{Ze^2}{r_1}\left\{1 - (E_K - E_{s1})\frac{4}{a_o e^2} r_1^2 \exp(-Zr_1/a_o)\right\}"$$

Here Z is the atomic number of the scatterer, $-e$ the electron charge, r_1 the radial distance of the electron from the centre of the atom, a_o the first Bohr orbit radius, E_K the energy of the incident electron and $-E_{s1}$ the single electron K-shell binding energy. Van der Spuy commented "that for $Z = 79$, $E_K = 120$ keV, and $-E_{s1} = 13.605\ Z^2$ eV $= 84909$ eV, in our approximation, the second term in the curly brackets has a highest value $= -2.61$." The similarity between the complete expression in the curly brackets and the "correction factor" mentioned but rejected by Massey and Mohr is at least interesting. It seems that the ideas discussed by van der Spuy have not been extended to predict what effect on scattering properties they would have if all the atomic shells were considered and the

treatment were made fully relativistic. It is not impossible, however, that the earlier screening effect, as developed by Mohr and others, accounts for only part of the total effect of the atomic electrons on electron-nuclear scattering.

There have been, so far, no direct experiments performed to measure or detect a screening effect or, for that matter, any other effect due to the atomic electrons - such as that suggested by van der Spuy. There is, however, considerable indirect evidence that screening could explain at least some of the discrepancies between theory and experiment which have been found in electron scattering work. Some examples of this evidence can be found in electron polarisation measurements (Greenberg et al., 1960; Murray, 1960) and measurements of the Mott scattering asymmetry (Bienlein et al., 1959; Nelson and Pidd, 1959). Following this last work, Sherman and Nelson (Sherman and Nelson, 1959) compared unscreened theoretical values for electron scattering cross-sections and asymmetries (Sherman, 1956) with the corresponding screened values (Mohr and Tassie, 1954). They commented that "it is possible that the differences between the Mott asymmetries are attributable to numerical approximations more than to the effect of screening" but concluded that "the amount of the difference between the screened and unscreened field calculations of the Mott asymmetries at large scattering

angles at 121 keV, indicate the desirability of more detailed investigation of screening effects for all scattering angles. This is especially important if theoretical results for Mott scattering are to be used in the evaluation of experiments measuring electron polarization."

The previous sentence suggests that if a screening effect of some kind is present in electron-nuclear scattering, then the best type of experiment by which to look for it is a straightforward series of electron-nuclear scattering cross-section measurements - an experiment whose interpretation is not made more difficult by, for example, uncertainties in beta decay theory (as electron polarisation determinations can be). The only extensive series of measurements of this type is that of Spiegel and others mentioned earlier (Spiegel et al., 1959). They scattered monoenergetic electrons of energies 1.0, 1.75 and 2.5 MeV through angles of 30°, 60°, 90°, 120° and 150° from foils of aluminium, nickel, silver and gold and found that only for 1,000 keV electrons scattered by aluminium through 30° did the theoretical and experimental values of the cross-section agree within the limits of the experimental error. Generally speaking, the discrepancy increased with scattering angle for all scatterers at all three energies, and the authors commented that "perhaps an accurate

evaluation of the screening correction would remove this discrepancy."

It is probably a fair comment that a screening effect, about which comparatively little is known, has been used to help to explain a remarkably large number of experimental results. The work to be described is an attempt to find whether or not some such effect actually does play a part in electron-nuclear scattering. To avoid awkward terminology, the word "screening" will be assumed, from now on, to include <u>all</u> the effects in electron-nuclear scattering which might be caused by the atomic electrons.

CHAPTER 2

THE DESIGN OF THE EXPERIMENT: DISCUSSION OF THE RELEVANT PROPERTIES OF MOTT SCATTERING CROSS SECTIONS

If the atomic electrons are to play any part in an electron-nuclear scattering process, then the electron being scattered must, in its passage through the scattering atom, follow a path which for much of its length is near the atomic electrons. Assuming this, it follows that screening should not greatly affect large angle scattering or scattering of high energy electrons in both of which cases the electron being scattered must pass close to the nucleus of the atom. It was decided, therefore, to examine the scattering properties of low energy electrons (in the range 100-600 keV approximately) for small scattering angles (less than 90°). The scattering material chosen was gold, atomic number 79.

The experimental measurements decided on were very straightforward because of an interesting property of certain ratios of Mott scattering cross sections, which made it unnecessary to measure absolute Mott scattering cross sections. Let the theoretical Mott scattering cross sections be denoted by $\sigma_N(\Theta, E, Z)$ where Θ is the angle of scattering, E the energy of the incident electron and Z the atomic number of the scattering atom, no screening being allowed for. It turns out that for certain pairs of scattering angles Θ_1 , and Θ_2

(see Appendix 1) the ratio

$\rho = \sigma_N^-(\Theta_2, E, 79)/\sigma_N^-(\Theta_1, E, 79)$ is independent of E for energies in the range 200 keV to 1,000 keV to a good approximation. For energies below 200 keV, then, if $\Theta_1 > \Theta_2$, ρ increases as energy decreases. But if screening (a) affects the lower angle scattering cross section more than the higher angle one, (b) decreases the scattering cross section and (c) becomes more important as the energy of the incident electrons decreases, then it follows that screening should alter the variation of ρ with energy. Instead of first staying constant and then increasing, ρ should decrease as the energy decreases.

Because of the unsatisfactory nature of screening theory, it was impossible to influence the choice of Θ_1 and Θ_2 so that a definite screening effect could be measured. Instead, as shown in Appendix 1, Θ_1 and Θ_2 were chosen so that the ratio ρ was independent of energy to the best approximation. The actual values chosen were $\Theta_1 = 65^\circ$ and $\Theta_2 = 30^\circ$. In the course of the experiment it was decided to extend the measurements to include Θ_2 equal to 20° and 45°, to see if a dependence of screening on Θ_2 could be detected.

The energy independence of ρ allowed another important simplification to be made in the experimental arrangement. For it follows that, to a good approximation, the quantity

$$\sum_E \rho = \sum_E \frac{\sigma_N^-(\Theta_2, E, 79)}{\sigma_N^-(\Theta_1, E, 79)}$$

is also energy-independent, where the summation is over any range of energies lying between $\sim$ 200 keV and 1,000 keV. Thus, not only was it unnecessary to use monoenergetic electron beams, but it was also possible to allow a rather poor resolution in the focussing system (see Chapters 3 and 6) which produced the incident electron beams from the electrons emitted by a radioactive material. This simplification did not apply so well to energies below $\sim$200 keV, but it was considered that if screening were important at these energies, the theoretical and experimental values of $\sum_E \rho$ would still be different.

The cross sections $\sigma_N^-(\Theta, E, Z)$ used above refer to the scattering of electrons through an angle Θ as a result of one collision with one nucleus. When electrons with energies of the order 1 MeV and below are scattered from gold foils of the thicknesses available commercially ($\gtrsim$0.2 mgm. cm.$^{-2}$, see Chapter 5), many electrons suffer more than one scattering process during their passage through the foil. By making scattering measurements with gold foils of several thicknesses and using a suitable process for extrapolation, from the measurements, to zero foil thickness, data characteristic of single scattering can be found (Spiegel et al., 1959). This matter will be dealt with in Chapter 8 where the treatment of the experimental measurements is described.

CHAPTER 3

THE DEVELOPMENT OF AN ELECTRON FOCUSSING SYSTEM

Introduction

In any electron scattering experiment, the beam of incident electrons should be well defined geometrically and the energy or energy range of the electrons should be known. When the incident electrons are obtained from the β-particle continuum of a radioactive source, it is usually necessary to focus the electrons into an approximately parallel beam. As well as defining the beam geometrically, the focussing process usually produces a gain in intensity. It also produces energy selection because the degree of focussing depends on the energy of the electrons. In general, the better the energy selection, the lower is the intensity of the resulting beam, and some compromise must be made.

For the type of electron scattering measurements discussed in Chapter 2, good energy selection was not necessary. The apparatus to be described, therefore, was developed so that from a radioactive source of a few millicuries a beam of electrons could be obtained which was of sufficient intensity for electron-nuclear scattering measurements to be made quite readily. Subject to this condition, the energy-selection was made as good as possible.

In a realistic experimental arrangement for the study of electron scattering, a radioactive source of a

few millicuries might be placed about 50 cm. from a scattering foil. A simple calculation (Appendix 2) shows that if the time for carrying out a series of electron-scattering measurements is to be kept reasonably short (say several weeks) then the electrons from the source must be focussed such that for electrons in a given energy range the "focussed intensity" is two orders of magnitude greater than the corresponding "unfocussed intensity", i.e. the intensity of a beam going directly from the source to the foil. It was decided to try to obtain this degree of focussing by using what is probably the simplest possible focussing system - a magnetic lens. This is essentially a current-carrying, cylindrical coil of wire producing an axial magnetic field which bends the paths of electrons emitted by a source on the axis of the coil and so focusses these electrons (assuming that source position, coil current, electron energy etc. are all suitably chosen).

The Prototype Focussing System

Three suitable identical coils of copper wire were available and two of them were incorporated in an apparatus designed to find out whether or not an increase in intensity of two orders of magnitude was feasible. One coil was surrounded by mild steel shielding (see Fig. 3.1) so that its magnetic field was confined to a small volume between two pole pieces and

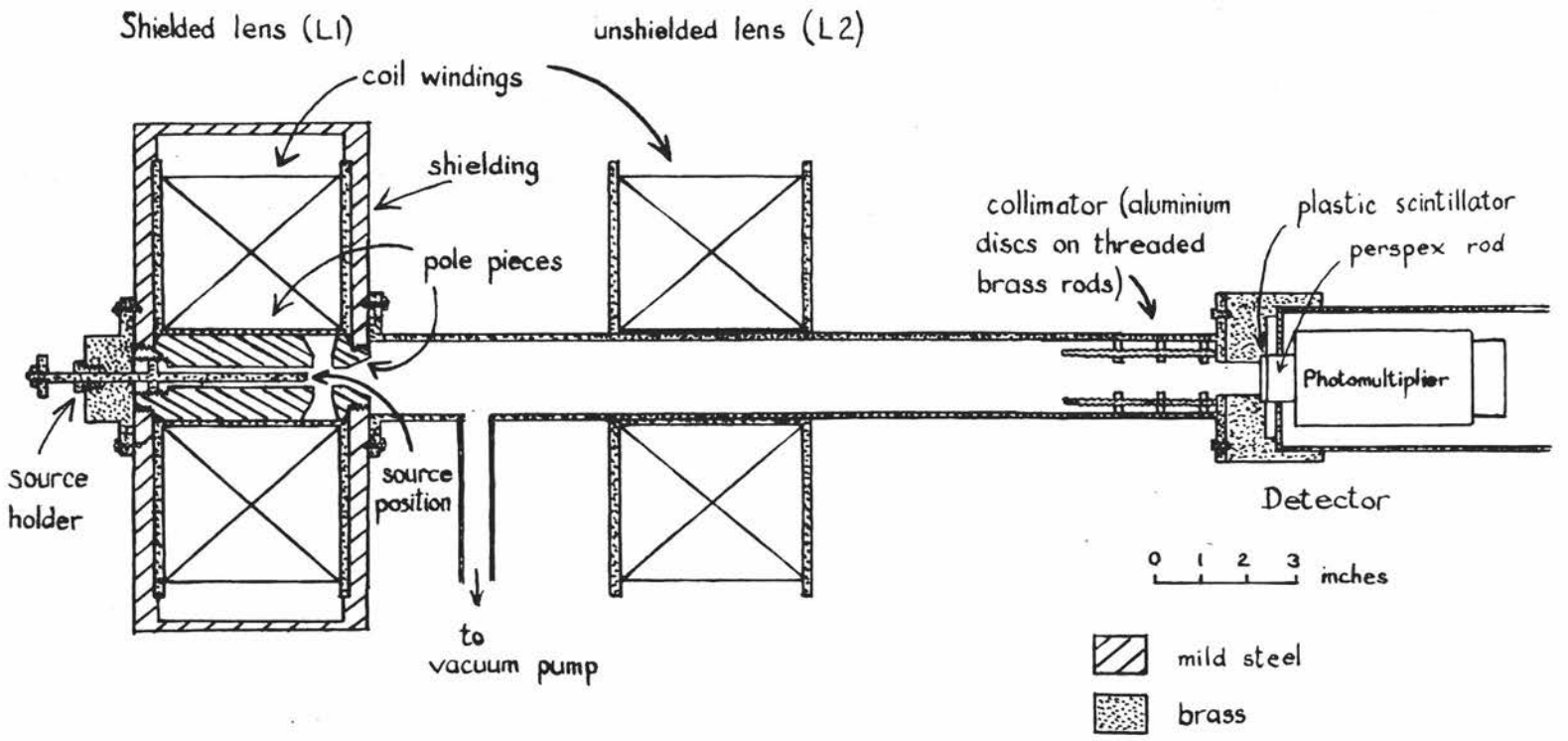

Fig 3.1 The prototype two-lens electron focussing system.

consequently made sufficiently intense for the focal length of the lens, L1, to be very small. The lens was, in effect, a "scaled-up" version of an electron microscope short-focus objective lens. The partly empirical equations and curves used in the design of the shielding are given in a paper by Durandeau and Fert (Durandeau and Fert, 1957). A summary of the relevant parts of this paper is given in Appendix 3. The main reason for examining the possibilities of using such a lens (in preference to others) was that an increase of two orders of magnitude would not be ruled out by the geometrical dimensions of the apparatus - see

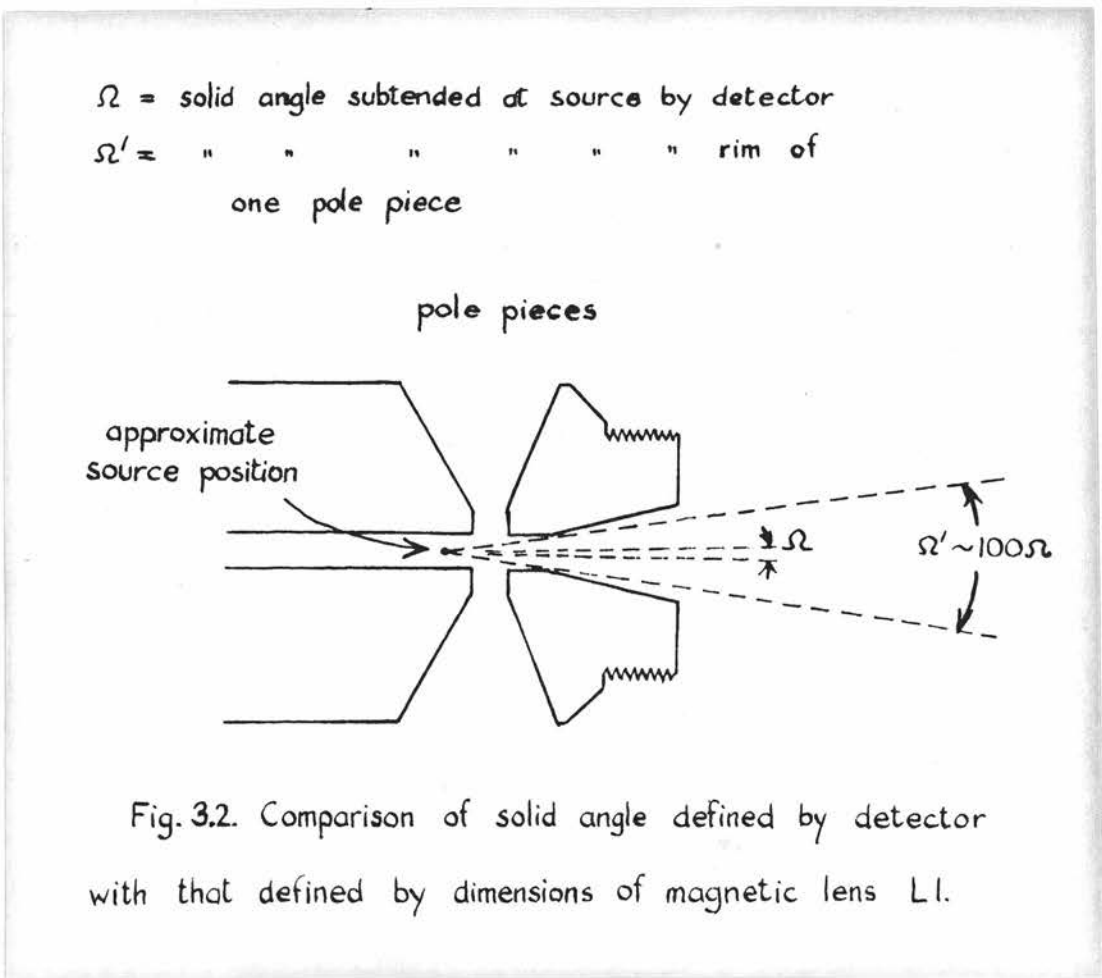

Fig. 3.2. Comparison of solid angle defined by detector with that defined by dimensions of magnetic lens L1.

Fig. 3.2. The second lens was left unshielded and was incorporated in the apparatus merely to see what effect it would have.

With the apparatus assembled essentially as in Fig. 3.1, the intensity of an unfocussed electron beam was measured (as the number of particles detected per unit time). A current was then passed through the shielded coil and this current - I1 - and the position of the source were varied to see what increase in counting rate was obtainable. To avoid what was thought might be excessive heating in the coil windings, the maximum current used was about 3 amps. The source position could be varied from about the middle of the gap between the pole pieces to about $\frac{1}{4}$ in. behind the gap. The first source used was sulphur - 35 (S^{35}) which gives electrons only, having an energy spectrum with an end point of 167 keV. The measurements indicated that under optimum conditions an increase in intensity by a factor of about 5 was possible.

Two more parameters were now introduced by passing a current through the unshielded lens and varying this current - I2 - and the position of the lens L2. It was found that a maximum increase in intensity of about 45 times was possible using both lenses and that with only L2 being used the corresponding factor was about 8. The measurements were extended using a phosphorus - 32 (P^{32}) source which, like S^{35}, is a

pure electron emitter but whose electron energy spectrum has an end point of 1710 keV. The measurements indicated that the maximum increase in intensity was about 45 times and was, to a first approximation, independent of energy for energies up to about 1,000 keV.

Although the overall result was encouraging, the performance of the shielded lens, L1, was disappointing. It was considered that part of the trouble was due to the source being a poor approximation to a point source (see Chapter 5). In fact, the internal diameter of the pole pieces was $\frac{3}{16}$ in. and the source diameter was estimated to be about $\frac{3}{32}$ in. As it seemed that a source of smaller diameter would be difficult to prepare, it was decided to improve the point source approximation by increasing the internal diameter of the pole pieces, and two new ones of internal diameter $\frac{3}{8}$ in. were made. The measurements previously described were repeated and the increases of intensity for L1 alone, L2 alone and L1 and L2 together were found to be approximately 10, 8 and 90 times respectively and were again essentially energy independent for energies up to about 1,000 keV.

With this crude apparatus, therefore, the necessary increase in intensity of two orders of magnitude was essentially achieved. There were several drawbacks, however, the most important ones being: the maximum current that the coils could comfortably cope with for,

say, several hours continuously was about 2 amps which the measurements indicated would limit the maximum energy to about 200 keV, which was far too low; once the source position was fixed, the source to detector distance was fixed and variations of beam intensity with position along the axis of the system were consequently not measurable; similarly, variations of the geometrical cross-section of the beam could not be measured; alignment of the apparatus was not possible - it was assumed that the magnetic and geometric axes of the components coincided. It was decided to build a new focussing system of the same type (i.e. two magnetic lenses, one of short focal length) but which did not suffer from the above list of defects.

The Magnetic Lenses of the Final Focussing System

Four brass and copper bobbins were constructed such that the outer diameter of the smaller two was equal to the inner diameter of the larger two, and from them two "double-bobbins" were made. A cross-section of one such double-bobbin is shown in Fig. 3.3. A spiral groove of section $\frac{1}{4}$ in. x $\frac{1}{8}$ in. cut into each bobbin and covered by a copper sleeve provided a conduit for water-cooling. Enamelled 13 s.w.g. copper wire was now wound on to each of the four bobbins by rotating each bobbin in a lathe and guiding the wire on by hand. Each layer of wire contained approximately 100 turns and there

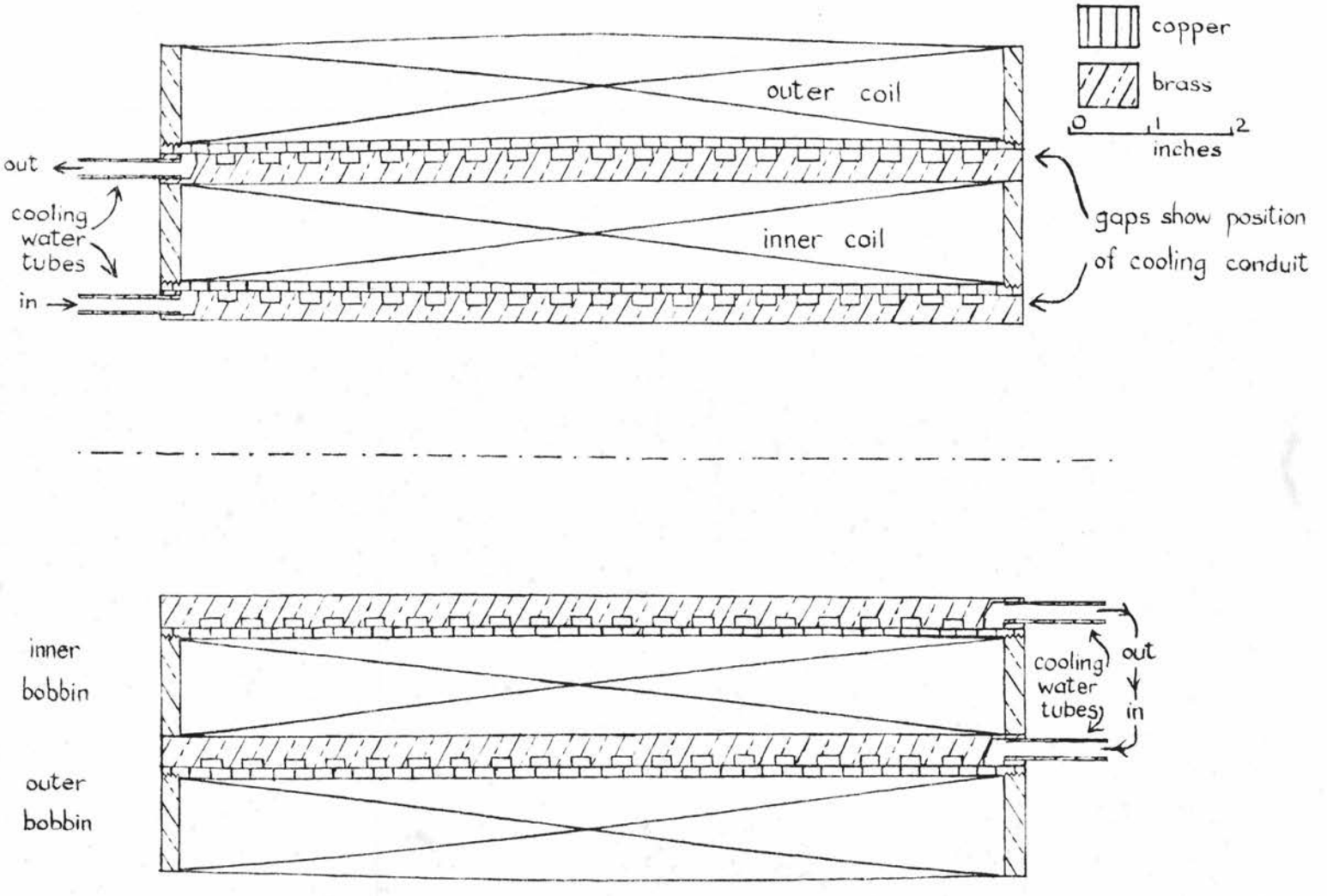

Fig. 3.3. Cross section of a lens coil showing double-bobbin structure.

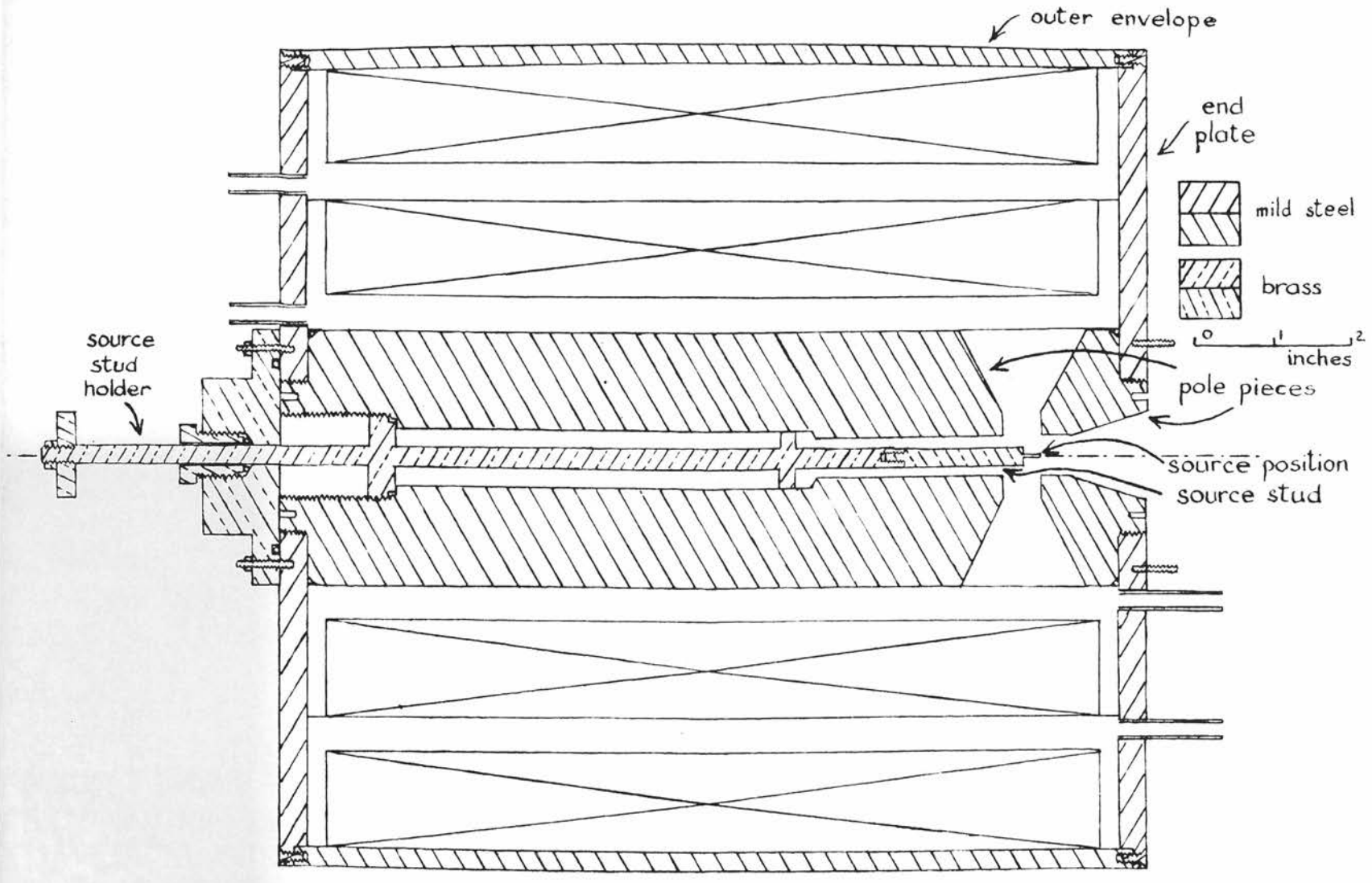

Fig.3.4. Cross section of L1 showing details of shielding and source holder

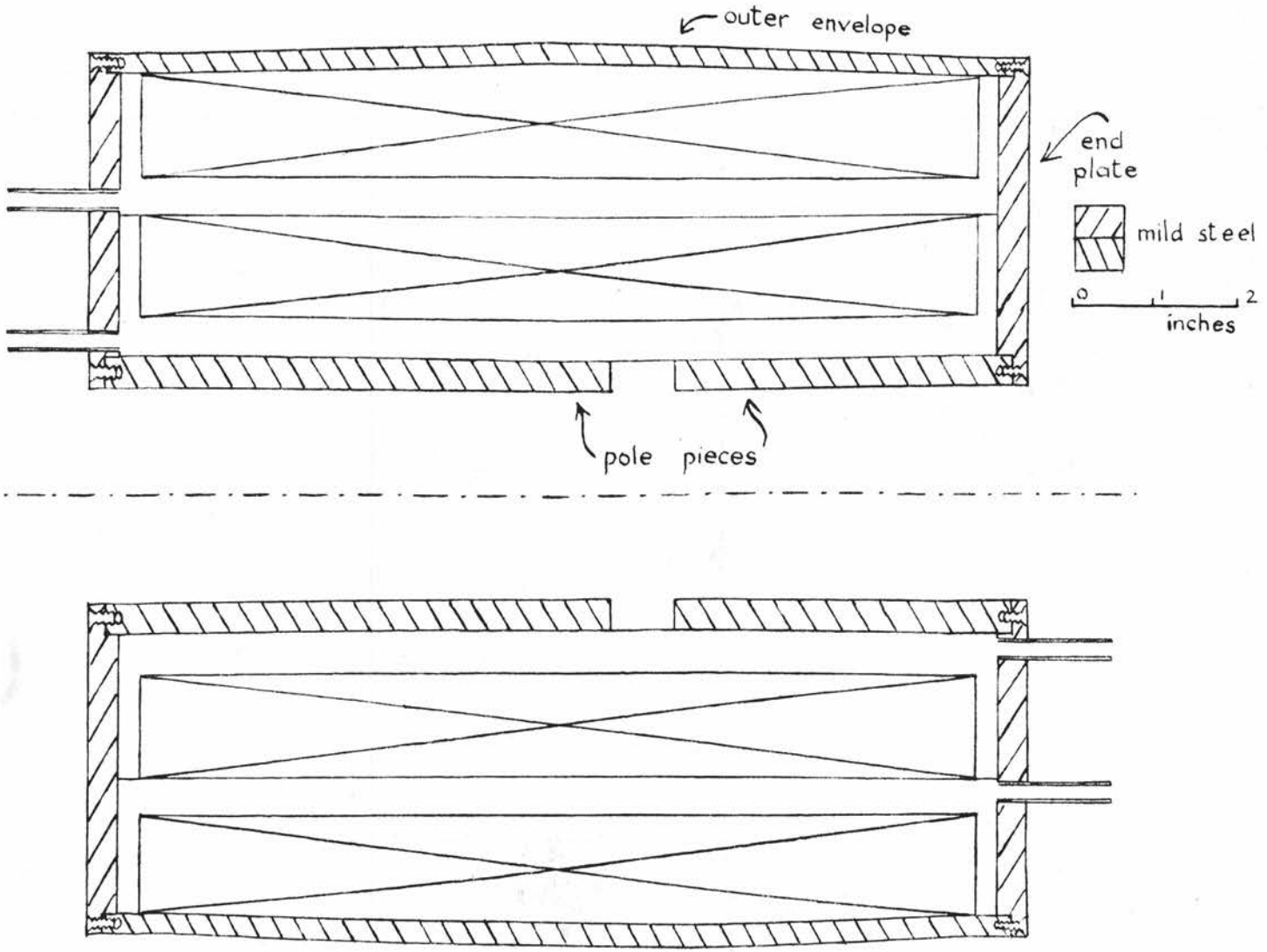

Fig. 3.5. Cross section of L2 showing details of shielding.

were 12 layers in the resulting larger diameter coils, 11 in the smaller. The winding of the coils became more difficult as the layer number increased, and less regular. However, by winding each magnetic lens coil in two stages (one on a smaller bobbin, the second on a larger one) this difficulty was reduced. A second advantage of the double-bobbin structure was that each resulting lens would have two cooling layers, with consequent better heat dissipation. The resistances of the larger diameter and smaller diameter coils were approximately 3.3 ohms and 2.2 ohms respectively.

This time, both lenses were shielded by bright mild steel. The details are shown in the cross-sections of the two lenses given in Figs. 3.4 and 3.5. The lens in Fig. 3.4, referred to as L1, was again a scaled-up version of an electron-microscope objective lens designed according to the data given by Durandeau and Fert. The internal diameter of the pole pieces was made $\frac{1}{2}$ in. in an attempt to make the point source approximation even better than in the prototype L1. The pole pieces of the second lens, L2 (which in the prototype system was unshielded), were much simpler (see Fig. 3.5) and were designed to find out whether or not there was an optimum L2 field extent. Four interchangeable pole pieces (essentially just lengths of steel tube) of different lengths were made. Measurements showed that the focussing properties of the resulting system were not strongly

dependent on the L2 field extents available but that, if anything, the field produced by the narrowest gap was the best (see page 26). The L2 pole pieces eventually used are shown in Fig. 3.5.

The source holder (see Fig. 3.4) consisted of two parts: the source stud and the stud holder into which it could be screwed. The longer pole piece was counter-bored and threaded at one end to take a threaded collar attached to the stud-holder. This allowed the source position, near the other end of this pole piece, to be adjustable through approximately 1 in.

The Final Focussing System

This second version of the focussing system was assembled on top of a wooden bench (Fig. 3.6). The short focus lens, L1, was clamped firmly to a wooden support which was bolted to the bench top. The axis of L1 was horizontal and arranged to be parallel to two cylindrical brass "rails" 11/16 in. in diameter and approximately 4½ ft. long. These rails were held in position by being bolted to two 6 ft. lengths of brass angle, the angles being bolted to the bench top. Four supports of adjustable length were fixed to the steel shielding of the second magnetic lens, L2, two to each side. To the ends of these supports wheels were attached such that L2 could run along the brass rails

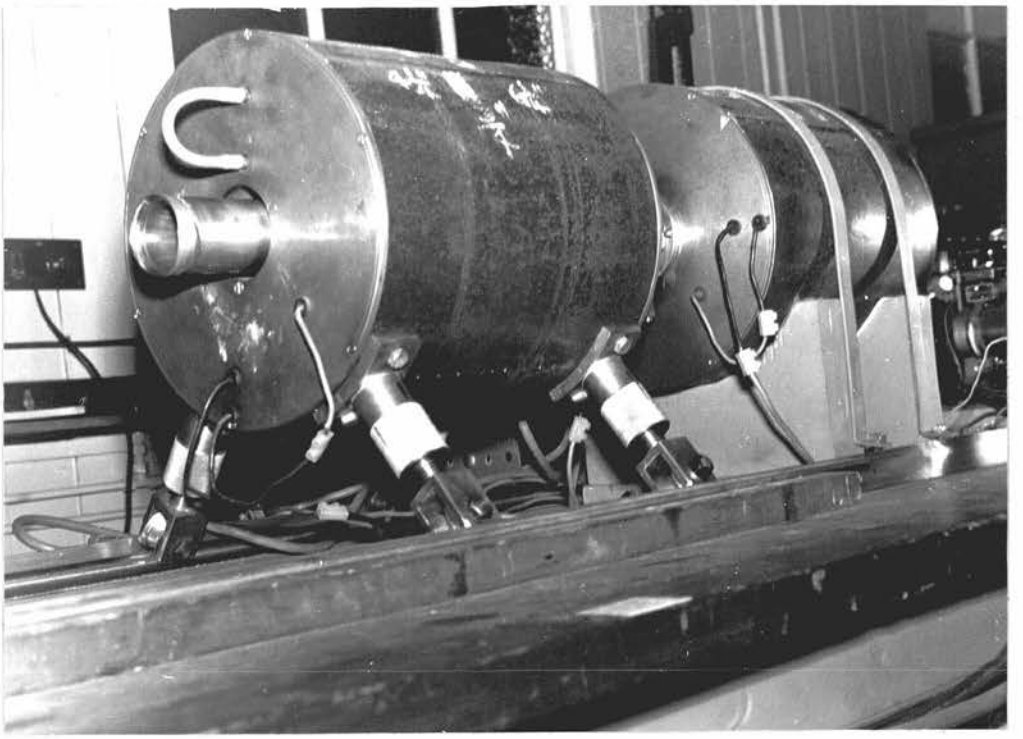

FIG. 3.6. The final focussing system.

and by adjusting the lengths of the supports the geometrical axis of L2 could be made to coincide with the fixed geometrical axis of L1. A brass tube, fixed to the end of L1 facing L2, passed through the middle of L2. A clearance of approximately $\frac{1}{4}$ in. between the outside diameter of this brass tube and the inside diameter of the L2 pole pieces allowed sufficient room for adjustment of L2.

An electron detection system, consisting of a plastic scintillator (type NE102, supplied by Nuclear Enterprises (G.B.) Ltd.), perspex light guide and

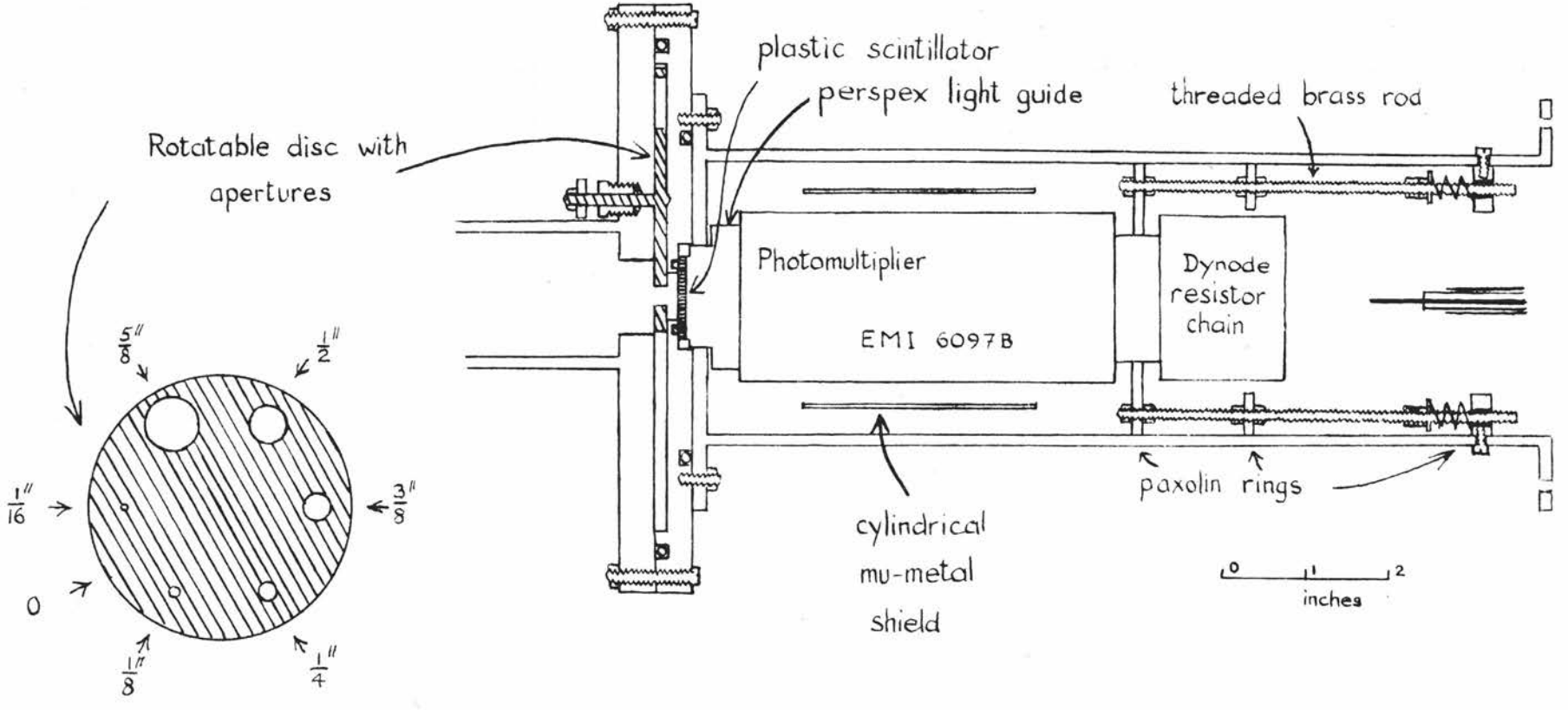

Fig.3.7. Variable aperture arrangement and details of photomultiplier tube mounting. The brass disc with apertures in could be set in any one of the seven positions indicated. The dimensions are the diameters of the apertures. The method of mounting the photomultiplier tube shown above was used in the assembly of the scattering chamber detection systems (chapter 4).

photomultiplier (E.M.I. type 6097) and mounted inside a brass tube of $3\frac{1}{2}$ in. outside diameter, was bolted to a combination of two brass plates (see Fig. 3.7). On the other side of the brass plates was fixed a brass tube which slid inside the brass tube fixed to L1 and passing through L2. This arrangement was supported on the rails by means of two supports fixed to one of the two brass

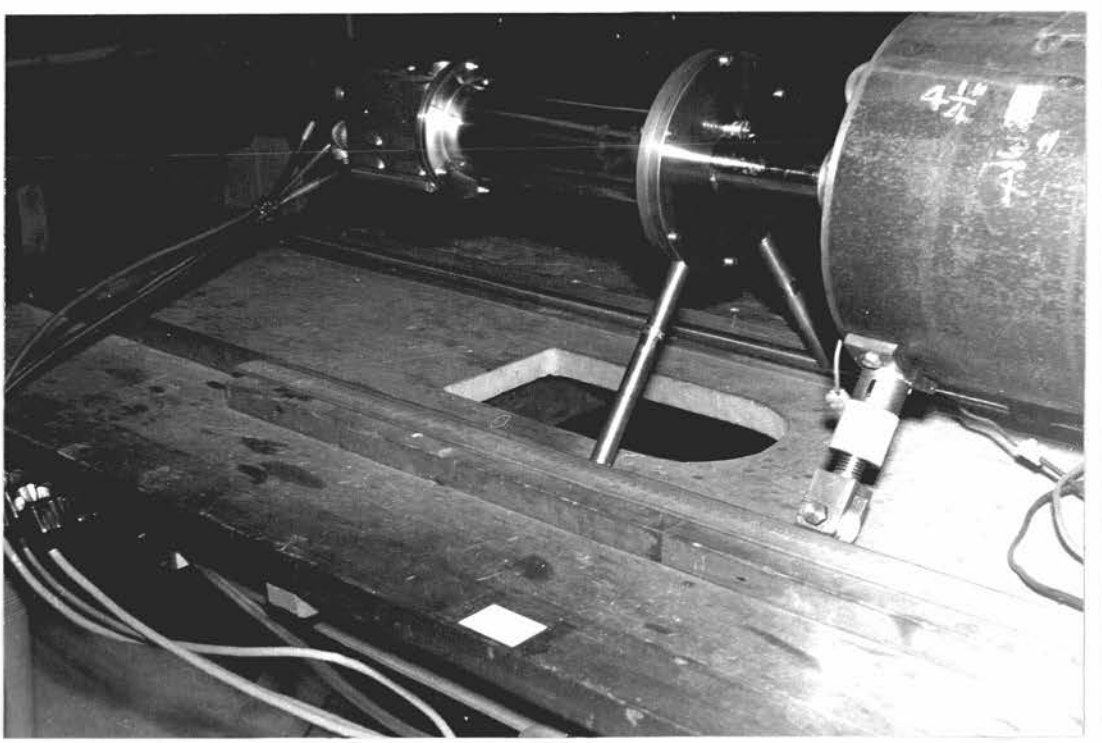

FIG. 3.8. The "variable aperture" detector unit.

plates (Fig. 3.8) and its position on the axis of the system could be varied. Holes were bored through the centres of these brass plates and between them a rotateable disc was arranged so that any of a number of

apertures could be set in the hole through the plates (Fig. 3.7). In this way, the effective size of the detector could be varied. With this arrangement the properties of the focussed electron beam were investigated to find the optimum values of source position, L2 position, L2 field extent, etc.

The Alignment of the Final Focussing System

The alignment of the apparatus was carried out after it had first been assembled and a rough check had been made that it was vacuum tight. It was dismantled then re-assembled bit by bit, the alignment being checked at each stage. Two brass discs were prepared which just slipped into the pole pieces of L1. In the centre of each disc a small hole of diameter approximately $\frac{1}{100}$" was bored. The line joining these "point apertures" was taken to define the geometrical axis of L1. Two similar apertures were prepared to fit the pole pieces of L2. One of them was inserted into the pole piece of L2 nearer to L1 and a light was placed at the other end of L2 (see Fig. 3.9). The L2 supports were adjusted until the three holes (one in L2 and two in L1) were in line - which occurred when light passed right through the system of apertures. The end of L2 next to L1 was now geometrically in line with L1. The procedure was repeated for the other end of L2 and a final adjustment made when all four apertures were in position (two in L1 and two in L2). It was found that L2 could be moved

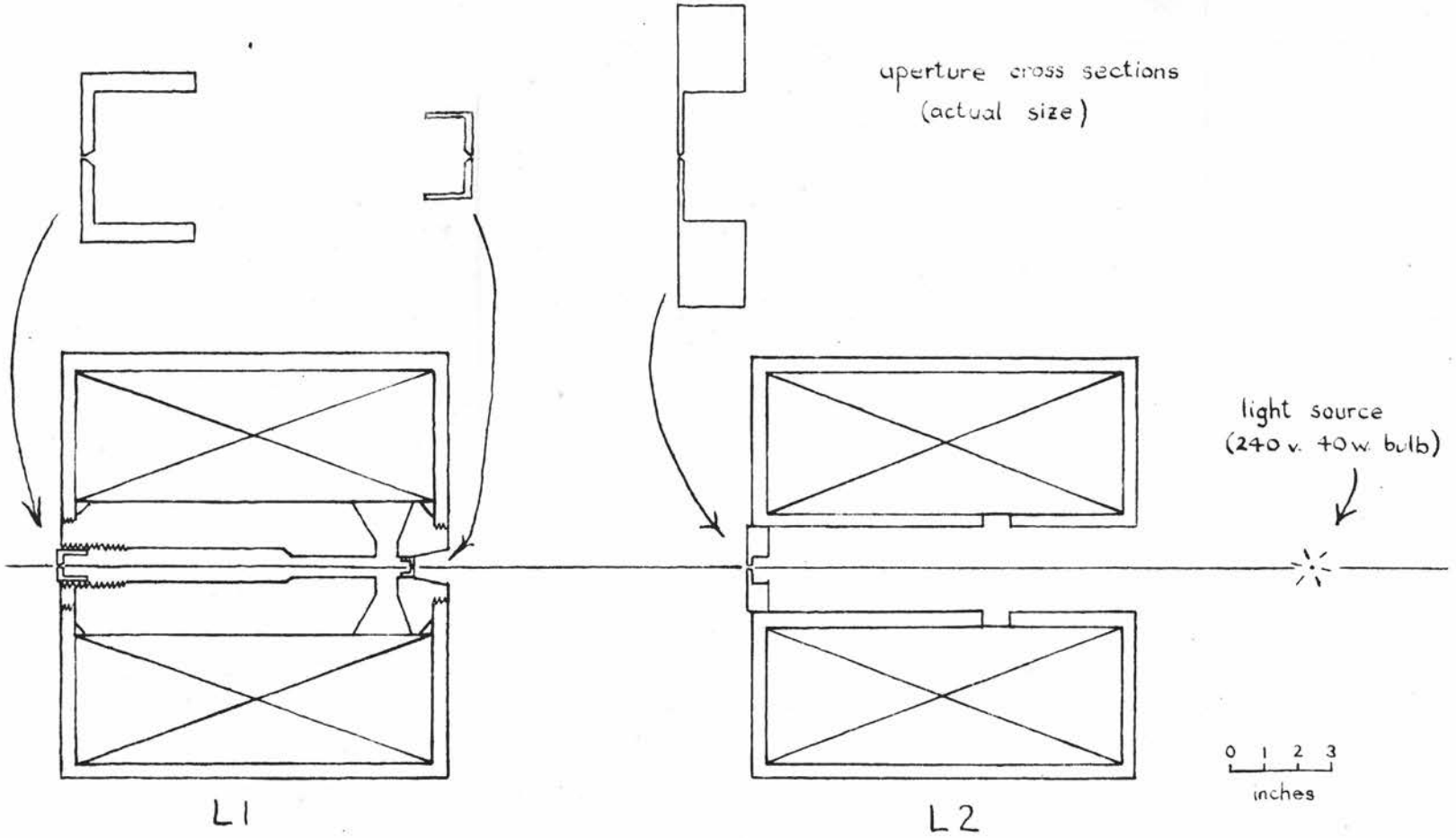

Fig. 39. Cross section of part of focussing system showing method of alignment and, at top, cross sections of some of the "point apertures" used.

along the rails through about 2 feet without the light, now passing through four apertures, being extinguished. The degree of alignment suggested by this was considered satisfactory. The same procedure was used to align both the brass tube leading from L1 through L2, and the device containing the rotatable aperture disc.

Focussing Properties.

The focussing properties of the system were investigated once the alignment was complete. It was first assumed that the magnetic axis and the geometrical axis (defined by the apertures discussed above) coincided. That this was only approximately true became apparent later (see Chapter 6). The three main properties of the beam which were investigated were its intensity, its geometrical cross-section and the energy resolution. The first two were examined using electrons from the β-spectrum of P^{32}. The last was examined using the Cs^{137} 625 keV internal conversion line and β-spectrum.

(i) Intensity

The intensity measurements were mainly made with the $\frac{3}{8}$" aperture in front of the detector and a simple collimator in front of the aperture (Fig. 3.10). For a source to detector distance of about 60 cm. an increase in intensity, compared with the unfocussed

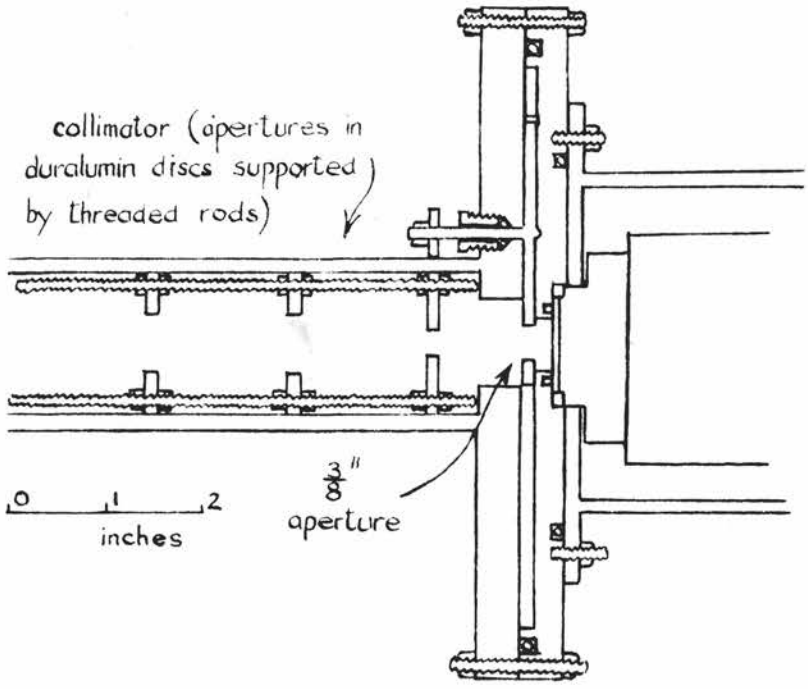

Fig. 3.10. Arrangement of collimator and aperture-disc in measurement of properties of focussing system.

intensity, of approximately 400 times was obtained using both lenses. An increase in intensity of about 20 times was obtainable using either lens alone. The beam intensity was not strongly dependent on either the position of the source relative to the L1 magnetic field or the distance between source and detector which could be varied between 60 cm. and 80 cm. approximately. It was found, however, that for larger source to L1 field distances smaller values of I1 were needed to focus electrons of a given energy. Similarly, the greater the source to detector distance the smaller was the optimum value of I2.

(ii) Geometrical extent

The geometrical extent of the focussed beam was found to be dependent on the size of the aperture of the collimator (Fig. 3.10) nearest to the detector. It was measured by noting the counting rates for the various sizes of aperture in the aperture disc. When the diameter of the final aperture in the collimator was $\frac{1}{4}$ in. it was found that for about the first 2 in. beyond the collimator, the beam diameter did not extend to more than about $\frac{3}{8}$ in. Using a smaller diameter final aperture in the collimator gave rise to a smaller diameter beam of lower intensity. It was considered that an incident beam of electrons of diameter $\frac{3}{8}$ in. could be tolerated

for the experiment being planned. The position of the scattering foil, however, would have to be quite close to the collimator. At this stage, various combinations of L2 pole pieces were tried. It seemed that the beam-produced by the pole pieces having the smallest gap ($\frac{3}{4}$ in.) had the smallest geometrical cross section, although the differences were small. All subsequent measurements, however, were made with the $\frac{3}{4}$ in. gap between the L2 pole pieces. The variation of beam cross section with position along the axis was investigated more fully when the whole scattering apparatus was assembled. Details are given in Chapter 6.

(iii) Resolution

The measurements described in the previous two sections were for a focussing system without a central "stop". No matter what focussing currents were used, electrons of all energies reached the detector although those focussed most strongly to the detector position were much more numerous than those whose energies were either so high that they were hardly focussed at all or so low that they were "focussed out of the beam" before it reached the detector position. It was decided, however, to try to improve the resolution of the system by including a stop in the L2 field (Figs. 3.11 and 3.12), the size of the stop being decided by the condition that the intensity of the beam was not decreased

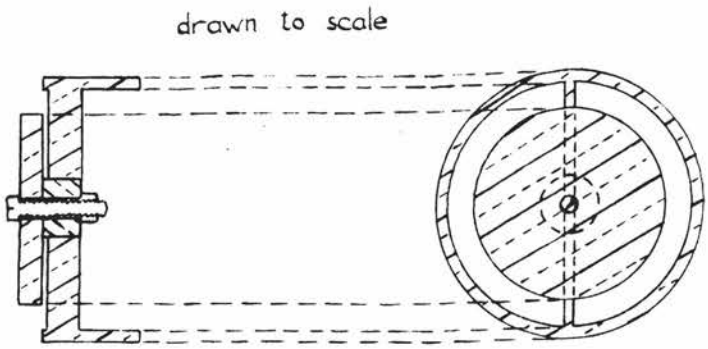

Fig.3.11. Details of central stop positioned in L2 field (see Fig. 3.12).

too greatly. Some idea of the resolution was found from measurements with the 625 keV internal conversion electrons from Cs^{137}. The procedure adopted was to fix the positions of all components and to observe how, for different sizes of the stop, the intensity of the focussed beam varied as I2 was varied while I1 remained at its optimum value. The curve of counting rate against I2 was plotted and ΔI2, the width at half-maximum found. The energy resolution of the focussing system could then be found from $\Delta I2/I2'$ where I2' is the optimum value of I2. Values of $\Delta I2/I2'$ of about 20% were obtainable without a serious loss in intensity. The final evaluation of the resolution was also made after the complete scattering apparatus was assembled and details are given in Chapter 6.

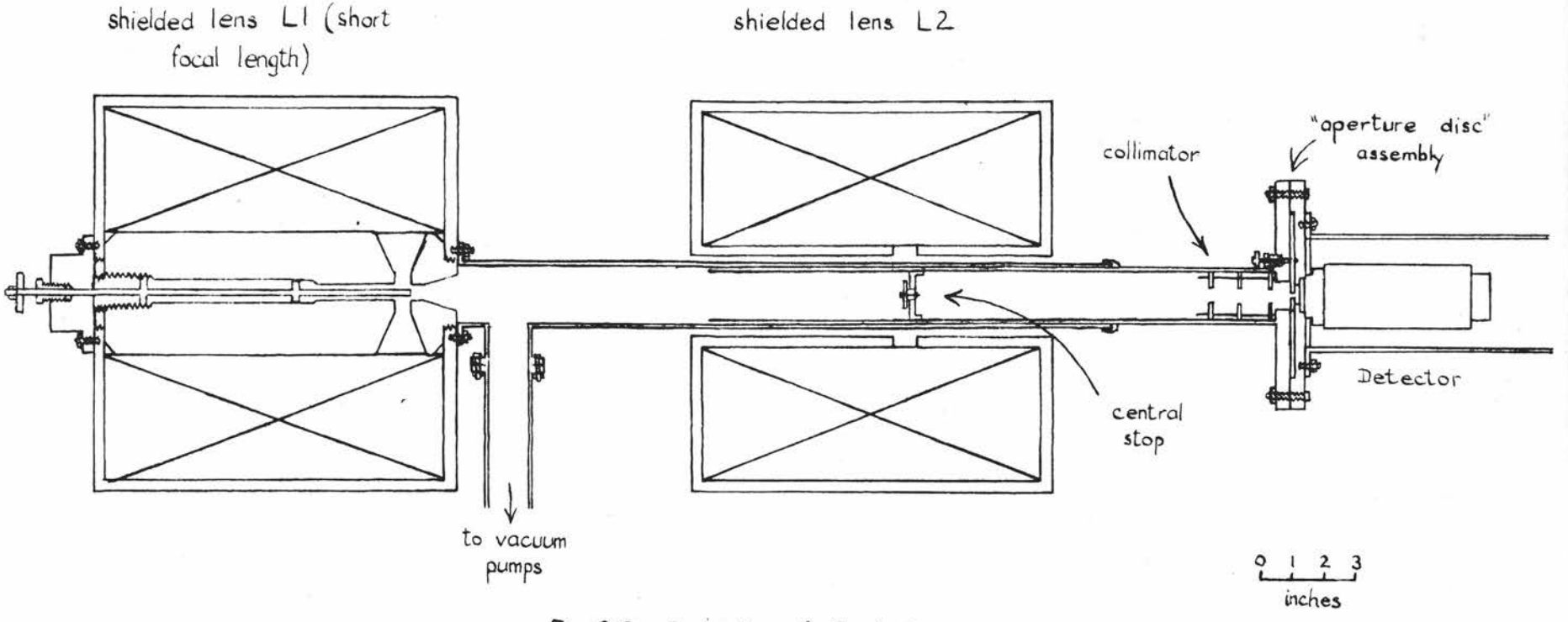

Fig.3.12. Details of final focussing system.

CHAPTER 4

THE COMPLETE SCATTERING CHAMBER ASSEMBLY

The Scattering Chamber

The main consideration in the design of the scattering chamber was that the procedure adopted in making the planned measurements be as simple as possible. A cylindrical chamber in which the angular position of the detector of the scattered electrons would be continuously variable over a large range seemed to be the best choice.

The brass cylinder used had an inside diameter of $9\frac{4}{5}$ in. and was $5\frac{1}{4}$ in. long. Two 12 in. outside diameter flanges were soldered to the ends of the cylinder (see Fig. 4.2) and two 12 in. outside diameter brass plates (only one shown in Fig. 4.2) were prepared to fit the flanges. The vacuum seal between plate and flange consisted of one $10\frac{1}{2}$ in. diameter O-ring which fitted into a circular groove in the flange.

One hole, $\frac{7}{8}$ in. diameter, was bored through each plate at a point $3\frac{7}{8}$ in. from the centre of the plate. A detector (described later) was inserted into the scattering chamber through this hole. A scale, graduated in degrees, was cut all the way round on the outside face of the plate. The angular setting of the detector could then be determined with the help of a reference line on a small brass bracket mounted on the flange -

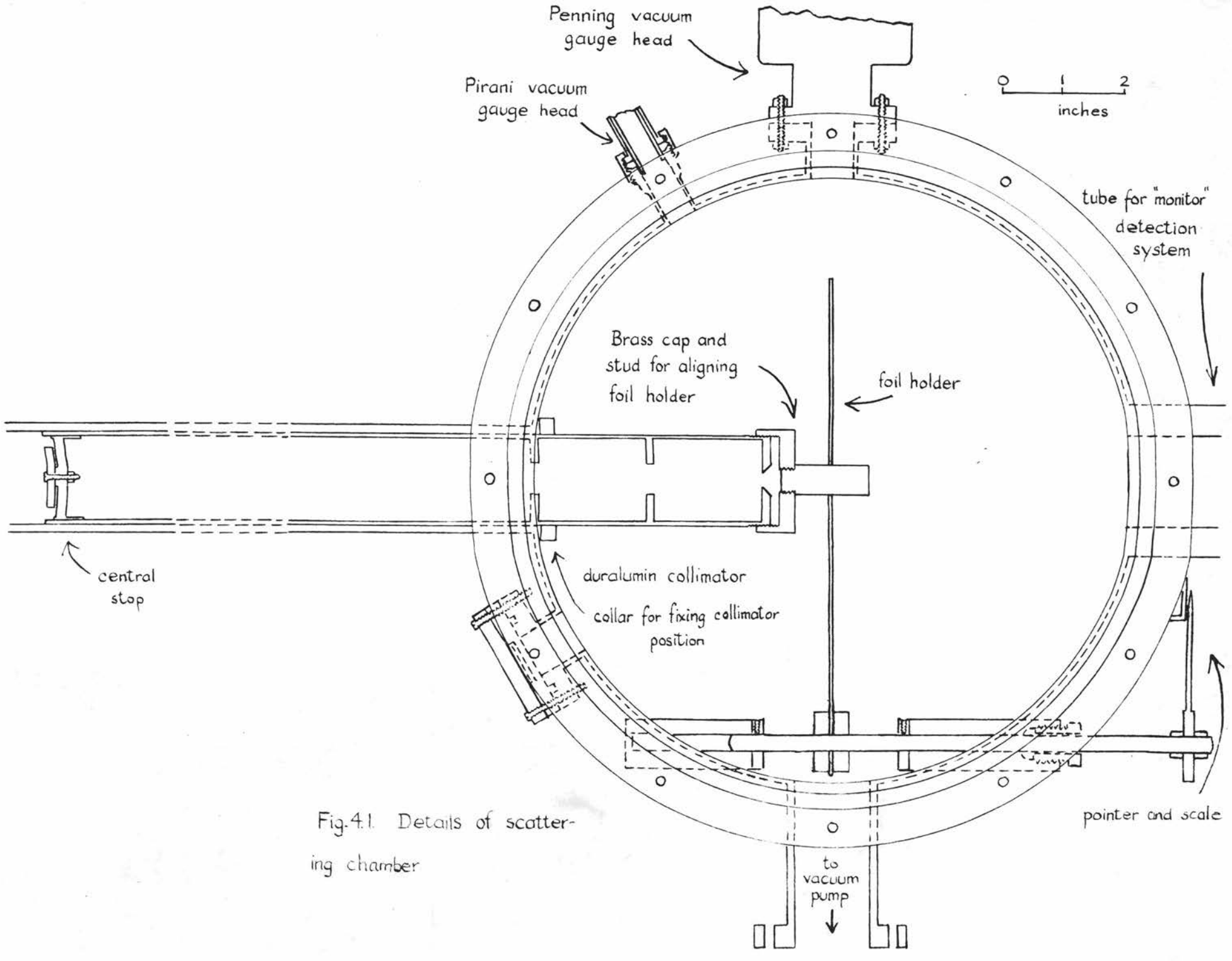

Fig. 4.1 Details of scattering chamber

Fig.4.2. Details of scattering chamber and "counter" detection system.

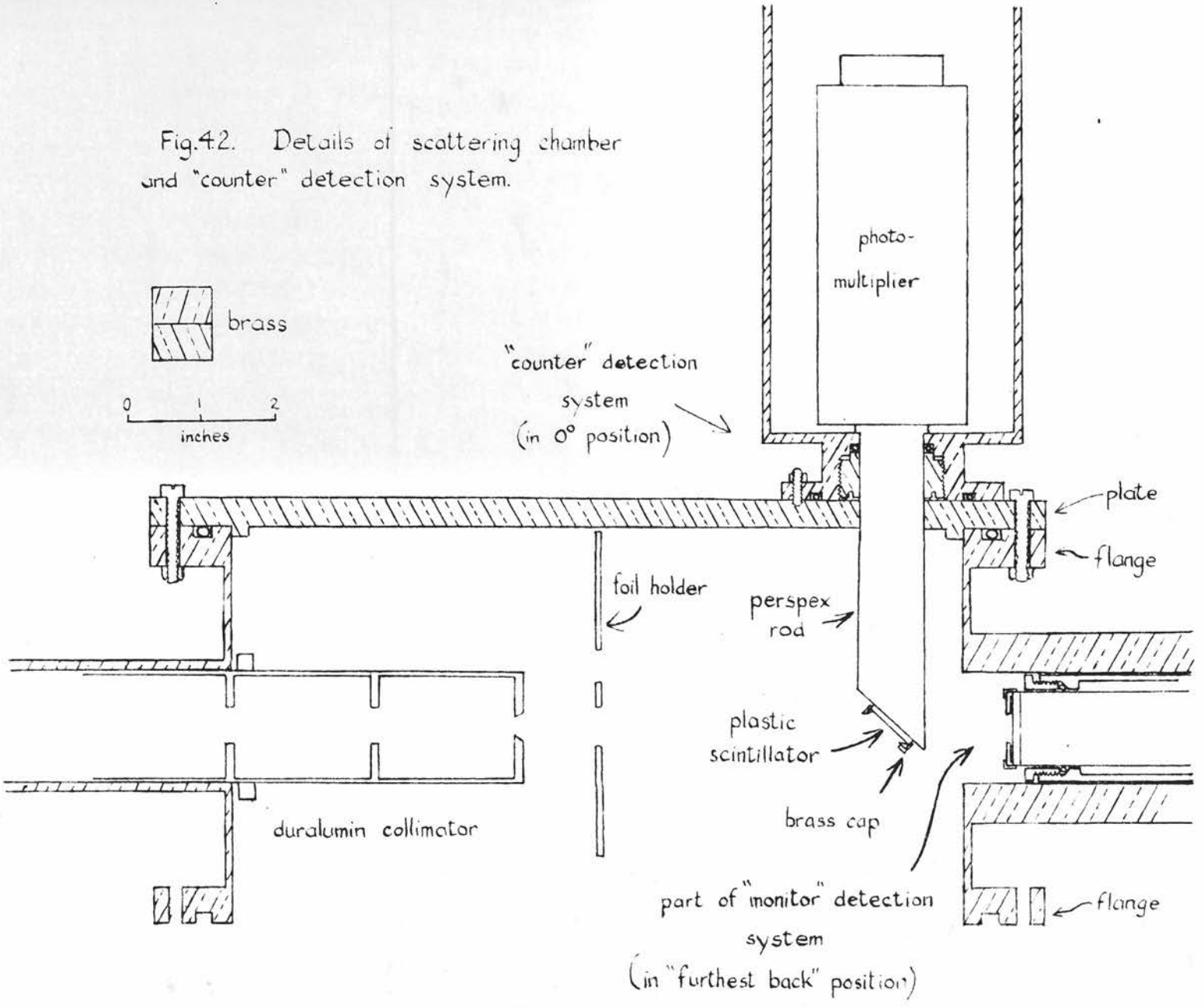

see Fig. 4.3. Into each flange twelve holes (OBA clearing) were drilled at 30° intervals around a circle $11\frac{2}{5}$ in. in diameter (see Fig. 4.1). Into each plate six slots were milled also on a circle $11\frac{2}{5}$ in. in diameter (see Fig. 4.3). The angle subtended at the centre of

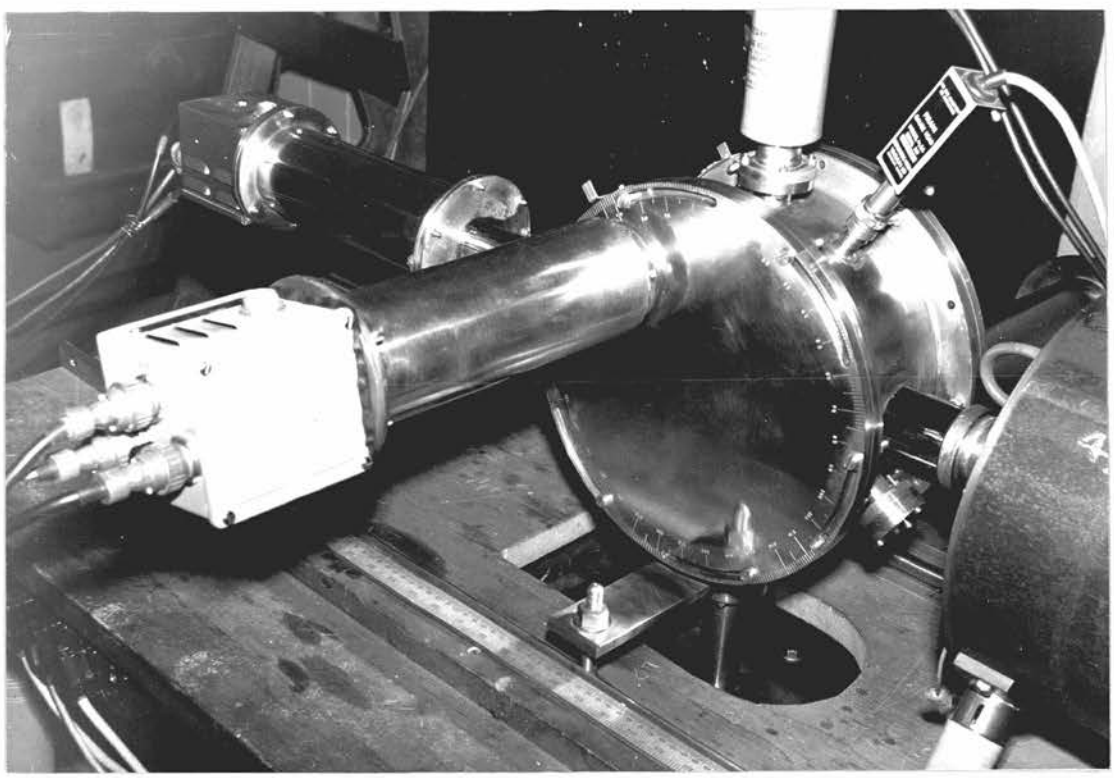

FIG. 4.3. The scattering chamber. The small bracket with the reference line for the angular scale on it is slightly above the centre of the photograph.

the plate by each slot was 36°. Each plate was held against its flange by means of six OBA bolts. The sizes and positions of the holes and slots allowed each plate to be fixed at any angular setting. When the

scattering chamber was in position, the plates were vertical.

Six cylindrical tubes of various dimensions (see Fig. 4.1) were soldered into the cylindrical chamber walls mid-way between the flanges. Two were fixed along what was the horizontal diameter of the chamber when it was in position. The electron beam entered the chamber through one of these, the monitoring system (Fig. 4.4) through the other. Another two were fixed along the vertical axis of the chamber. The lead to the vacuum pumps was attached to the lower of these two tubes and one of the vacuum gauge heads was fixed to the upper one. The second vacuum gauge head was fixed to the fifth tube set in the top half of the chamber at 30° to the vertical. The final tube, set in the lower half of the chamber at 30° to the horizontal, was included in the construction to allow for the possibility of electrical connections being made <u>inside</u> the chamber. In the work to be described, this tube was permanently sealed.

Near the bottom of the cylinder, $\frac{3}{4}$ in. from one of the flanges, two bearings were soldered (see Fig. 4.1). In these bearings was located a spindle to which the scattering foil holder (described later) could be fixed.

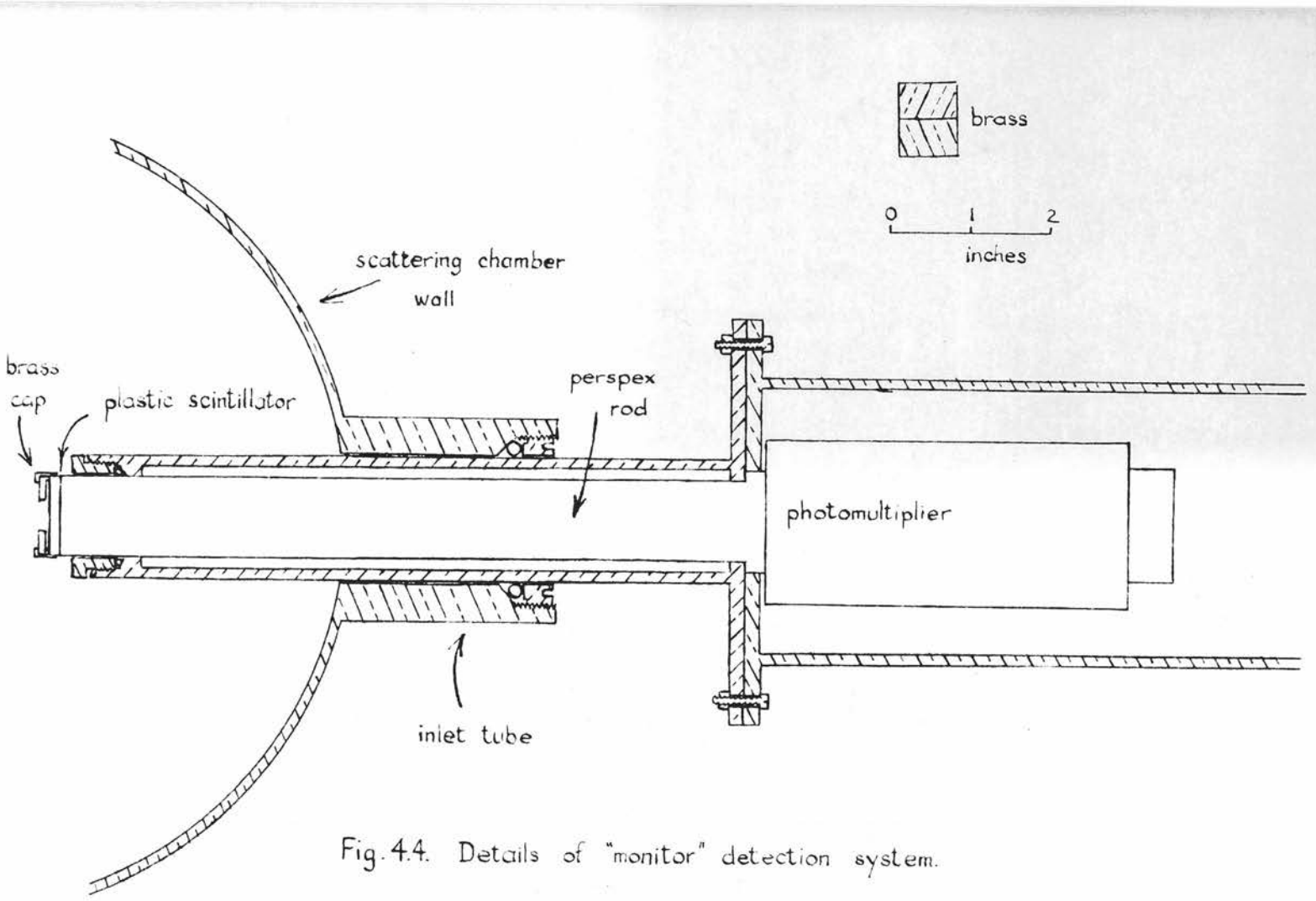

Fig. 4.4. Details of "monitor" detection system.

The Detection Systems

Provision was made in the apparatus for three detection systems - the "monitor", to check the incident beam, and, in each plate, a system referred to as a "counter" to measure the intensity of the scattered beam.

The monitor (Figs. 4.2 and 4.4) consisted of a disc of plastic scintillator 1 in. in diameter and $\frac{1}{10}$ in. thick fixed to a perspex light guide 1 in. in diameter and $8\frac{3}{4}$ in. long. The other end of the perspex rod was kept in optical contact with the photomultiplier by a thin layer of viscous silicone oil (Nuclear Enterprises (G.B.) Ltd.). By means of a brass "cap" and apertures of various sizes in brass discs $\frac{1}{8}$ in. thick and 1 in. in diameter (see Fig. 4.5), the effective size of the monitor scintillator

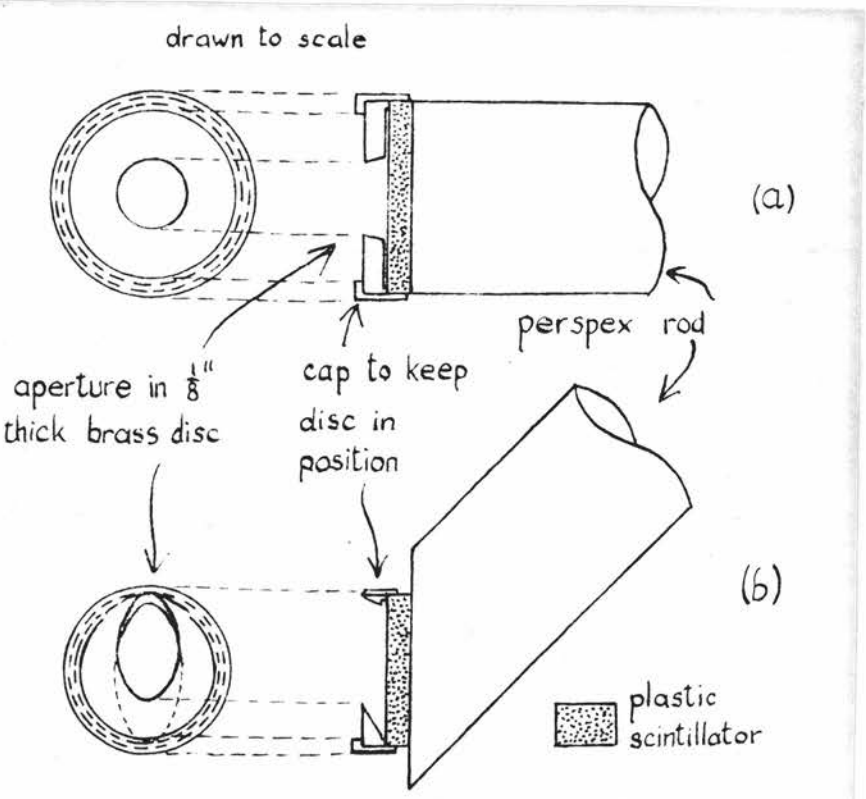

Fig. 4.5. Details of brass cap and aperture devices used with monitor (a) and counter (b).

could be varied. The photomultiplier was held in position (Fig. 4.4) inside a light-tight brass tube of $3\frac{1}{2}$ in. outside diameter. Attached to this tube was another one of $1\frac{1}{2}$ in. outside diameter which slid through the monitor inlet tube fixed to the scattering chamber. The monitor assembly was held in position by means of "distance pieces" (Fig. 4.6) and the arrangement was kept

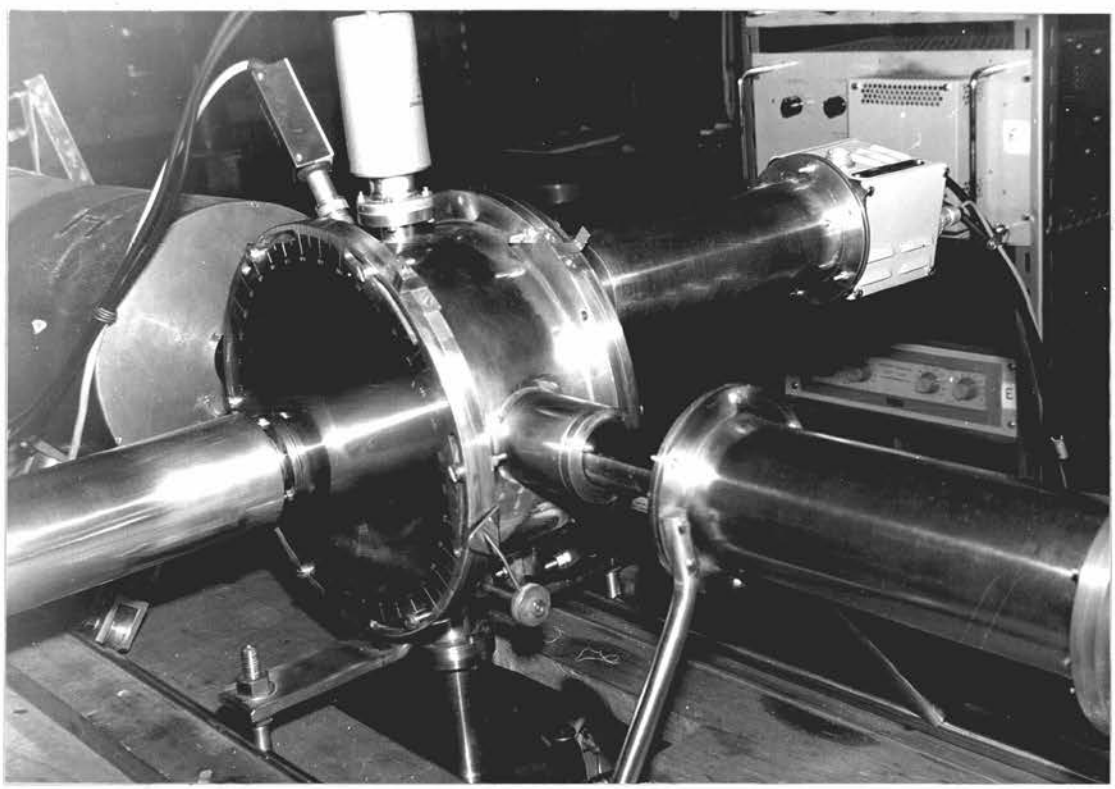

FIG. 4.6. The scattering chamber. The "distance piece" between the monitor assembly (right) and the monitor inlet tube (centre of photograph) is darker in colour than the rest of the apparatus in this region.

vacuum tight by means of two O-ring joints (Fig. 4.4).

The counter assembly (Fig. 4.2) was similar to the monitor assembly in that it used the same type of

photomultiplier, a perspex light-guide and the same type of plastic scintillator. The perspex rod, however, was narrower, being $\frac{7}{8}$ in. in diameter and was sufficiently long for the scintillator to lie in the plane mid-way between the chamber flanges (and so containing the path of the incident beam). The plastic scintillator disc, of $\frac{13}{16}$ in. diameter and $\frac{1}{10}$ in. thick was mounted at 45° to the axis of the perspex rod (Figs. 4.2 and 4.5). As with the monitor assembly, the effective size of the counter scintillator was defined by an aperture in a brass disc held in position by a brass cap. Again, two O-ring joints were required for vacuum tightness.

The Collimator

Inside the brass tube through which the incident electron beam entered the scattering chamber a collimator and a central stop were fixed (Figs. 3.11, 4.1 and 4.2). The optimum size and position of the brass stop (near one end of the duralumin tube) were found experimentally. Inside the other end of the duralumin tube were three apertures cut in duralumin discs $\frac{1}{4}$ in. thick, forming a collimation system. The end aperture was $\frac{1}{4}$ in. in diameter and was bevelled as shown to reduce scattering from it. The other two apertures were $\frac{1}{2}$ in. in diameter and were not bevelled. The distance between the two end apertures of the collimation system was approximately 4 in. The outside of the end of the duralumin tube which

protruded into the scattering chamber was threaded to take a brass cap used in adjusting the position of the foil holder (see later). The complete assembly of collimator plus stop was held in position by means of a duralumin collar which was fixed to the duralumin tube by means of three screws. This collar was kept in contact with the inside wall of the scattering chamber (see Figs. 4.1 and 4.2).

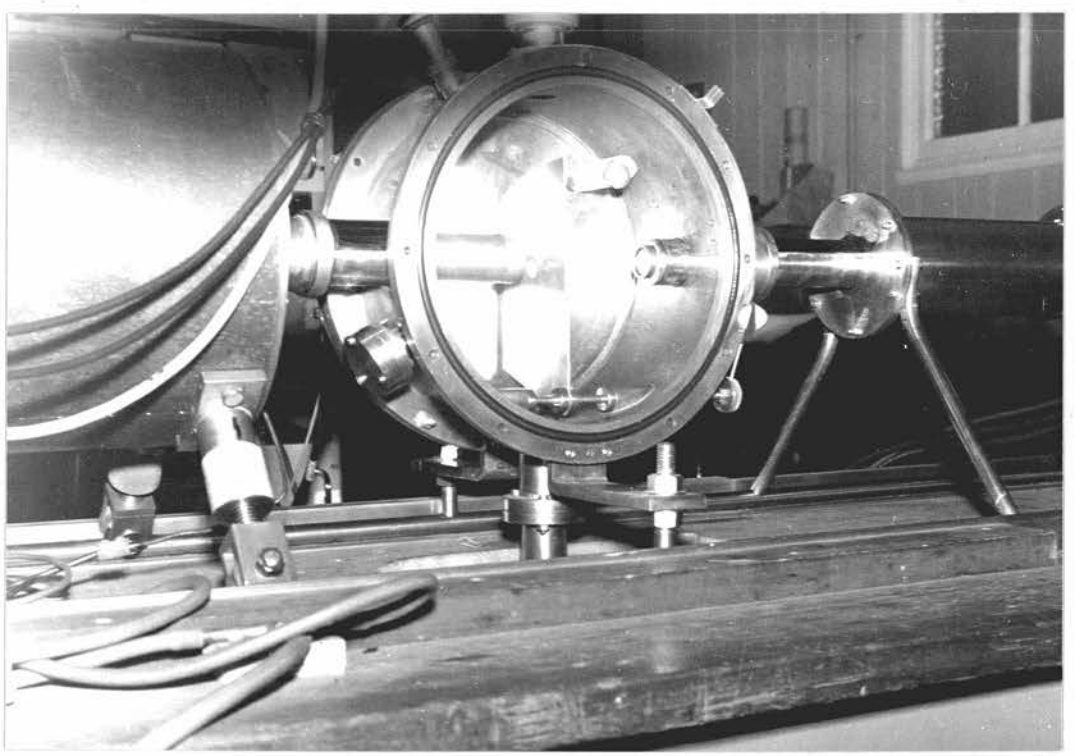

FIG. 4.7. The inside of the scattering chamber.

The Foil Holders

The foil holders (Figs. 4.1, 4.2, 4.7 and 4.8) used consisted of sheets of aluminium $\frac{1}{32}$ in. thick in which two holes were drilled such that when the holder was attached to the spindle, either of the holes could be set in the centre of the scattering chamber. Two brass collars were positioned near the centre of the spindle (Fig. 4.1). One of them was held fixed by means of a screw, the second was moveable. The foil holder was slipped on to the spindle by means of the slot cut in the bottom corner, and held against the fixed brass collar by the moveable one. Collars and holder were held together by means of two threaded studs which were fixed to one collar and passed through the fixing holes in the other collar and the small slots in the foil holder. Before the nuts were tightened to fix the holder rigidly to the spindle, the brass cap was screwed on to the end of the collimator tube. A brass stud was inserted through one of the holes of the foil holder and screwed into the cap (see Fig. 4.1). A pointer attached to the end of the spindle protruding from the chamber was adjusted to be in line with one of the two lines on a scale fixed to the chamber wall (Fig. 4.6). When it was thus ensured that the hole was in line with the geometrical axis of the collimator the nuts were tightened on the fixing collar studs and the brass cap-and-stud assembly removed. The positions of the holes in the foil holder and the two lines on the scale were such that once the

above procedure had been carried out, each of the holes could be brought into the centre of the scattering chamber by setting the pointer on one or other of the lines on the scale. In the work to be described, one of the holes was covered with a scattering foil and the other left blank and used for the adjustment of the holder.

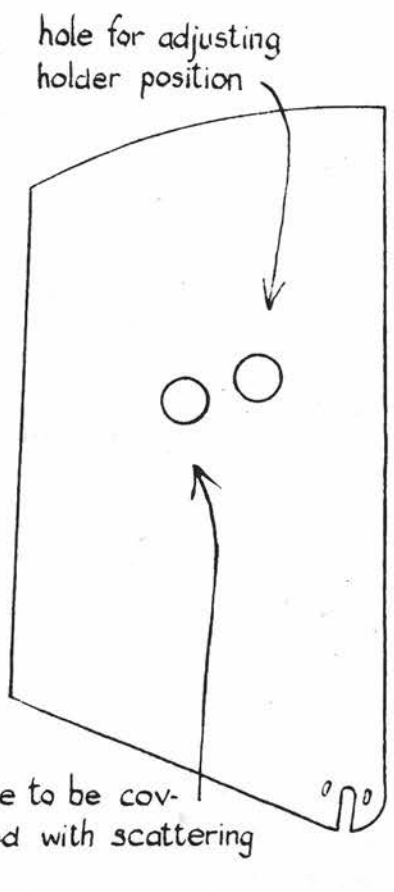

Fig. 4.8. Foil holder, made from $\frac{1}{32}$" thick aluminium sheet

CHAPTER 5

SOURCE AND FOIL PREPARATION

The Radioactive Sources

Four radioactive materials were used as sources of electrons: sulphur-35 (S^{35}), phosphorus-32 (P^{32}), caesium-137 (Cs^{137}) and thorium B (Th B) or lead-212 (Pb^{212}). The S^{35}, P^{32} and Cs^{137} were obtained from the U.K.A.E.A. Radiochemical Centre, Amersham, as, respectively, a sulphate in dilute sodium chloride solution, an orthosphosphate in dilute hydrochloric acid and caesium nitrate in nitric acid. Each was deposited on the end of a source stud by evaporation one drop at a time. Source studs were of brass for S^{35} and P^{32}, but of duralumin for Cs^{137}. The ThB source was collected on the end of a conducting (brass) source stud exposed in a radiothorium pot. The preparations of the Cs^{137} source and the ThB source will be described in more detail. The preparations of the S^{35} and P^{32} sources are essentially the same as that of Cs^{137}.

10 mc. of Cs^{137} were obtained in a solution of volume approximately 1 cc. This was evaporated down to about 0.2 cc., then transferred one drop at a time on to the aluminium foil at the tip of the source stud (see Fig. 5.1). The transfer was done by means of a syringe made from a piece of glass capillary tube and a short length of wire which formed the plunger. The diameter

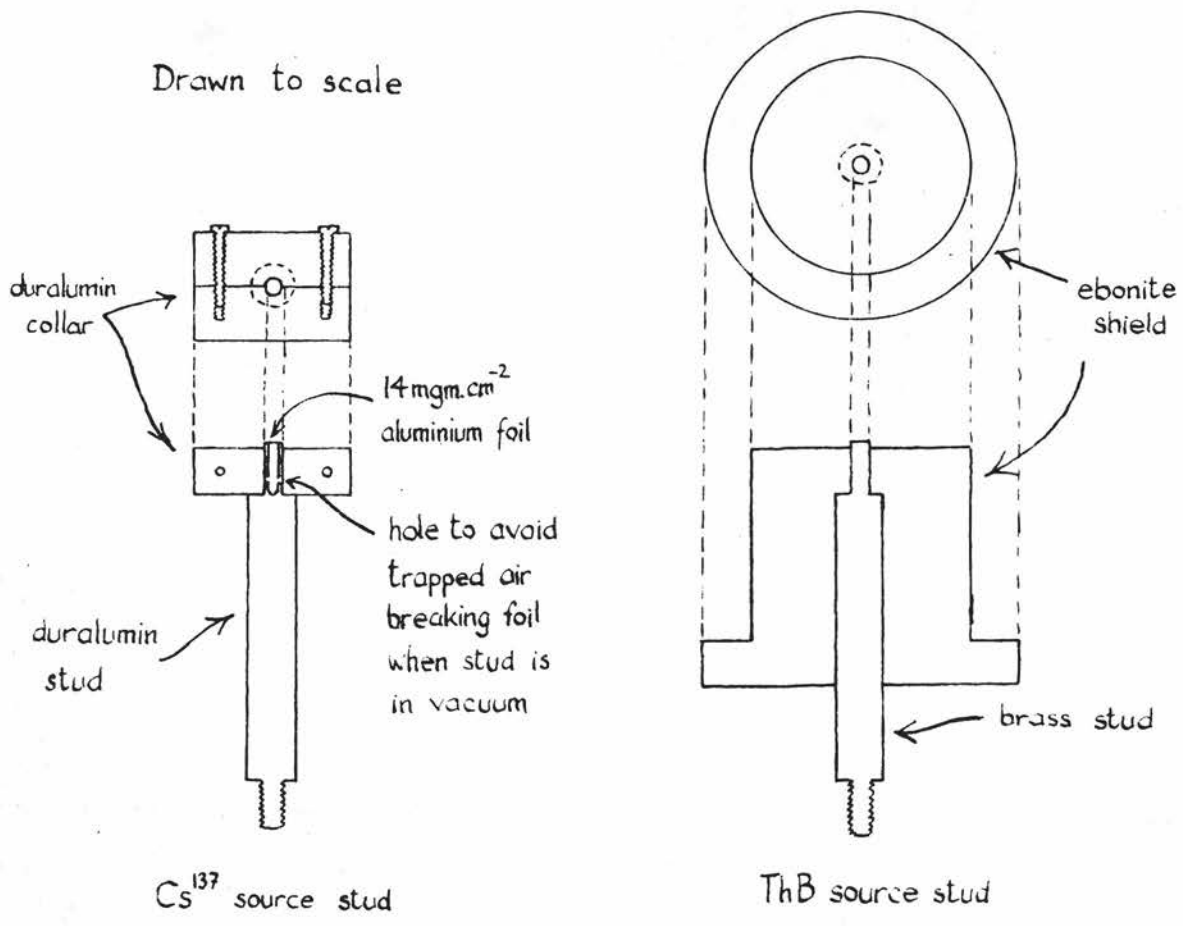

Fig. 5.1. Source stud details.

of the tip of the stud was approximately 1/16 in. A duralumin collar was fixed around the end of the stud to prevent any source material which might be accidentally dropped from contaminating the sides of the stud. When the transfer was completed, the collar was removed and a thin covering of "Zapon" lacquer put on the tip of the source stud. This was done by dropping on to the stud tip a drop of solution consisting of one part (by volume) of lacquer to one part of acetone. The purpose of the coating of lacquer was to prevent any of the deposit from flaking off inside the apparatus. As a final check that none of the source material would come off under vacuum, the source was put in a glass vessel and the air pumped out. No activity was subsequently detected in the glass vessel or the pumping line after the source was removed.

The brass source stud used for the ThB source (Fig. 5.1) had the same dimensions as the duralumin one used for the Cs^{137}. The stud fitted an ebonite holder so that only the tip protruded. The ebonite holder fitted into the top of a pot containing an open source of radiothorium. A positive potential (relative to the pot) was applied to the stud. This led to thorium A (ThA), a decay product of radiothorium, being deposited on the tip of the stud. The ThA decays quickly to ThB which emits a strong conversion line of electrons of energy 148 keV. These line electrons were used in some of the measurements described later.

The Scattering Foils

The scattering material used throughout was gold in the form of gold leaf. Three thicknesses were available: 0.24, 1.22 and 1.55 mgm. cm^{-2}. These values were found by weighing a leaf of the foil on an analytical balance capable of weighing correct to 0.2 mgm. and dividing by the area of the leaf which was ~ 100 cm^2. Considerable difficulty was found in mounting the foils without their becoming warped. The procedure eventually adopted was as follows. A piece of

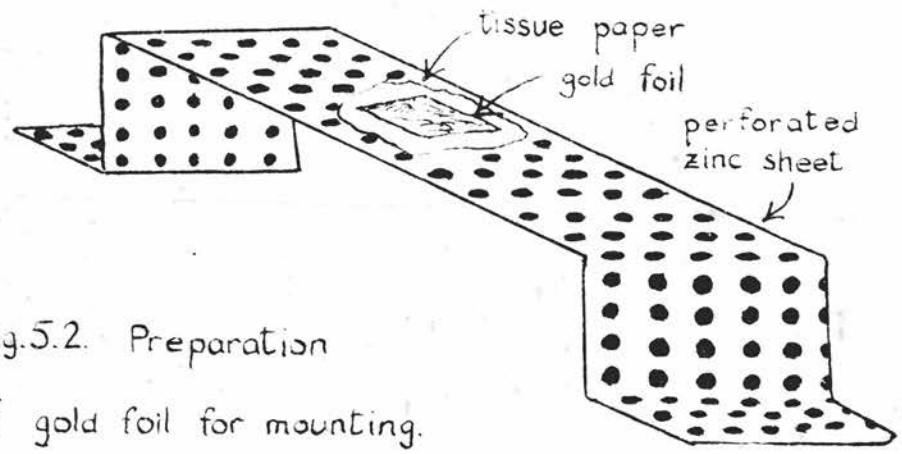

Fig.5.2. Preparation of gold foil for mounting.

perforated zinc sheet was bent into the shape shown in

Fig. 5.2. On the top surface was laid a square of gold foil (approximately $\frac{3}{4}$ in. square) separated from the perforated surface by a piece of tissue paper. A thin layer of "Zapon" lacquer was spread around the hole in the foil holder which was to be covered by the foil (Fig. 4.8). The holder was lowered slowly on to the piece of gold foil. It was found that by blowing gently through the hole in the foil holder on to the foil, the foil was kept very flat until it adhered to the holder. The tissue paper was then removed and the lacquer allowed to dry. By having the foil lying on a perforated surface no air was trapped momentarily between the foil and the surface during the mounting process, and so no distortions of the foil were produced because of this trapped air.

Six foils were used for the measurements: the three mentioned above and three composite foils of thicknesses 0.48, 0.72 and 0.96 mgm. cm^{-2} formed from two, three and four layers, respectively, of the 0.24 mgm. cm^{-2} foil. Naturally the complete mounting process could not be used for these last three foils, and their quality suffered.

CHAPTER 6

THE ASSEMBLY OF THE COMPLETE APPARATUS

The complete system was assembled and alignment was carried out as explained in Chapter 3, except that now the scattering chamber was in place of the variable aperture arrangement. The chamber itself was supported on the brass rails (see Figs. 6.1 and 4.7).

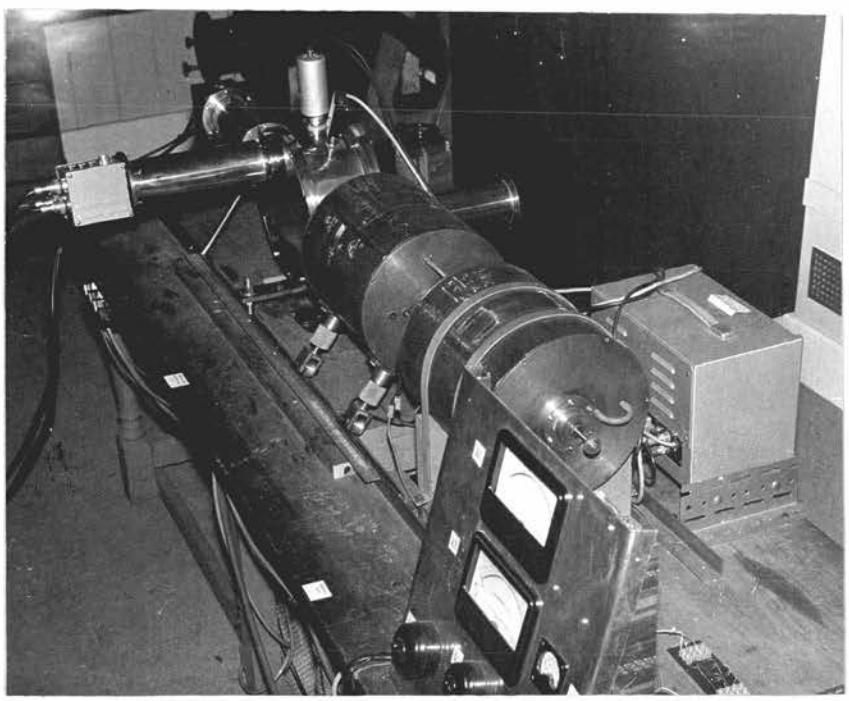

FIG. 6.1. The complete apparatus.

A check was made of the vacuum obtainable with a single stage rotary pump (type 1S50) and an oil diffusion

pump (type F203), both manufactured by Edwards High Vacuum Ltd. Without any special cooling, a pressure of 4×10^{-5} torr was easily obtainable, the pressure being measured by a Penning vacuum gauge. After ten hours continuous pumping, the pressure was between 3×10^{-5} and 4×10^{-5} torr, which seemed to be the limit of the system.

L2 was set at its optimum position relative to L1, and the scattering chamber was set in such a position relative to L2 that the beam produced by the focussing system had its smallest geometrical cross section at the centre of the chamber. To make the efficiency of light collection of the monitor and counter detection systems as high as possible, the perspex light-guides were well polished and the plastic scintillators and the ends of the light guides to which they were attached were coated with a thin layer of magnesium oxide.

Before any scattering measurements were attempted checks were made that

(a) the beam entered the scattering chamber along the main axis of the apparatus,

(b) the size of the stop in the magnetic field of L2 gave the best compromise between intensity and resolution of the incident beam,

(c) the pairs of values of I1 and I2 were the optimum values for the energy ranges focussed.

Two additional checks were made after the scattering measurements were completed but will be described

here. They were

(d) the determination of the ranges of energy of the electrons in the four beams obtained from the Cs^{137} continuum and hence of the energy resolution of the focussing system, and

(e) a check of the divergence of the incident beams of electrons.

Incident beam direction - (a)

To check (a) the monitor, with a $\frac{3}{8}$in. diameter aperture in front of the scintillator, was set so that its position coincided with the position that the counter would occupy if the counter were set at 0^{o}. The 625 keV internal conversion electrons from the Cs^{137} source were focussed at the position occupied by the monitor by a suitable choice of I1 and I2 and the optimum values of I1 and I2 found empirically (these ought not to be the same as the optimum values for focussing the 625 keV electrons most strongly at the foil position, i.e. the centre of the scattering chamber). The lengths of the supports of L2 were varied until the maximum monitor counting rate was obtained. Fortunately, this occurred just before the limits of adjustment of L2 were reached. It was clear from this that the geometrical axis of the apparatus (defined by the small apertures in the brass discs used in the alignment process - see Chapter 3) did not coincide with the magnetic axis.

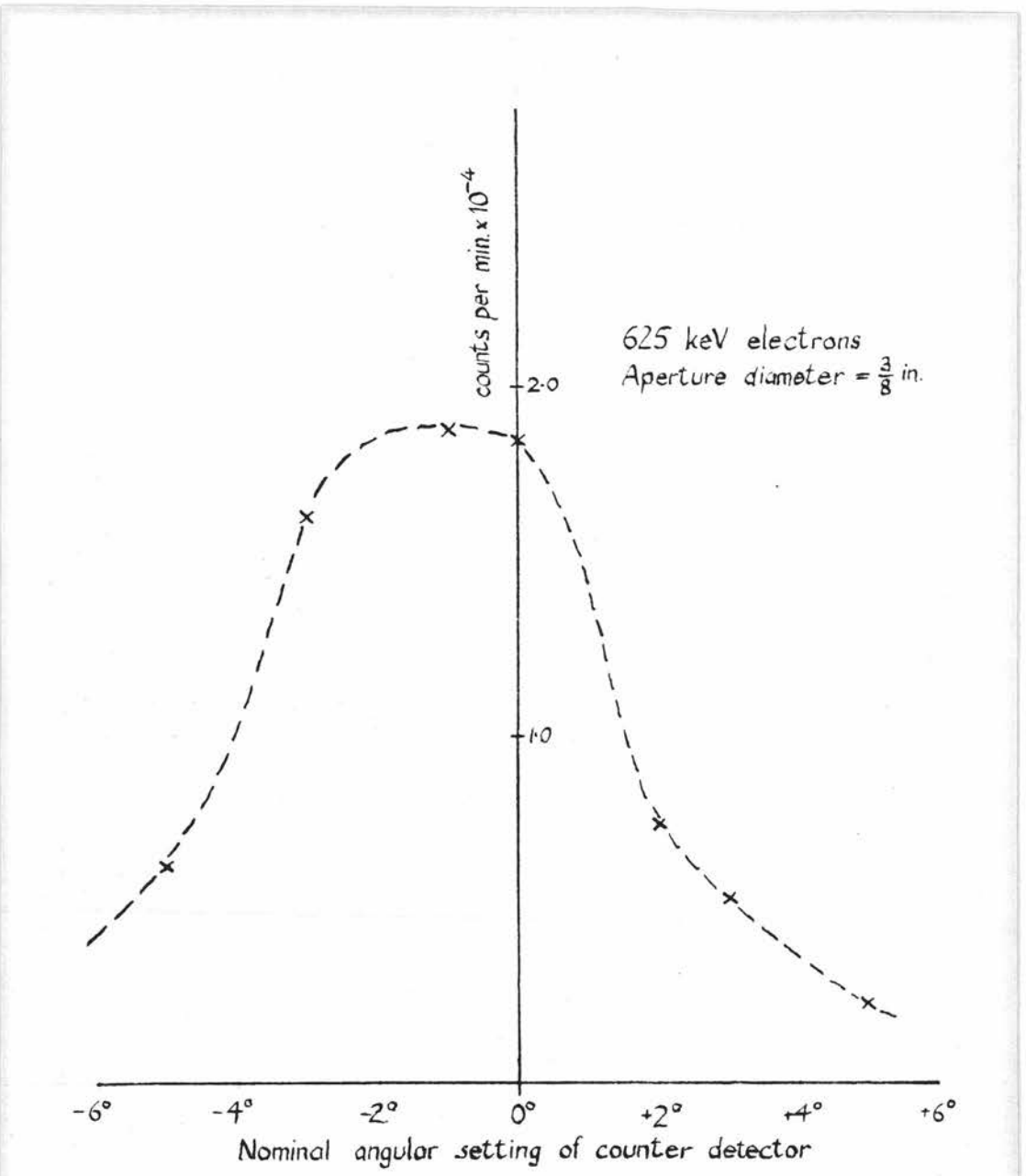

Fig. 6.2. Variation of counting rate with position of counter detector.

The monitor was now fixed in its "furthest back" position, in which position the plastic scintillator was approximately 1 in. up the monitor inlet tube and so outside the scattering chamber. The reference line for the counter scale had been set by eye. The counter was set at a nominal position of 0° and, using the same values of I1 and I2 as were used with the monitor detector, the counter counting rate was measured. In this and in all later measurements with the counter detection system, a $\frac{3}{8}$ in. diameter aperture was positioned in front of the counter scintillator (see Fig. 4.5). The semi-angle subtended by the aperture at the centre of the scattering chamber was approximately 3°. The measurements were extended to nominal angles in the range -5° to $+5^{\circ}$. The reference line position was in error by about 1° and it was re-set (Fig. 6.2).

Incident beam intensity and resolution - (b)

To check (b), several sizes of stop were tried in the L2 magnetic field. The smaller the stop diameter, the greater was the intensity but the poorer the resolution. Most of the measurements were made with the 625 keV line electrons and the resolution was measured from the variation of intensity of the electron beam at the foil position with I2 for the optimum value of I1 (see Chapter 3, pages 26 and 27). The final choice was a stop diameter of 1 in. and a resolution $\Delta I2/I2'$,

Fig.6.3. Variation of counting rate with I2 when I1 set at optimum value for 625 keV line electrons from Cs^{137}

Measurements made with monitor detection system at foil position.
Aperture diameter = $\frac{3}{8}$ in.

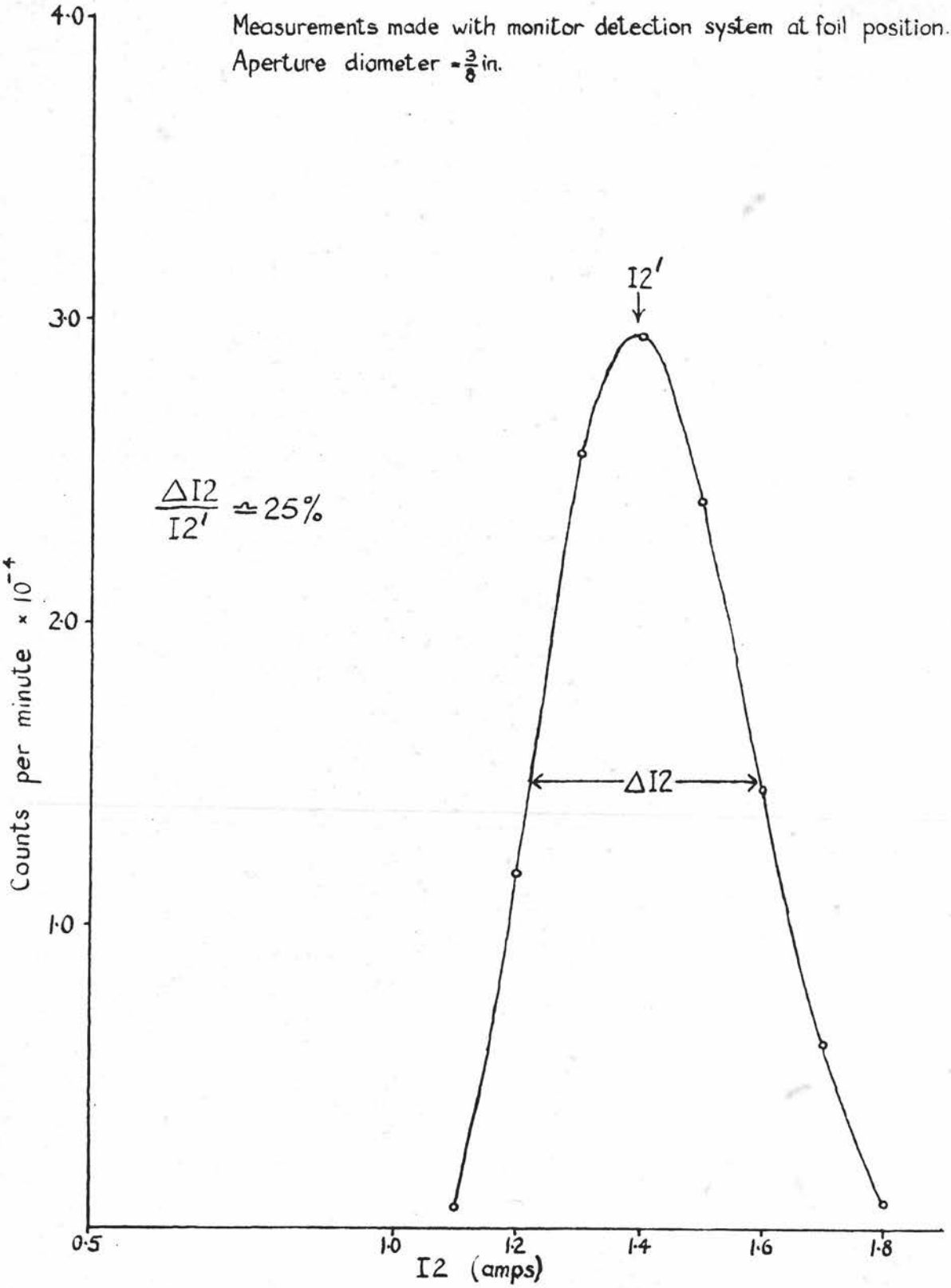

of 25% (Fig. 6.3). The resolution in terms of energy will be dealt with under (d).

Optimum values of I1 and I2 - (c)

In checking (c) it was decided first of all to use four different energy ranges from the lower energy electrons of the continuum of Cs^{137}, choosing them such that, in spite of the poor resolution of the focussing system, there was no appreciable overlap between ranges. The optimum values of I1 and I2 for the 625 keV line electrons had already been determined, and also the voltage distribution of the pulses produced by these electrons. Assuming that the voltage of the maximum of the pulse height distribution was proportional to the mean energy of the electrons producing the pulses, it was possible to choose I1 and I2 such that the mean energies of the electrons selected from the β-particle continuum ranged from ~100 keV to ~350 keV. The final stage of the calibration was carried out later. For each of the four values of I1 chosen, the variation of beam intensity (at the foil position) with I2 was found and the optimum values of I2 noted. Plots of the five pulse height distributions from the Cs^{137} source are shown in Fig. 6.4.

Fig. 6.4. Pulse height distributions for electrons from Cs^{137} and ThB at optimum focussing conditions.

Measurements made with monitor detection system at foil position. Aperture diameter = $\frac{3}{8}$ in.

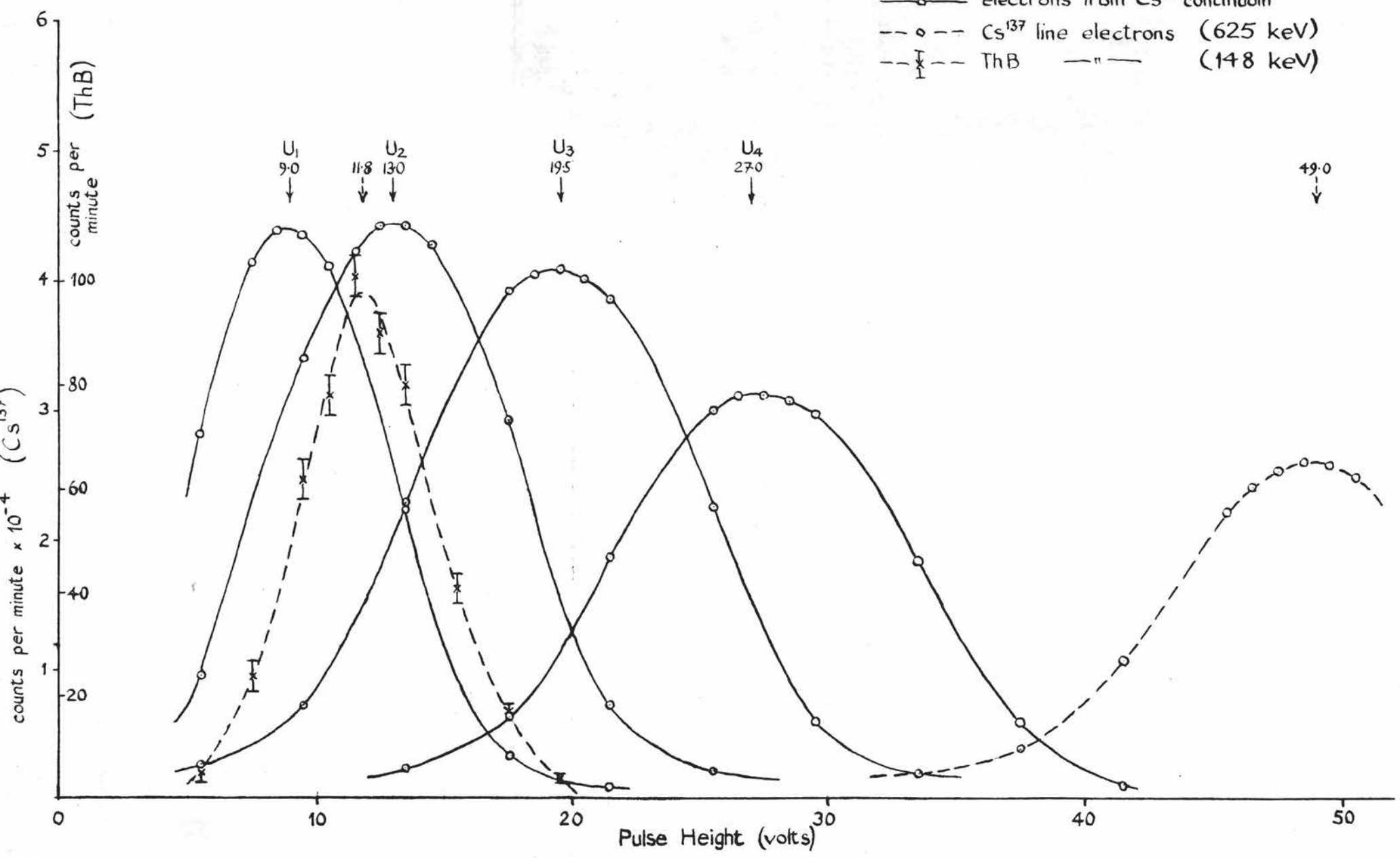

Energy ranges and energy resolution - (d).

These were determined with the help of electrons of two conversion lines: the 625 keV line from Cs^{137} and the 148 keV line (the "F line") from ThB. Optimum values of I1 and I2 for these energies were found and from the pulse height distributions for the two resulting electron beams, Fig. 6.4, corresponding values of electron energy and voltage at the maximum of the pulse height distribution were found. A straight line through these fixed points was drawn (Fig. 6.5) having an equation $E = 12.8U - 3.2$ where E is the electron energy in keV and U the pulse height in volts. From the pulse height distributions for the electrons focussed from the Cs^{137} continuum, the voltages corresponding to the maxima, U_1, U_2, U_3 and U_4 say, were found (Fig. 6.4). It was then assumed that the values of energy, E_1, E_2, E_3 and E_4, obtained from the above equation (see Fig. 6.5) were equal to the mean energies of the electrons in the four beams.

An approximate measure of the range of energies in each beam was found from the mean energy and the resolution of the focussing system determined earlier in terms of the current I2. Plots of the optimum values of I1 and I2 against mean energy E are straight lines to a good approximation (Fig. 6.6). The optimum value of I2 can be expressed as a function of mean electron energy E: $I2 = 0.0018E + 0.3$ where I2 is measured in amps and

Fig. 6.5. Variation of the mean electron energy (E) with the voltage (U) at the maximum of the pulse height distribution produced by these electrons.

Measurements made with monitor detection system at foil position. Aperture diameter = $\frac{3}{8}$ in.

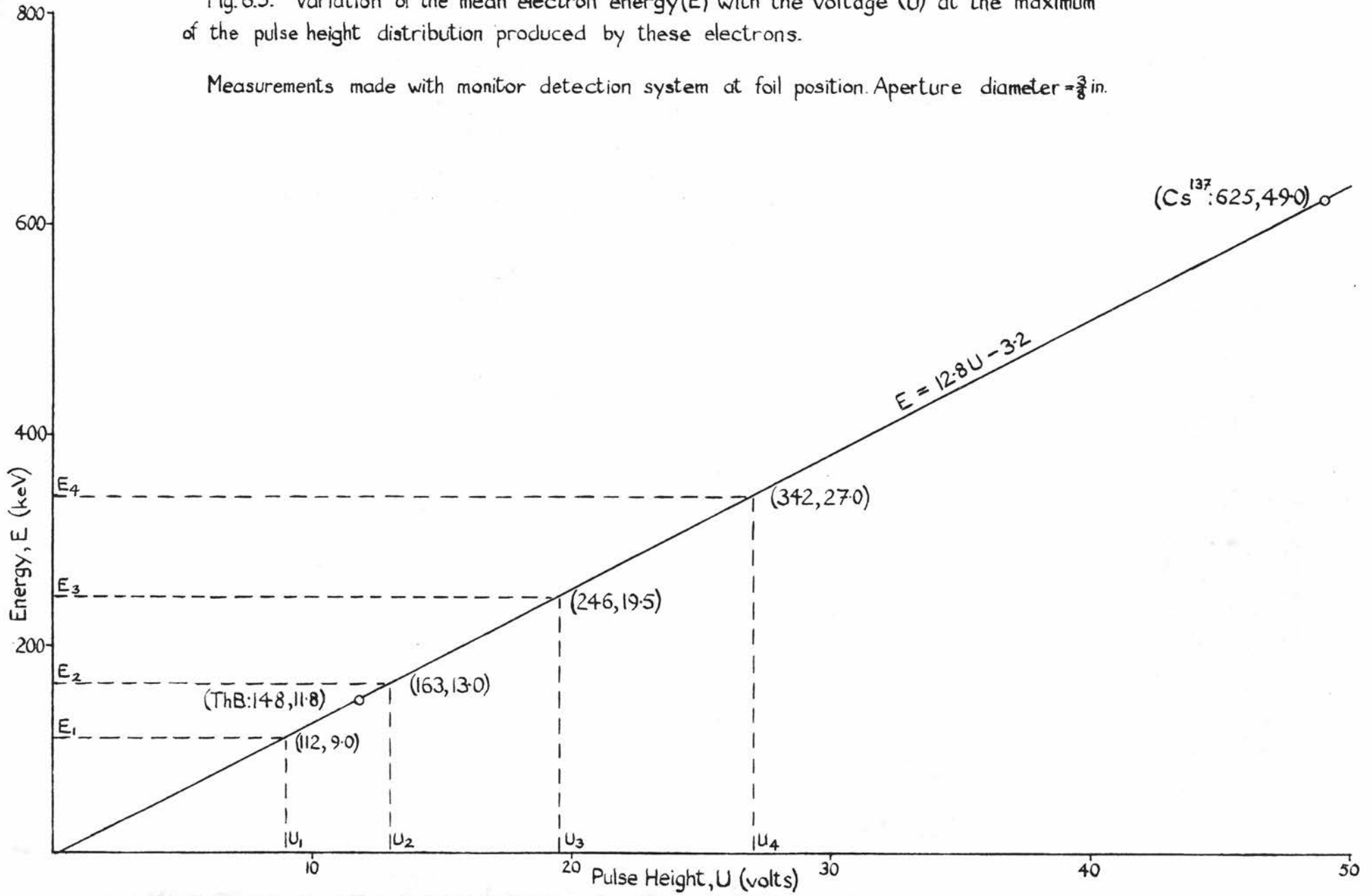

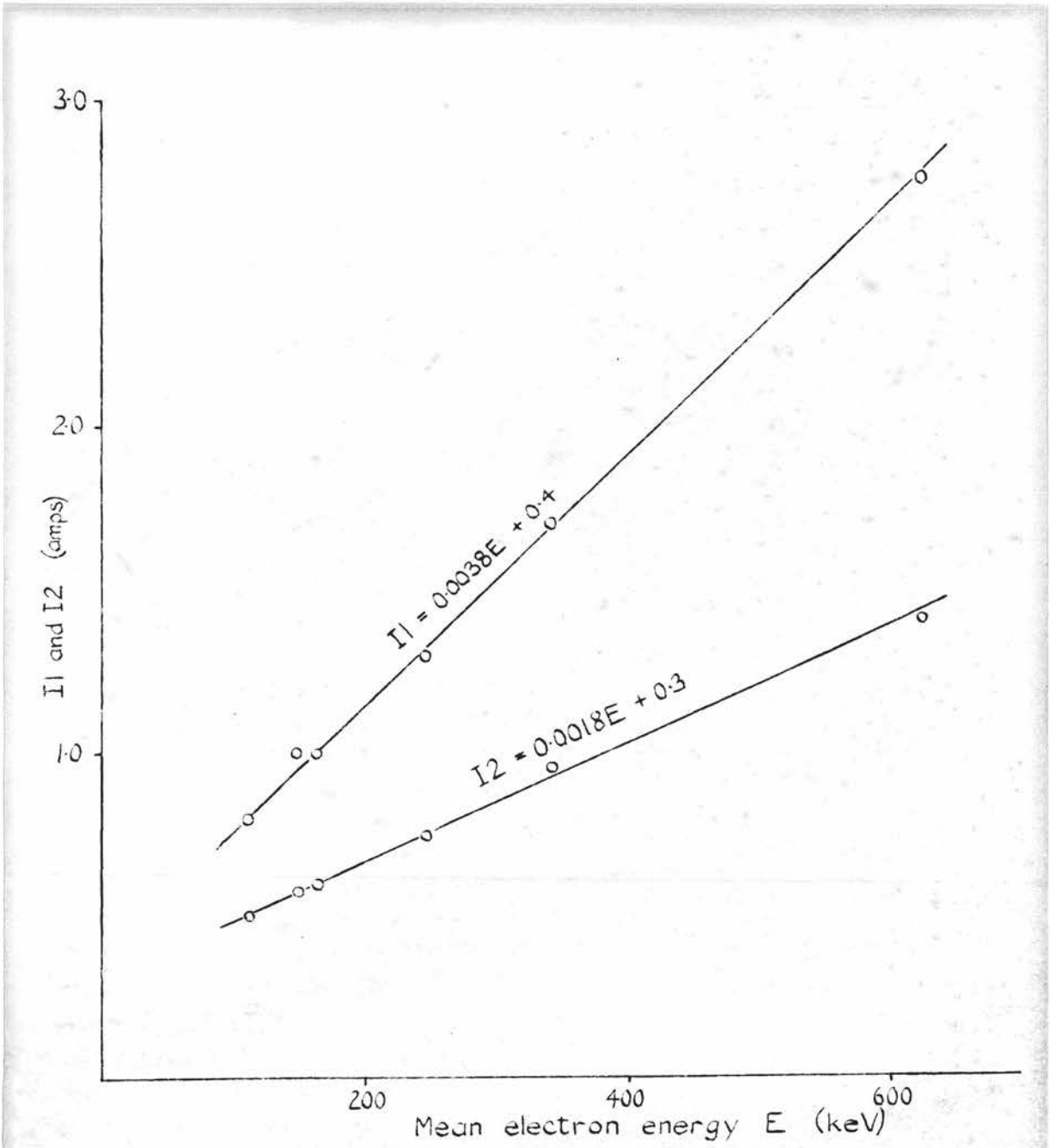

Fig.6.6. Variation of optimum values of I1 and I2 with E.

E in keV. From this equation, it follows that $\frac{\Delta E}{E} = (1 + \frac{1000}{6E}) \frac{\Delta I2}{I2}$. Suppose that $\Delta I2/I2$ is replaced by $\Delta I2/I2'$ which was found experimentally to be 25% for an energy of 625 keV (see Fig. 6.3). Then if this value for the "resolution" in terms of I2 is assumed valid for all energies in the range being used ($\sim$100 keV to $\sim$600 keV), the resulting values of $\frac{\Delta E}{E'} = \frac{\Delta E}{E'} = (1 + \frac{1000}{6E'}) \times 25\%$ are measures of the ranges of energy in the focussed electron beams. For a given I2', $E' \pm \frac{\Delta E}{2}$ are the energies of the electrons whose intensities are only half of their maximum possible focussed intensities. These values of $\Delta E/E'$, Table 6.1, are actually too large, because the focussing and consequent energy-selecting of L1 have been neglected. As the energy-selection by L1 is poor compared with that by L2, however, the errors in the values of $\Delta E/E'$ will be small.

Energy Range	Focussing Current (amps) I1'	I2'	Mean Energy (keV) E'	$\frac{\Delta E}{E'}$ (approx.)	Approx. Range of Energies (keV)
1	0.8	0.50	112	60%	80 - 145
2	1.0	0.60	163	50%	120 - 205
3	1.3	0.75	246	40%	195 - 295
4	1.7	0.95	342	35%	280 - 400
5	2.75	1.40	625	Cs^{137} line	
6	1.0	0.575	148	ThB line	

TABLE 6.1. Approximate ranges of energy in the electron beams.

The divergence of the incident beam - (e)

This was investigated by measuring (with the monitor) the intensity of the beam for each pair of optimum values of I1 and I2 at several positions along the horizontal axis of the scattering chamber (Fig. 6.7). Pulse height spectra were obtained for each position and for three different sizes of aperture in front of the monitor scintillator ($\frac{1}{4}$ in., $\frac{3}{8}$ in., and $\frac{1}{2}$ in.). Typical spectra for electrons of mean energy 246 keV obtained with a $\frac{3}{8}$ in. aperture in front of the monitor scintillator are given in Fig. 6.8. The maxima of these pulse height spectra are plotted as a function of monitor position in Fig. 6.7, as well as those of the 625 keV line electrons. It may be concluded that there is little spreading of the beam for about two inches beyond the end of the collimator and that the beam diameter at the foil position is $\sim\frac{3}{8}$ in. By the time the beam reaches the monitor inlet tube, however, it has spread out to more than $\frac{1}{2}$ in. in diameter, but an upper limit for the diameter cannot be found from the measurements made.

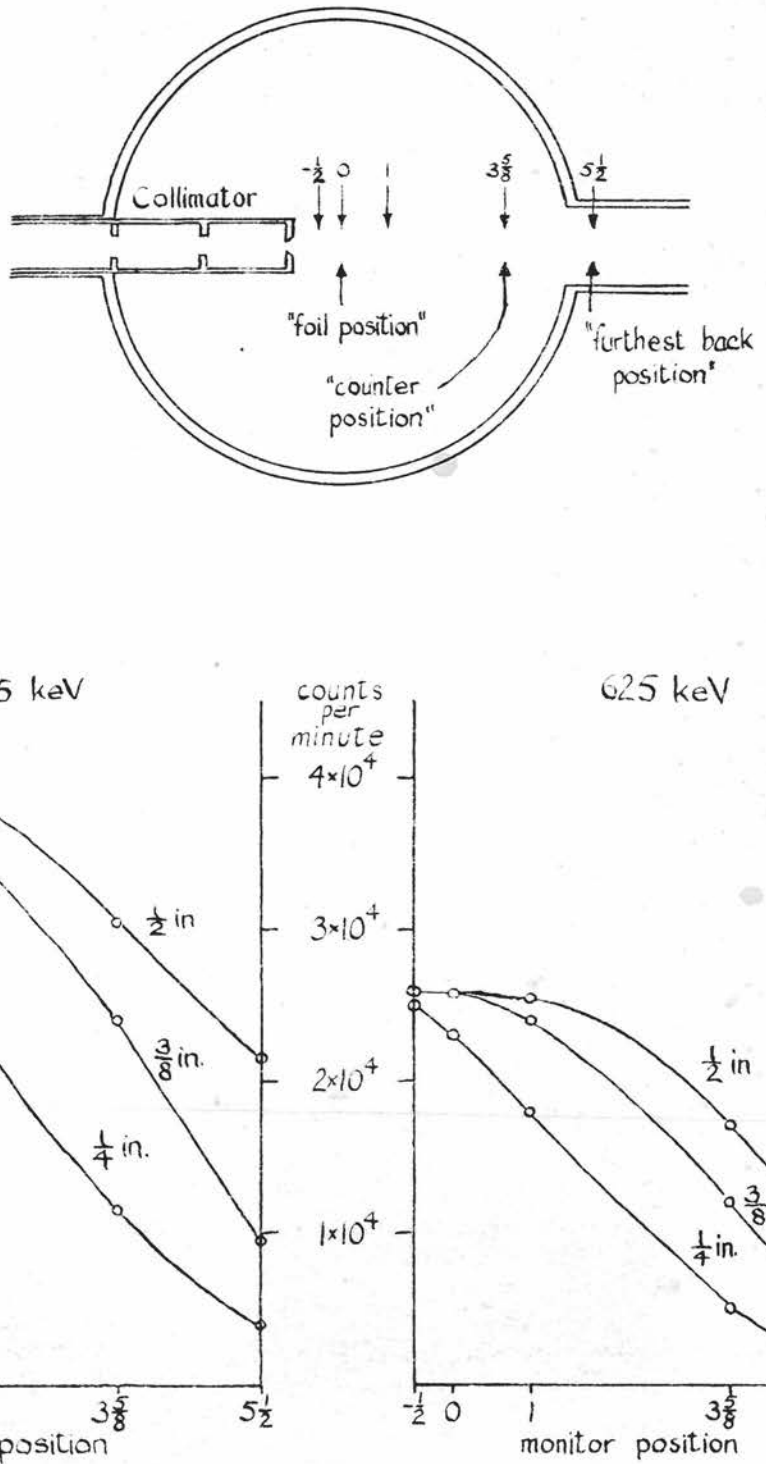

Fig. 6.7 Top: Monitor positions

Bottom: Variation of values of maxima of pulse height distributions with position of monitor. Aperture diameters and electron energies as indicated.

Fig. 6.8. Variation of pulse height distributions from 195-295 keV electrons (under optimum focussing conditions) with monitor position as indicated (see Fig 6.7)
Aperture diameter = $\frac{3}{8}$ in.

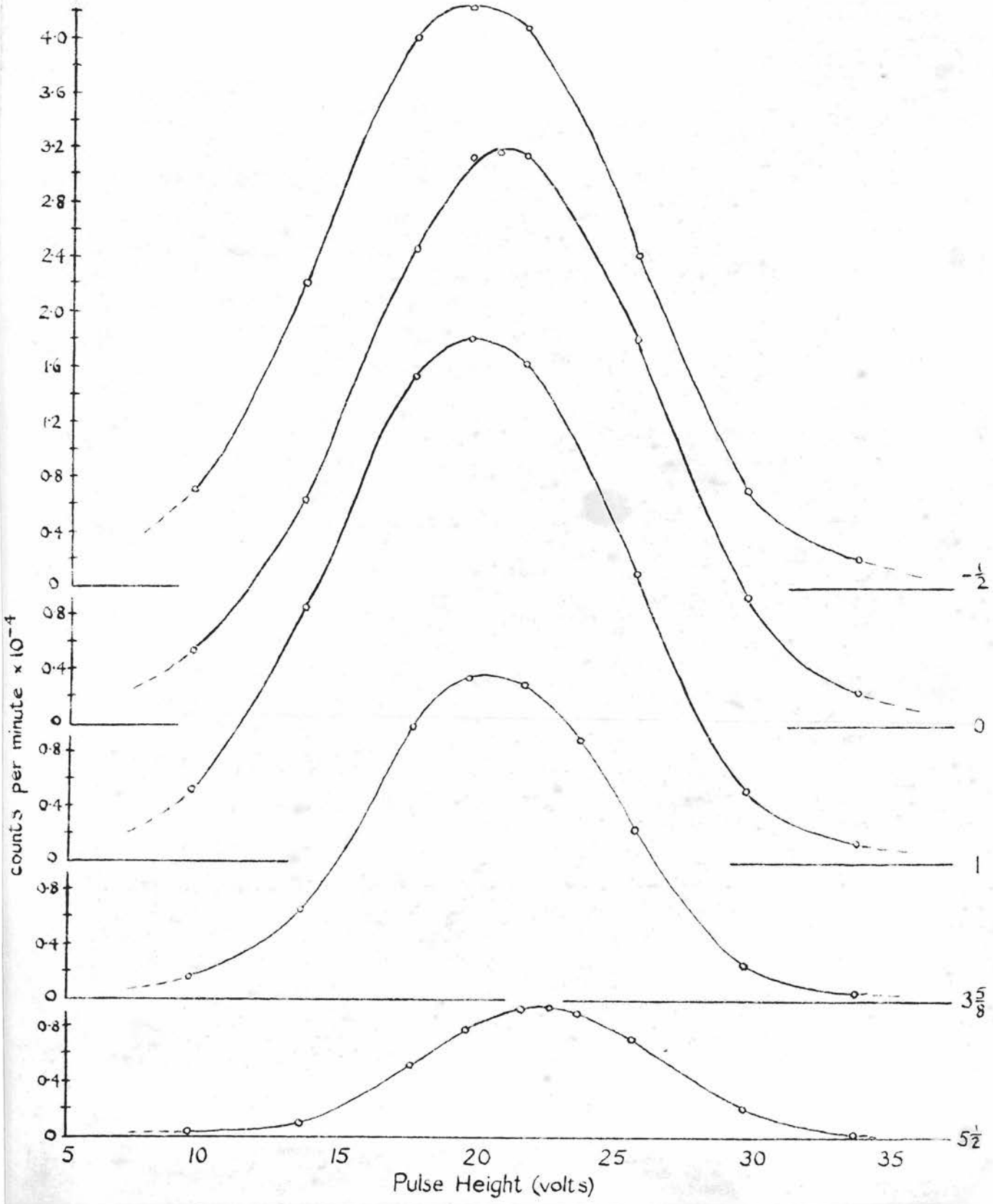

CHAPTER 7

ELECTRON SCATTERING MEASUREMENTS

Procedure

The electron scattering measurements were planned to lead to experimental values of the Mott (or electron-nuclear) scattering cross section ratio $\sigma_N^-(30^\circ, E, 79)/\sigma_N^-(65^\circ, E, 79) = \varrho(30^\circ, 65, E)$ for various electron energies E. The measurements were extended to allow comparisons to be made with $\varrho(20^\circ, 65^\circ, E)$ and $\varrho(45^\circ, 65^\circ, E)$.

The experimental procedure was as follows. The monitor was set in its furthest back position and was used to provide a check on the intensity of the incident beam. The counter was set at one angle, say 30°, and the counting rates (a) with no foil in position and (b) with a gold foil in position at the centre of the chamber were measured for incident electrons with energies in the ranges 1, 2, 3 and 4 (Table 6.1, page 47). The counter was then set at the second angle, say 65°, and the measurements were repeated. The complete procedure was repeated for other thicknesses of gold foil. Six foil thicknesses were used: 0.24, 0.48, 0.72, 0.96, 1.22 and 1.55 mgm. $cm.^{-2}$. The measurements were extended to counting rates at 20° and 45° so allowing comparisons with $\varrho(20^\circ, 65^\circ, E)$ and $\varrho(45^\circ, 65^\circ, E)$ to be made.

The scattering at 30° and 65° was measured for the 625 keV line electrons from the Cs^{137} source (Energy

range 5). Because of low counting rates, the thinnest foil (0.24 mgm. cm.$^{-2}$) was not used, and even with the foils used counting times were rather long. No corresponding measurements at 20° and 45° were attempted.

Because of the finite dimensions of the counter detector ($\frac{3}{8}$ in. diameter) and the beam ($\sim\frac{3}{8}$ in. diameter), the counter accepted electrons scattered through a range of angles centred roughly on the angle at which the counter was fixed. These ranges were calculated from the geometry of the apparatus and are given in Table 7.1.

Angular Position of Counter	Approx. Maximum Range of Scattering Angles
20°	14° - 26°
30°	24° - 35°
45°	40° - 50°
65°	60° - 72°

TABLE 7.1. Ranges of Scattering Angles.

Only one of the two "counter" detection systems included in the scattering chamber construction (see Chapter 4) was used in the measurements being described.

Adjustments of Counting Electronics

The counting electronics was arranged as shown in Fig. 7.1. From a single E.H.T. Supply Unit output, two independently variable outputs were produced by the potentiometer unit, one going to the counter photomultiplier and the other to the monitor photomultiplier.

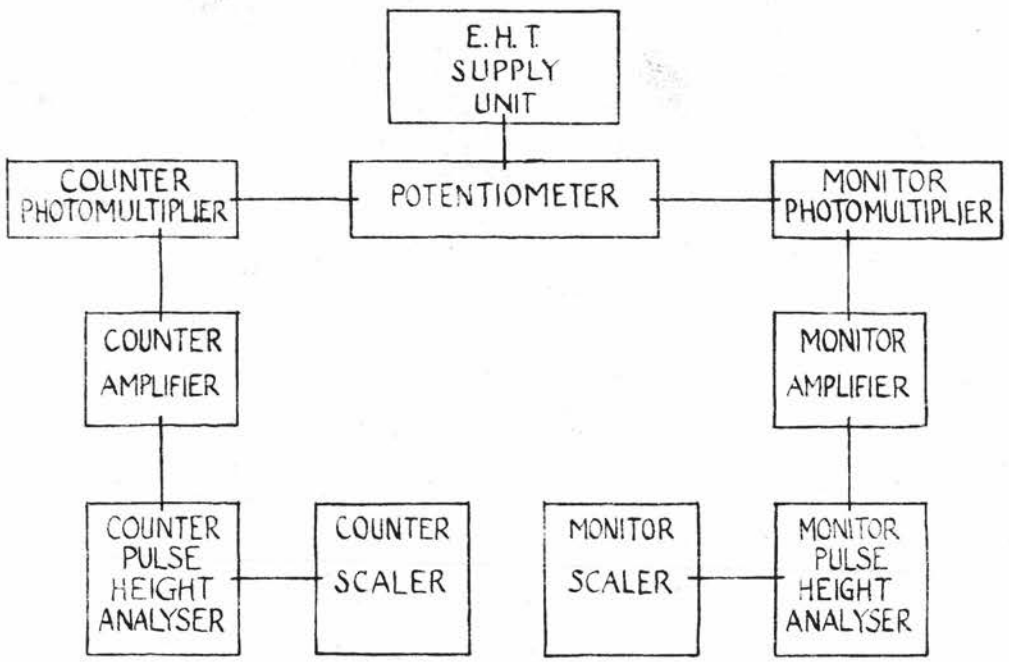

Fig.7.1. Block diagram of counting electronics arrangement.

The pulse height analysers were of the single channel type.

To determine the settings of the various units, the following measurements were made. Firstly, pulse height distributions were obtained with the monitor for the five beams from the Cs^{137} source. A $\frac{3}{8}$ in. diameter aperture was used in front of the monitor plastic scintillator and the distributions were obtained for three monitor positions: foil position (i.e. centre of scattering chamber), counter position (i.e. the position that the counter would occupy when set to 0^{o}) and furthest back position (i.e. with the monitor plastic scintillator in a position approximately 1 in. up the monitor inlet tube to the scattering chamber). As the monitor moved from position one to two to three, the maxima of the pulse height distributions moved to higher voltages (indicating a slightly higher mean energy of the electrons being counted) and the areas under the pulse height distribution curves decreased (indicating that the beam was spreading out). For the line electrons, of course, only the second change was observed. The pulse height distributions for the 625 keV (line) electrons and the 195-295 keV electrons are shown in Fig. 7.2. It was decided to use the counting rate of the monitor in the furthest back position with the monitor pulse height analyser channel set on the maximum of the pulse height distribution <u>for the furthest back position</u> as a measure of the intensity of the electron beam at the <u>foil</u> position. Thus in monitoring the 195-275 keV electrons, the monitor pulse

Fig. 7.2. Variation of pulse height distributions with monitor positions (as indicated) for (a) 195-295 keV electrons – energy range 3 – and (b) 625 keV electrons – energy range 5. Aperture diameter = $\frac{3}{8}$ in.

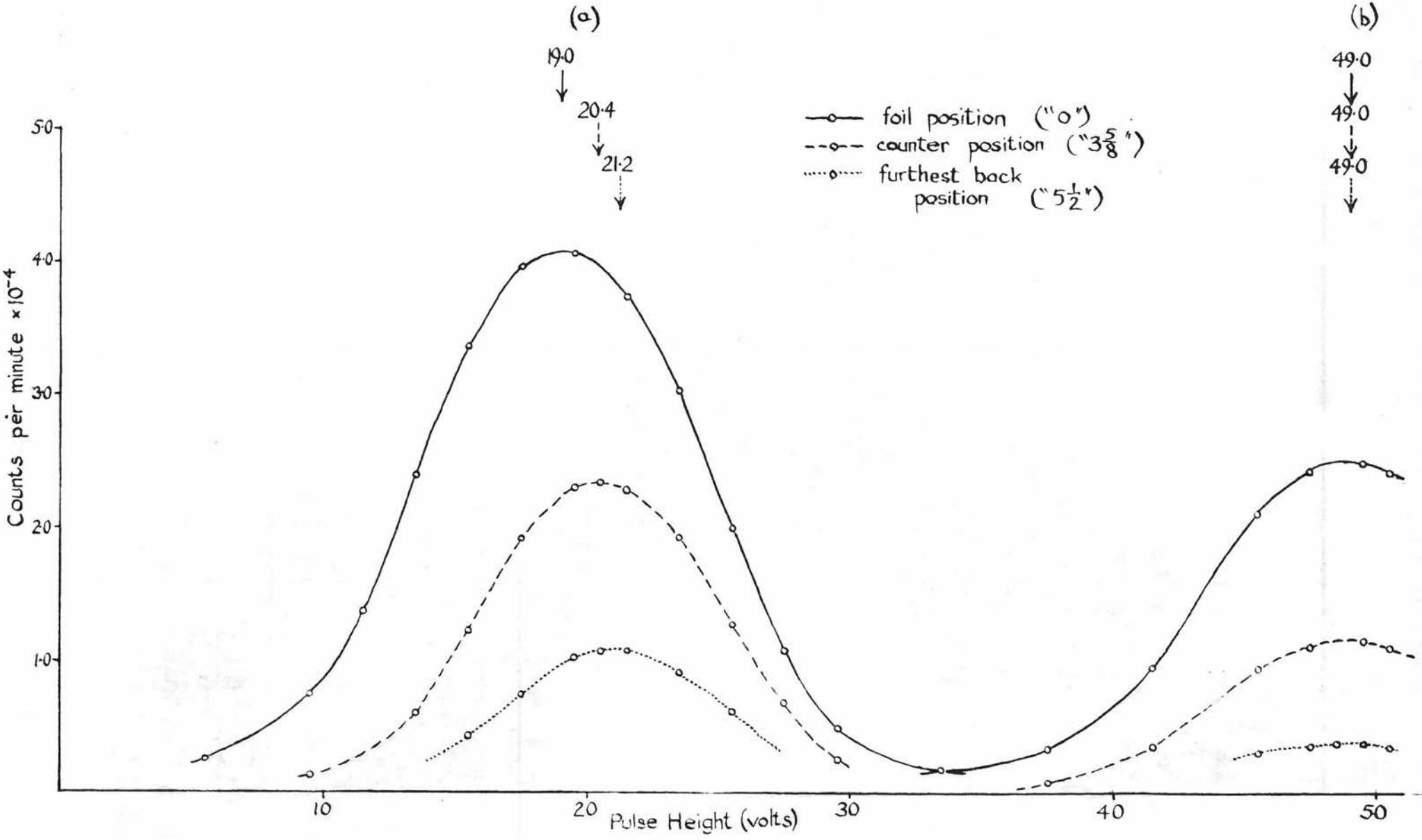

height analyser channel was 19-22 volts.

With the monitor still in the furthest back position, the counter (also with a $\frac{3}{8}$ in. diameter aperture in front of the plastic scintillator) was set in the 0^{o} position. By adjusting various voltages, the maximum of the pulse height distribution for the lowest energy (80-145 keV) electrons was made to occur at the same voltage setting on the counter pulse height analyser as on the monitor analyser when the monitor was in the counter position. Keeping the counter electronics settings fixed, the pulse height distributions for the electron beams of higher energies were measured. The maxima of the counter pulse height distributions were at higher voltages than the maxima of the monitor distributions for the three beams of higher energy electrons (Fig. 7.3). Allowance was made for this when setting the counter electronics for scattering measurements. Thus for the 195-295 keV electrons, the monitor maximum voltage is 20.4 volts while the counter maximum is 22.8 volts (Fig. 7.3). The monitor voltage of the maximum at the foil position is 19.0 volts (Fig. 7.2). The counter voltage for the foil position, were it possible to put the counter there, would be approximately $22.8 - (20.4 - 19.0) \sim 21$ volts. Now elastically scattered electrons with energies in the range 195-295 keV detected by the counter should give a pulse height distribution with a maximum at this same voltage. The counter pulse height analyser channel

Fig. 7.3. Pulse height distributions for electrons in energy ranges 1-4 (Table 6.1.) as measured by monitor (—o—) and counter (- - x - -). All measurements made at "counter position". Aperture diameters = $\frac{3}{8}$ in

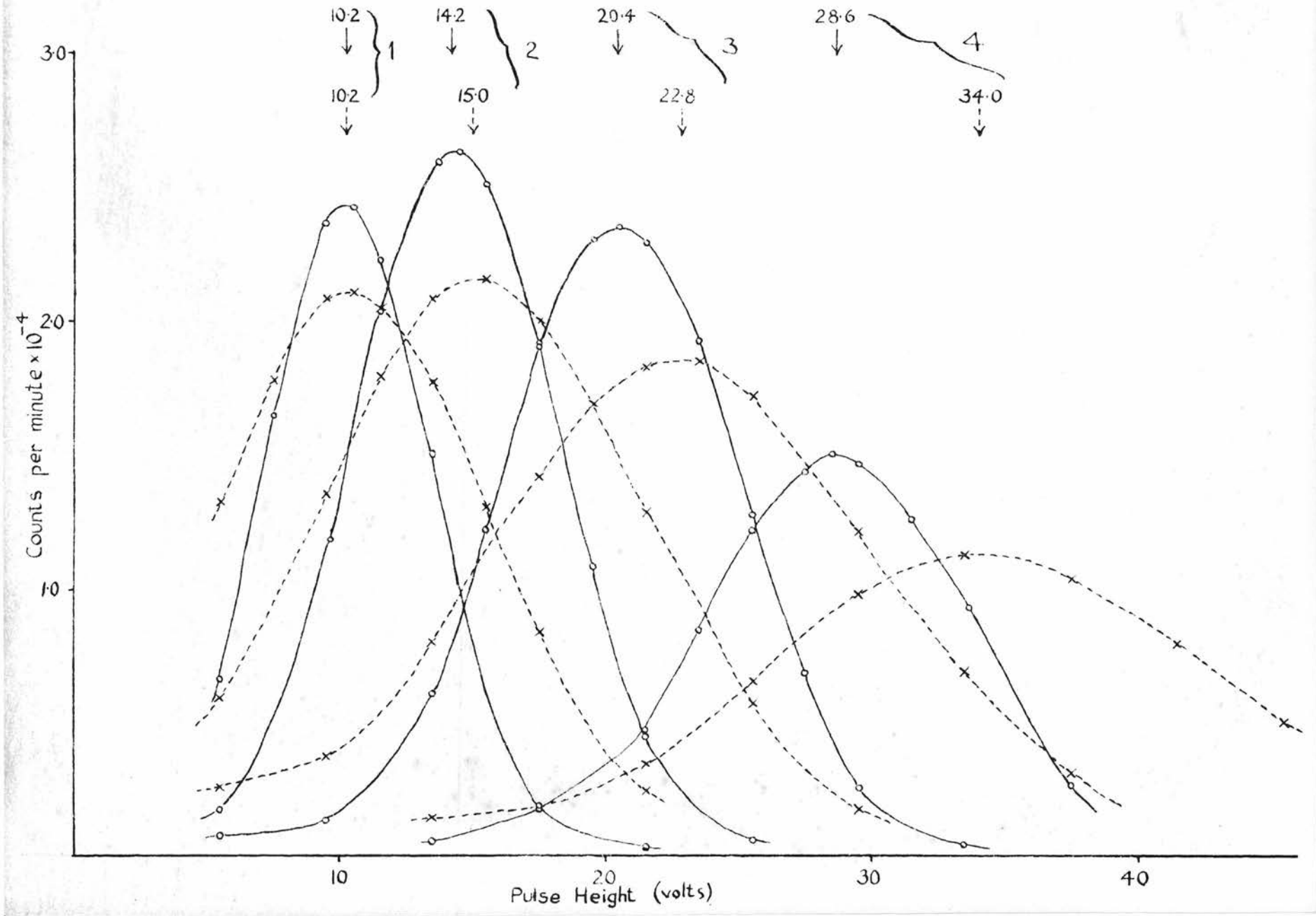

should therefore be centred on 21 volts when counting the scattered 195-295 electrons. The channel chosen was 17-24.5 volts, the width (7.5 volts) being the maximum available from the pulse height analyser used. The analyser could have been used as a discriminator, and all pulses greater than, say, 8 volts counted. It was found that when this was done the relative increase in the background counting rate (i.e. when the incident beam passed through the blank in the foil holder) was much greater than the relative increase in the total counting rate (i.e. when the foil was in position). To avoid the higher background counting rate, therefore, a 7.5 volt channel was used for all the measurements of the scattered electrons except for those with the 625 keV line electrons. For these, all pulses greater than 50 volts were counted. An additional benefit of counting pulses corresponding to the maximum of the distribution produced by the elastically scattered electrons was that virtually all those pulses produced by electrons suffering (inelastic) electron-electron (or Møller) scattering would lie outside the chosen channel and so would not be counted.

Stability of the Incident Beam

The stability of the incident electron beam was determined by the stability of the focussing currents I1 and I2. The counting rate from the monitor was used mainly as a check for accidents, such as source coming off the source stud, scattering foil breaking, scattering

foil holder slipping, etc. For the lower current settings, the current stabiliser coped adequately (see Appendix 4) with fluctuations in the mains voltage supply to the rectifier. For the higher current settings a close watch had to be kept on the readings on the ammeters A1 and A2 which gave the values of I1 and I2. Fortunately, the currents for optimum focussing conditions were, with one exception (I1 for the 625 keV electrons), always very close to values corresponding to whole numbers of divisions on the ammeter scales. The currents actually used where those given by whole numbers of divisions (with the one exception given above, where an ammeter setting mid-way between two scale divisions was used). Because of this, it was very easy to notice very slight changes in the ammeter needle positions and to re-set the currents by adjusting the appropriate control rheostats. Actually, except for certain times of day (e.g. noon) the mains supply voltage was extremely stable and it is unlikely that current variations of more than $\pm\frac{1}{2}\%$ occurred while scattering measurements were being made.

Numerical Data

The values of the counting rates for the various energy ranges, foil thicknesses (τ) and scattering angles ($\ominus$) used are given in Table 7.2.

τ (mgm. cm^{-2})	Θ 20°	30°	45°	65°	Mean electron energy (keV)
0.24	3132 ± 19	837 ± 7	239 ± 8	74 ± 2	112
0.48	4085 ± 28	1498 ± 12	443 ± 9	142 ± 5	
0.72	4230 ± 22	1766 ± 13	581 ± 9	209 ± 6	
0.96	4027 ± 28	1933 ± 20	726 ± 10	251 ± 8	
1.22	3284 ± 25	2012 ± 13	952 ± 14	362 ± 5	
1.55	2593 ± 23	1837 ± 15	1064 ± 17	431 ± 8	
0.24	2457 ± 17	585 ± 6	150 ± 4	49.5 ± 1.5	163
0.48	4027 ± 27	1172 ± 9	309 ± 6	95 ± 2	
0.72	4527 ± 22	1481 ± 10	400 ± 3	141 ± 5	
0.96	4730 ± 29	1731 ± 18	537 ± 8	168 ± 5	
1.22	4161 ± 28	2039 ± 13	760 ± 11	273 ± 5	
1.55	3416 ± 26	2129 ± 15	978 ± 14	358 ± 6	
0.24	1384 ± 12	296 ± 9	67 ± 2	24 ± 1	246
0.48	2571 ± 21	599 ± 6	134 ± 3	43 ± 1.5	
0.72	3257 ± 18	801 ± 8	179 ± 4	62 ± 1.5	
0.96	3443 ± 24	1037 ± 11	237 ± 4	75 ± 2	
1.22	3912 ± 27	1322 ± 10	398 ± 7	117 ± 3	
1.55	3714 ± 25	1729 ± 13	589 ± 9	187 ± 4	
0.24	456 ± 4	82 ± 1	20.4 ± 0.6	6.3 ± 0.4	342
0.48	910 ± 11	172 ± 3	39.5 ± 1	12.7 ± 0.5	
0.72	1204 ± 11	256 ± 2	59.5 ± 2	18.6 ± 1.0	
0.96	1485 ± 13	340 ± 4	67 ± 2	21.5 ± 1.0	
1.22	1959 ± 19	518 ± 5	120 ± 3	34 ± 1	
1.55	2219 ± 19	729 ± 7	191 ± 4	51 ± 2	
0.48	-	90 ± 2	-	5.4 ± 0.2	625
0.72	-	131 ± 3	-	8.0 ± 0.4	
0.96	-	165 ± 4	-	10.4 ± 0.4	
1.22	-	273 ± 4	-	13.6 ± 0.6	
1.55	-	441 ± 5	-	22.4 ± 0.7	

TABLE 7.2. Values of electron scattering counting rates (counts per min.) for various electron energies, foil thicknesses τ and scattering angles Θ.

CHAPTER 8

RESULTS AND CONCLUSIONS

Introduction

It is shown in Appendix 2 that if N_i electrons are incident per second on a scattering foil of area A_1 containing n nuclei per unit area, then N_S, the number of electrons scattered once by a nucleus through a mean angle Θ into a solid angle Ω_2, may be written

$$N_S = N_i \times A_1 n \times \bar{\sigma}_N(\Theta) \times \Omega_2 \text{ per second}$$
$$= N_i \times A_1 \alpha \tau \times \bar{\sigma}_N(\Theta) \times \Omega_2 \text{ per second} \qquad (8.1)$$

where n is proportional to τ, the thickness of the scattering foil, and α is constant for a given scattering material. In practice, equation (8.1) does not hold because electrons are counted which are scattered more than once (i.e. suffer multiple scattering) during their passage through the scattering foil. To allow for this, N_S', the number of electrons counted per second, may be written

$$N_S' = N_S \times f(\Theta, E, \tau) \qquad (8.2)$$

where E is the mean energy of the electrons being scattered. Equations (8.1) and (8.2) can be combined to give

$$\frac{N_S'}{\tau} = N_1 A_1 a \bar{\sigma}_N(\Theta) \Omega_2 \times f(\Theta, E, \tau)$$

$$= \text{constant} \times \bar{\sigma}_N(\Theta) \times f(\Theta, E, \tau) \qquad (8.3)$$

In the measurements described in the previous chapter N_1, a and Ω_2 were all constant for a given range of energies in a beam of incident electrons. N_1 was constant within the limits of the setting and the stability of the focussing currents I1 and I2. a is constant for a given scattering material (see Appendix 2), and gold was used throughout. Ω_2 was the solid angle subtended at the centre of the scattering chamber by the constant area of the counter detector which was at a fixed radial distance from the centre of the chamber. The values of N_S' being known for given E and τ at two scattering angles Θ_1 and Θ_2, it follows from equation (8.3) that

$$\frac{N_S'(\Theta_2)}{N_S'(\Theta_1)} = \frac{\bar{\sigma}_N(\Theta_2)}{\bar{\sigma}_N(\Theta_1)} \times \frac{f(\Theta_2, E, \tau)}{f(\Theta_1, E, \tau)} \qquad (8.4)$$

The ratio of cross sections $\bar{\sigma}_N(\Theta_2)/\bar{\sigma}_N(\Theta_1)$ can be found from the measured values of N_S' using equation (8.4), provided the function $f(\Theta, E, \tau)$ is known.

$f(\Theta, E, \tau)$ is, however, so complicated a function that its derivation is usually carried out with certain approximations. For example, Chase and Cox (Chase and Cox, 1940) showed that it could be expressed

$$f(\Theta, E, \tau) = 1 + \varepsilon^2(\operatorname{cosec}^2 \frac{\Theta}{2} - \tfrac{1}{2}) \qquad (8.5)$$

where ε^2 is the "mean square deflection of electrons having a mean length of path in the foil equal to that of the electrons deflected at the angle Θ from the direction of incidence". Chase and Cox's approximation in deriving (8.5) was that τ was sufficiently small for it to be possible to neglect terms involving powers of ε above the second. (It is well established experimentally that if a parallel beam of electrons passes through an "absorber" - a foil, say - then the emerging beam is divergent, and the divergence increases with the thickness of the absorber). The dependence of ε on E and τ was investigated theoretically by Williams (Williams, 1939 and 1940; in summarised form - Kulchitsky and Latyshev, 1942). Very approximately, ε^2 was found to be proportional to τ for a given value of E.

However, as $\tau \to 0$, $\varepsilon^2 \to 0$ and $f(\Theta, E, \tau) \to 1$. If foils of several thicknesses are available, it is unnecessary to know an expression for $f(\Theta, E, \tau)$. Instead, a limiting value of, say, N_S'/τ as $\tau \to 0$ will provide a value proportional to $\tilde{\sigma}_N(\Theta)$ - see equation (8.3) - and this limiting value can be obtained by extrapolation from measured values of N_S'/τ plotted against τ or some function of τ. This was, for example, the method used by Spiegel and others in arriving at values of absolute electron-nuclear scattering cross sections (Spiegel et al., 1959).

It was decided to use the extrapolation method to find limiting values of N_S'/τ . From these limiting values, $\bar{\sigma}_N(\Theta_2)/\bar{\sigma}_N(\Theta_1)$ could be found from equation (8.4) with $f(\Theta_2, E, \tau) \equiv f(\Theta_1, E, \tau) \equiv 1$. Values of N_S'/τ (Table 8.1) were calculated from the experimental data given in Table 7.2. From the values of N_S'/τ , however, it is clear that the Chase and Cox correction factor cannot be applied to approximately half of them because they <u>decrease</u>, as τ increases, for lower energies and lower scattering angles. From the above discussion, N_S'/τ ought to <u>increase</u> as τ increases. It was felt that this difference in behaviour might be caused by the values of τ used being too large, in which case the Chase and Cox correction would be invalid or insufficient. More consideration was therefore given to the properties of multiple scattering.

<u>Properties of Multiple Scattering</u>

Suppose that electrons are scattered from a thick foil and that the deflection of each electron from its incident direction is the resultant of a large number of small deflections due to a large number of collision processes. The problem of finding the resultant distribution of electrons, with respect to angle, is essentially statistical and the distribution is, to a good approximation, Gaussian (Williams, 1939 and 1940).

τ (mgm. cm^{-2})	Θ 20°	30°	45°	65°	E (keV)
0.24	13050 ± 70	3490 ± 30	995 ± 30	308 ± 8	112
0.48	8510 ± 60	3120 ± 25	925 ± 20	296 ± 5	
0.72	5880 ± 30	2455 ± 20	805 ± 15	290 ± 6	
0.96	4200 ± 30	2015 ± 15	755 ± 10	262 ± 8	
1.22	2690 ± 20	1650 ± 15	780 ± 10	297 ± 5	
1.55	1670 ± 15	1185 ± 10	685 ± 10	278 ± 5	
0.24	10240 ± 70	2440 ± 25	625 ± 15	206 ± 6	163
0.48	8390 ± 60	2440 ± 20	645 ± 15	198 ± 4	
0.72	6290 ± 30	2055 ± 15	555 ± 5	196 ± 7	
0.96	4425 ± 25	1805 ± 20	560 ± 10	175 ± 5	
1.22	3410 ± 25	1670 ± 10	620 ± 10	224 ± 4	
1.55	2205 ± 20	1375 ± 10	630 ± 10	231 ± 4	
0.24	5770 ± 50	1235 ± 35	280 ± 10	100 ± 4	246
0.48	5355 ± 45	1250 ± 15	280 ± 5	90 ± 3	
0.72	4525 ± 25	1115 ± 10	250 ± 5	86 ± 2	
0.96	3580 ± 25	1080 ± 10	250 ± 5	78 ± 2	
1.22	3210 ± 20	1085 ± 10	325 ± 5	96 ± 2.5	
1.55	2395 ± 15	1115 ± 10	380 ± 5	121 ± 2.5	
0.24	1900 ± 15	342 ± 4	85 ± 2.5	26 ± 1.5	342
0.48	1895 ± 20	358 ± 6	82 ± 2	26.5 ± 1	
0.72	1675 ± 15	356 ± 3	83 ± 3	26 ± 1.5	
0.96	1550 ± 15	354 ± 4	70 ± 2	22.5 ± 1	
1.22	1610 ± 15	425 ± 4	98 ± 2.5	28 ± 1	
1.55	1430 ± 10	470 ± 5	123 ± 2.5	33 ± 1.5	
0.48	-	187 ± 4	-	11.2 ± 0.8	625
0.72	-	182 ± 4	-	11.1 ± 0.5	
0.96	-	172 ± 4	-	10.8 ± 0.4	
1.22	-	224 ± 3	-	11.1 ± 0.4	
1.55	-	285 ± 3	-	14.5 ± 0.5	

TABLE 8.1. Values of N'_s/τ for various mean electron energies E, scattering angles Θ and foil thicknesses τ.

The probability of scattering into a solid angle $d\Omega$ about a direction Θ relative to the direction of incidence may be written:

$$P(\Theta)d\Omega = \frac{1}{2\pi\varepsilon^2} \exp(-\Theta^2/2\varepsilon^2)d\Omega \qquad (8.6)$$

where $P(\Theta)$ is the expression for a Gaussian distribution in two dimensions. As before, ε^2 is the mean square deflection. The counting rate G at an angle Θ will be proportional to $P(\Theta)$:

$$G = \frac{\text{constant}}{2\pi\varepsilon^2} \exp(-\Theta^2/2\varepsilon^2) \qquad (8.7)$$

and the counting rate per unit foil thickness will be

$$\frac{G}{\tau} = \frac{\text{constant}}{2\pi\varepsilon^2\tau} \exp(-\Theta^2/2\varepsilon^2) \qquad (8.8)$$

To obtain an idea of how G/τ depends on τ, the approximate substitution $\varepsilon^2 = k\tau$ where k is a constant (see page 59) can be used. Then

$$\frac{G}{\tau} = \frac{\text{constant}}{2\pi k\tau^2} \exp(-\Theta^2/2k\tau) = F(\tfrac{1}{\tau}) \qquad (8.9)$$

As $1/\tau \to 0$ and as $1/\tau \to \infty$, $G/\tau = F(1/\tau) \to 0$; and G/τ has a maximum value at $\Theta^2 = 4k\tau = 4\varepsilon^2$, or $\Theta = 2\varepsilon$.

In practice, the distribution of the scattered electrons will not behave as above for the two limiting situations. As $1/\tau \to \infty$, the number of collisions suffered by the scattered electrons will become so few that the statistical treatment will become invalid. The

distribution will tend to the distribution for single scattering of electrons. As $1/\tau \to 0$, energy losses by electrons during their passage through the foil mean that if the detection system is sensitive to electrons of a given energy or energy range, then the counting rate, G', will decrease more quickly than G, as τ increases. These properties are shown in Fig. 8.1.

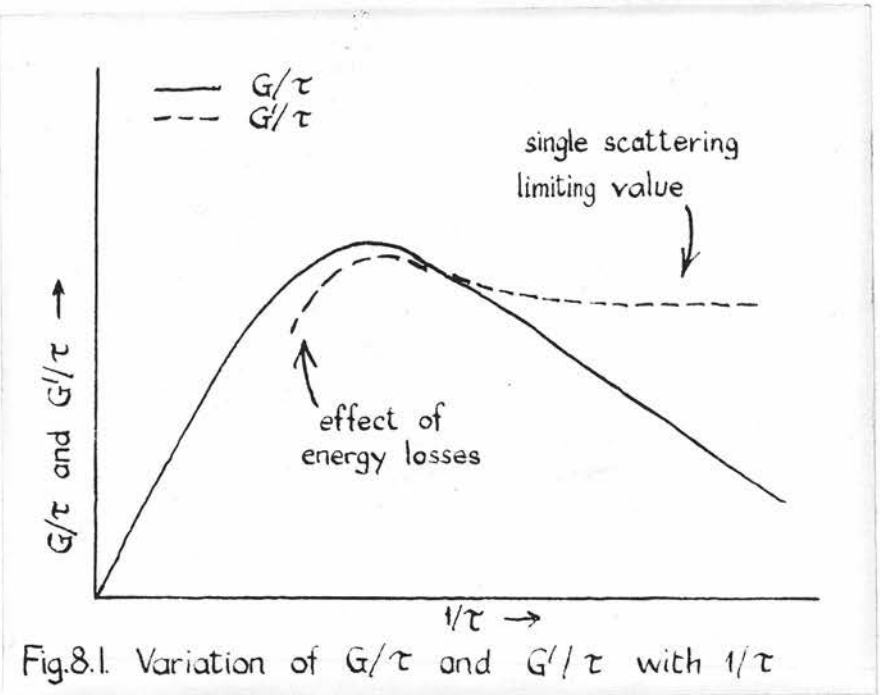

Fig.8.1. Variation of G/τ and G'/τ with $1/\tau$

Results.

The values of N_S'/τ were plotted as functions of $1/\tau$, see Figs. 8.2 - 8.5, for the energy ranges and scattering angles used. The curves drawn through the various sets of points are those that seemed, to the

Fig. 8.2. Variation of counts per minute per unit foil thickness with $1/\tau$ where τ = foil thickness in mgm. cm.$^{-2}$ Mean electron energies as indicated. Errors are counting errors only.

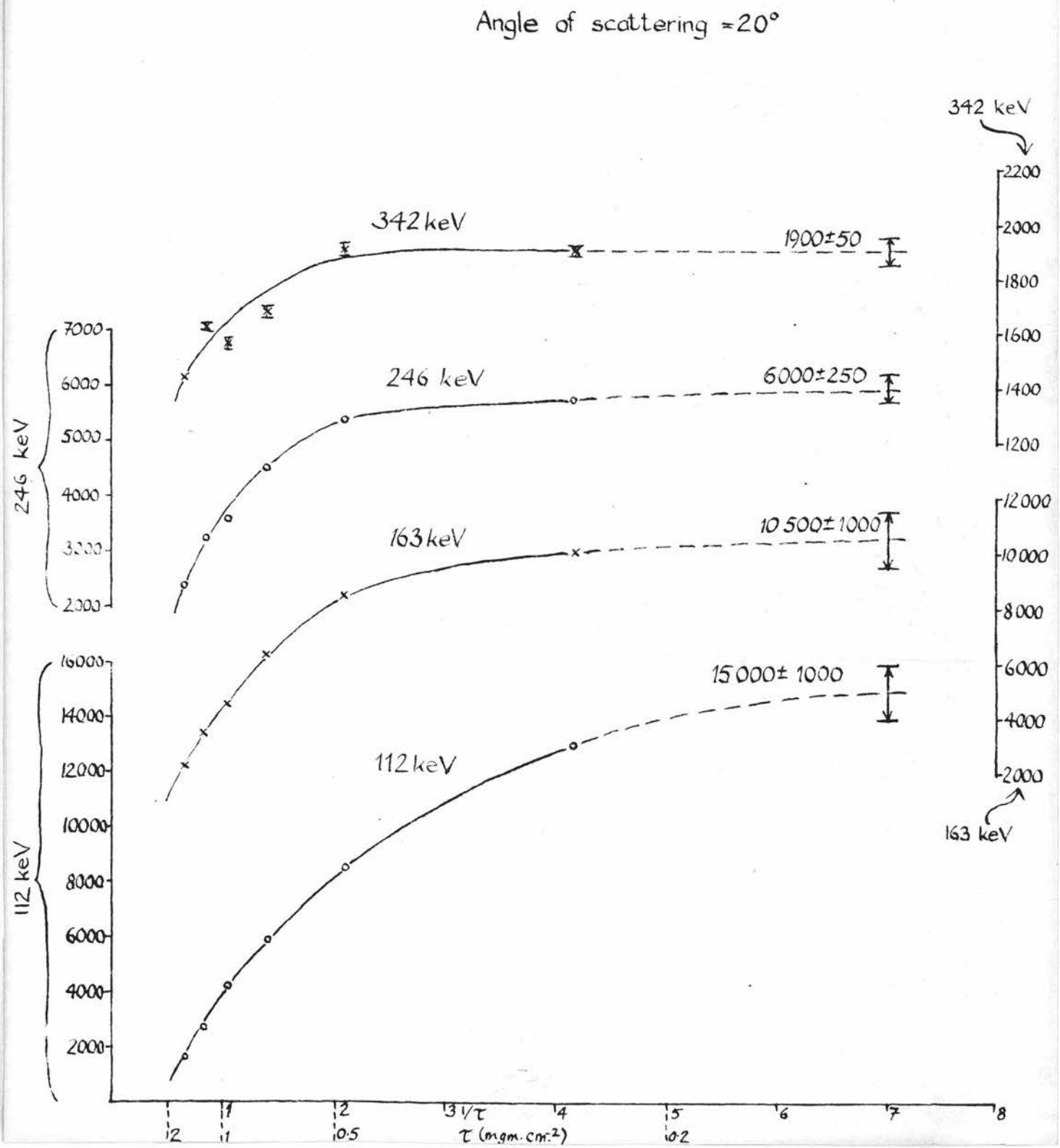

Fig. 8.3. Variation of counts per minute per unit foil thickness with $1/\tau$ where τ = foil thickness in mgm.cm.$^{-2}$ Mean electron energies as indicated. Errors are counting errors only.

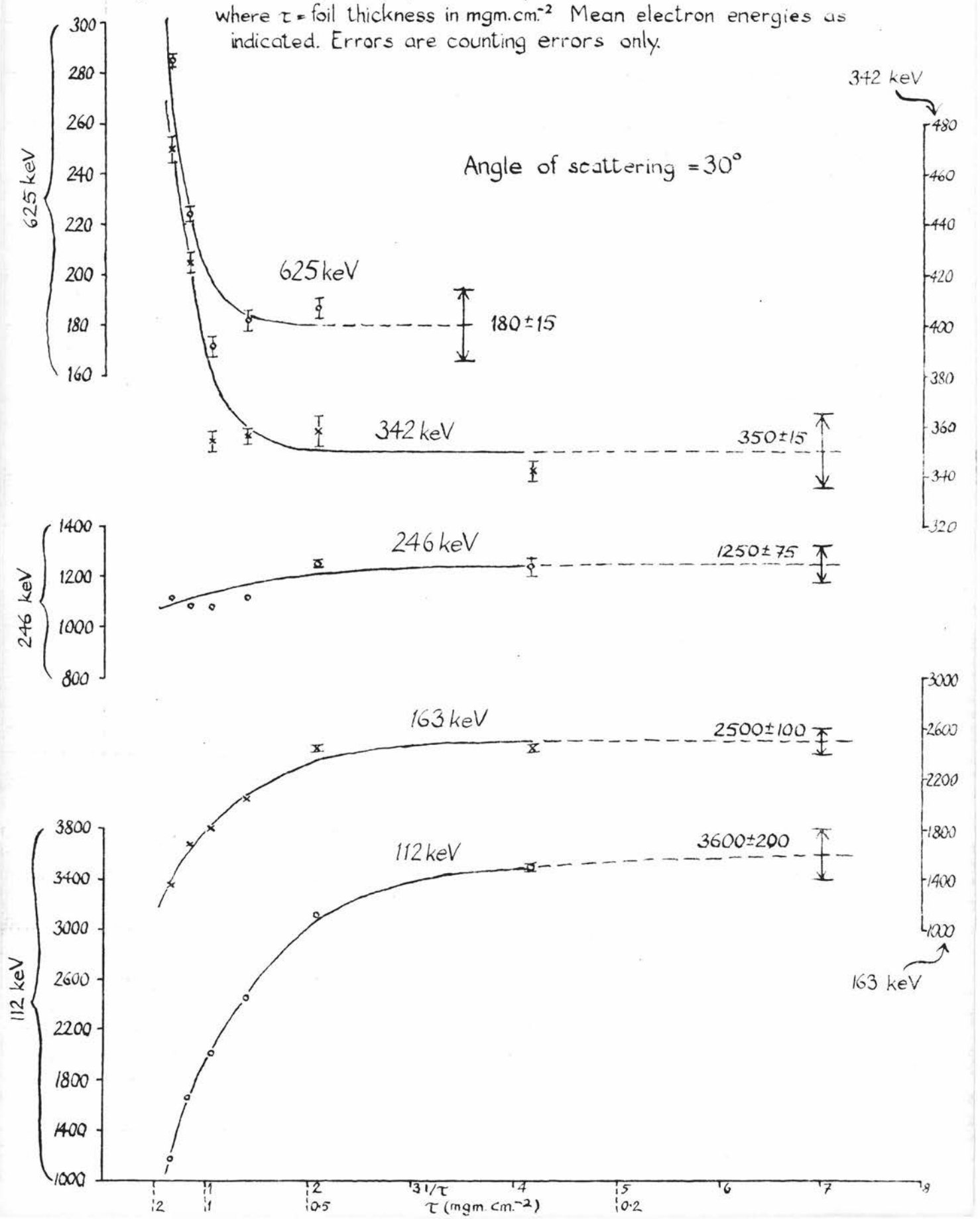

eye, to fit the points best. These curves may be interpreted as being different parts of the curve for G'/τ (Fig. 8.1), depending on the energy and scattering angle. With the exception of the curve for 112 keV electrons being scattered through 20°, limiting values as $1/\tau \rightarrow \infty$ (i.e. $\tau \rightarrow 0$ and the distribution becomes more and more of the single scattering type) are clearly indicated. This is especially true where N_S'/τ <u>decreases</u> to its limiting value as $1/\tau \rightarrow \infty$ (higher energies, higher scattering angles). For those cases where N_S'/τ <u>rises</u> to its limiting value, then (see Fig. 8.1) either the maximum values of N_S'/τ are not noticeably greater than the single scattering values or the smallest value of τ was too large for the decrease from the maximum to the single scattering values of N_S'/τ to be observed. Thus the limiting values of the curves (inserted, in Figs. 8.2 - 8.5, at the right hand ends of each curve) are either equal to or greater than the single scattering values. The errors assigned to these limiting values were chosen to be compatible with the counting errors of the plotted points (when these errors were large enough to be shown) and the scatter of the points about the curve through them.

These single scattering values of N_S'/τ are listed in Table 8.2. Ratios of electron-nuclear scattering cross sections have been calculated from them and these ratios are given in Table 8.3.

Mean energy (keV) \ Scattering angle	20°	30°	45°	65°
112	15000 ± 1000	3600 ± 200	1000 ± 50	305 ± 15
163	10500 ± 1000	2500 ± 100	600 ± 50	200 ± 15
246	6000 ± 250	1250 ± 75	275 ± 25	90 ± 15
342	1900 ± 50	350 ± 15	82 ± 6	26 ± 2
625	-	180 ± 15	-	11 ± 1

TABLE 8.2. Limiting values of N'_S/τ (no. of electrons scattered per minute per unit foil thickness).

Mean energy (keV) \ Cross section ratio	$\frac{\sigma_N^-(45°)}{\sigma_N^-(65°)}$	$\frac{\sigma_N^-(30°)}{\sigma_N^-(65°)}$	$\frac{\sigma_N^-(20°)}{\sigma_N^-(65°)}$
112	3.3 ± 0.2	12 ± 1	49 ± 4
163	3.0 ± 0.3	12.5 ± 1	53 ± 6
246	3.1 ± 0.4	14 ± 2.5	67 ± 12
342	3.2 ± 0.3	13.5 ± 1	73 ± 6
625	-	16.5 ± 2	-

TABLE 8.3. Experimental values of the ratios of electron-nuclear scattering cross sections investigated.

The experimental and the theoretical values of the ratios of cross sections measured are plotted in Figs. 8.6 - 8.8. The experimental values of the electron-nuclear scattering cross section ratios are in good agreement with the theoretical values (with no screening allowed for) for scattering angles of 45° and 65°. Discrepancies appear when the smaller scattering angle has the values 30° and 20°.

Discussion

That the agreement between the experimental cross section ratios and the theoretical curve plotted in Fig. 8.8 is good suggests that the extrapolated values N_S'/τ for $\Theta = 65^{\circ}$ and $\Theta = 45^{\circ}$ are not greatly different from what might be expected theoretically, at least for energies in the range $\sim$100 keV to $\sim$400 keV. It follows, therefore, that the discrepancies between theory and experiment indicated by Figs. 8.7 and 8.6 are introduced by the extrapolated values of N_S'/τ for $\Theta = 30^{\circ}$ and $\Theta = 20^{\circ}$.

There are two such discrepancies. The first one is the difference between the general trend of the theoretical curves and the trend suggested by the experimental values. As the energy decreases from $\sim$400 keV, the theoretical curve firstly remains approximately constant then increases. The experimental points suggest that (a) as energy decreases, the value of

Fig. 8.6. Comparison between theoretical and experimental values of ϱ

—o— $\varrho = \sigma_N^-(20°, E, 79) / \sigma_N^-(65°, E, 79)$ – Mott theory – no screening

– – – $\sigma_R(20°, E, 79) / \sigma_R(65°, E, 79) = 91{\cdot}7$ – Rutherford theory

I experimental values for angles of scattering of 20° and 65°

× above experimental values corrected for range of scattering angles.

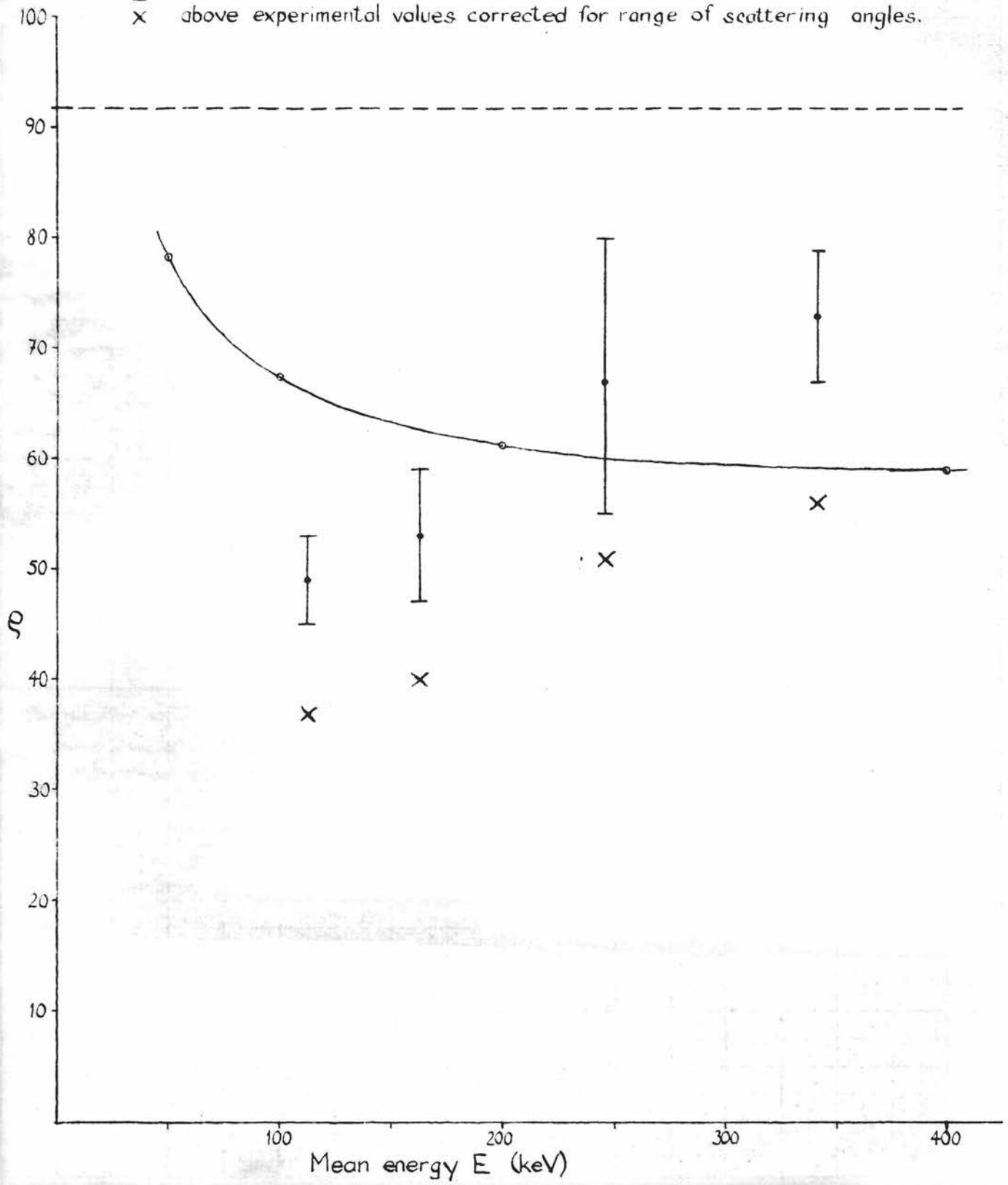

Fig. 8.7. Comparison between theoretical and experimental values of ϱ

—o— $\varrho = \bar{\sigma_N}(30°, E, 79) / \bar{\sigma_N}(65°, E, 79)$ - Mott theory - no screening.

– – – $\bar{\sigma_R}(30°, E, 79) / \bar{\sigma_R}(65°, E, 79) = 18{\cdot}6$ - Rutherford theory.

I experimental values for angles of scattering of 30° and 65°.

× above experimental values corrected for range of scattering angles.

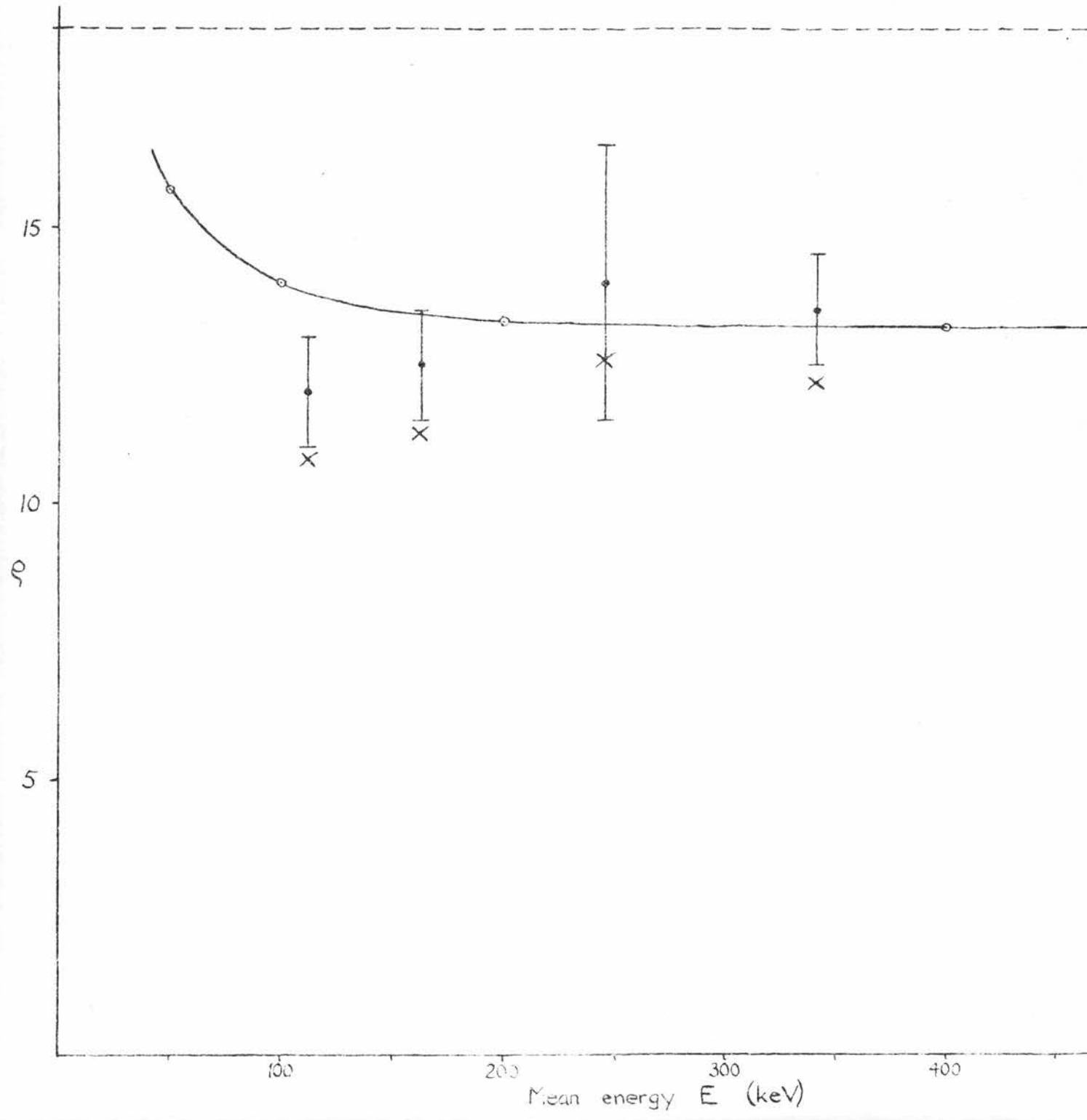

Fig. 8.8 .Comparison between theoretical and experimental values of ϱ

—o— $\varrho = \bar{\sigma_N}(45°, E, 79) / \bar{\sigma_N}(65°, E, 79)$ – Mott theory – no screening.

– – – $\sigma_R(45°, E, 79) / \sigma_R(65°, E, 79) = 3{\cdot}89$ – Rutherford theory.

I experimental values for angles of scattering of 45° and 65°.

× above experimental values corrected for range of scattering angles.

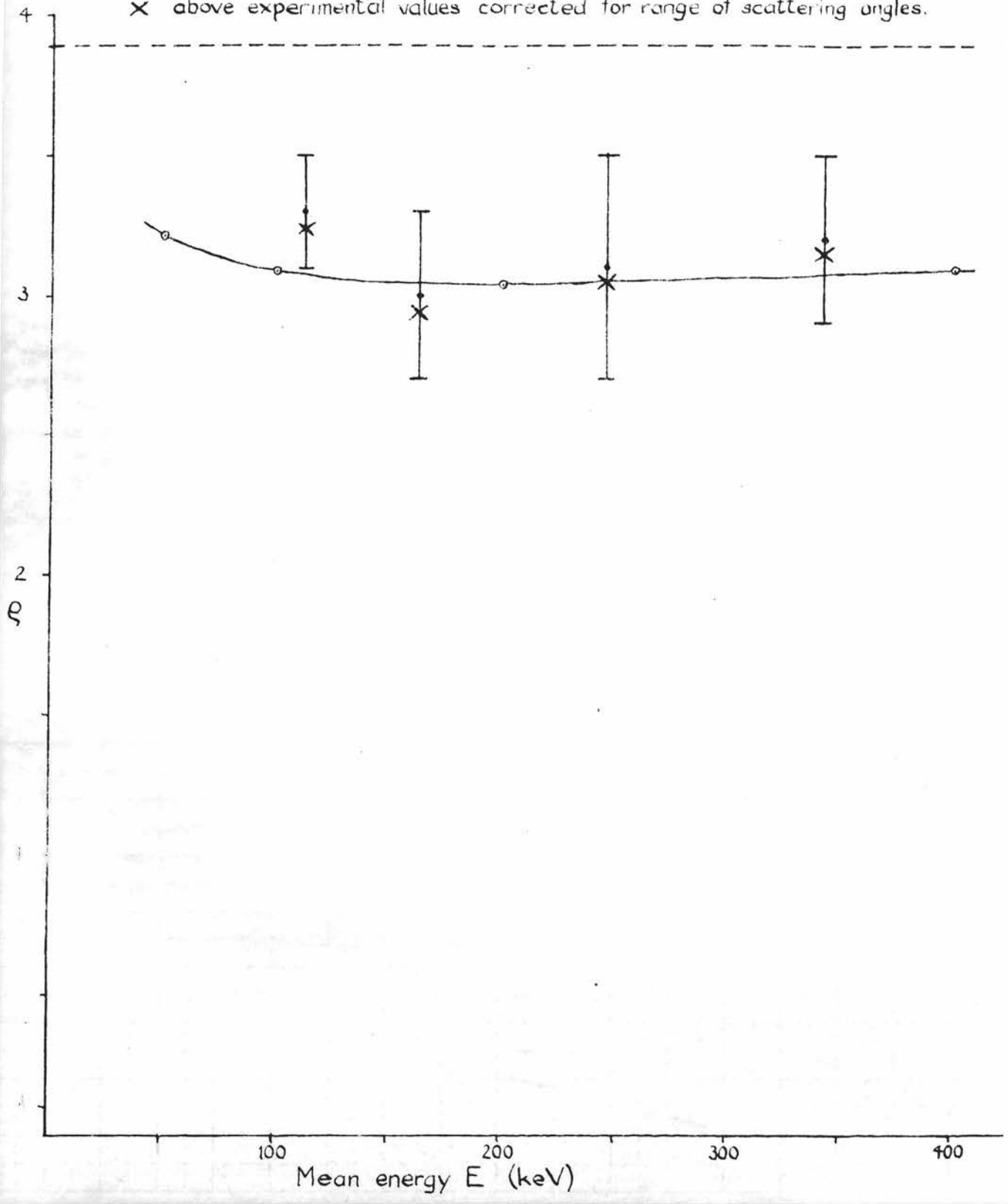

$\sigma_N^-(30^\circ)/\sigma_N^-(65^\circ)$ is firstly constant and then decreases and (b) as energy decreases, the value of $\sigma_N^-(20^\circ)/\sigma_N^-(65^\circ)$ decreases. The 625 keV value of $\sigma_N^-(30^\circ)/\sigma_N^-(65^\circ)$ is not, at the moment, being considered. The second discrepancy is that it seems that the differences between theory and experiment are not consistent, especially for the $\sigma_N^-(20^\circ)/\sigma_N^-(65^\circ)$ measurements. Here, the measured cross section ratios are too high at the higher energies and too low at the lower.

Unless the interpretation of the measurements and the extrapolation process described earlier are seriously in error, the first discrepancy described in the previous paragraph cannot be easily explained except in terms of a screening effect. If this explanation of the first discrepancy is accepted, then the second discrepancy is an indication that the experimental points are still all too large. This, however, is quite reasonable. The counter detector accepts a large range of scattering angles, approximately 10 degrees (Table 7.1, page 50). Over such a range of scattering angle the electron-nuclear cross section varies approximately as the Rutherford cross section, i.e. as $\text{cosec}^4 \frac{\Theta}{2}$ where Θ is the angle of scattering. Because of the rapid variation of $\text{cosec} \frac{\Theta}{2}$ with Θ, particularly at smaller values of Θ, the mean value of $\text{cosec}^4 \frac{\Theta}{2}$ over the range

$\Theta' \pm \Phi$ (i.e. $\frac{1}{2\Phi}\int_{\Theta'-\Phi}^{\Theta'+\Phi} \mathrm{cosec}^4 \frac{\Theta}{2}\, d\Theta = A(\Theta')$) is not equal to $\mathrm{cosec}^4 \frac{\Theta'}{2}$. Values of $A(\Theta')$ and $\mathrm{cosec}^4 \frac{\Theta'}{2}$ were calculated for $\Theta' = 20^\circ$, 30°, 45° and 65° and $\Phi = 5^\circ$. The ratios $A(\Theta')/\mathrm{cosec}^4 \frac{\Theta'}{2}$ (Table 8.4), are estimates of by how much the observed counting rates can be too large. The ratios $\left(A(\Theta')/\mathrm{cosec}^4 \frac{\Theta'}{2}\right) \Big/ \left(A(65^\circ)/\mathrm{cosec}^4 \frac{65^\circ}{2}\right)$ are estimates of by how much the plotted experimental points in Figs. 8.6 to 8.8 can be higher than the values given by the theoretical curve.

Θ'	$A(\Theta')$	$\mathrm{cosec}^4 \frac{\Theta'}{2}$	$\frac{A(\Theta')}{\mathrm{cosec}^4 \frac{\Theta'}{2}}$	$\frac{A(\Theta')}{\mathrm{cosec}^4 \frac{\Theta'}{2}} \Big/ \frac{A(65^\circ)}{\mathrm{cosec}^4 \frac{65^\circ}{2}}$
20°	1415	1100	1.29	1.24
30°	253	223	1.14	1.10
45°	50	47	1.06	1.02
65°	12.5	12	1.04	1

TABLE 8.4. Values of $A(\Theta')$, $\mathrm{cosec}^4 \frac{\Theta'}{2}$ and various ratios of them (see text).

These estimates are only approximate. The assumed spread in scattering angle ($\pm 5^\circ$) is that determined by the geometry of the apparatus. This, however, was considered good enough for an order of magnitude

calculation. The dependence of $(A(\Theta')/\text{cosec}^4 \frac{\Theta'}{2})/(A(65^\circ)/\text{cosec}^4 \frac{65^\circ}{2})$ on Θ is shown in Fig. 8.9. It

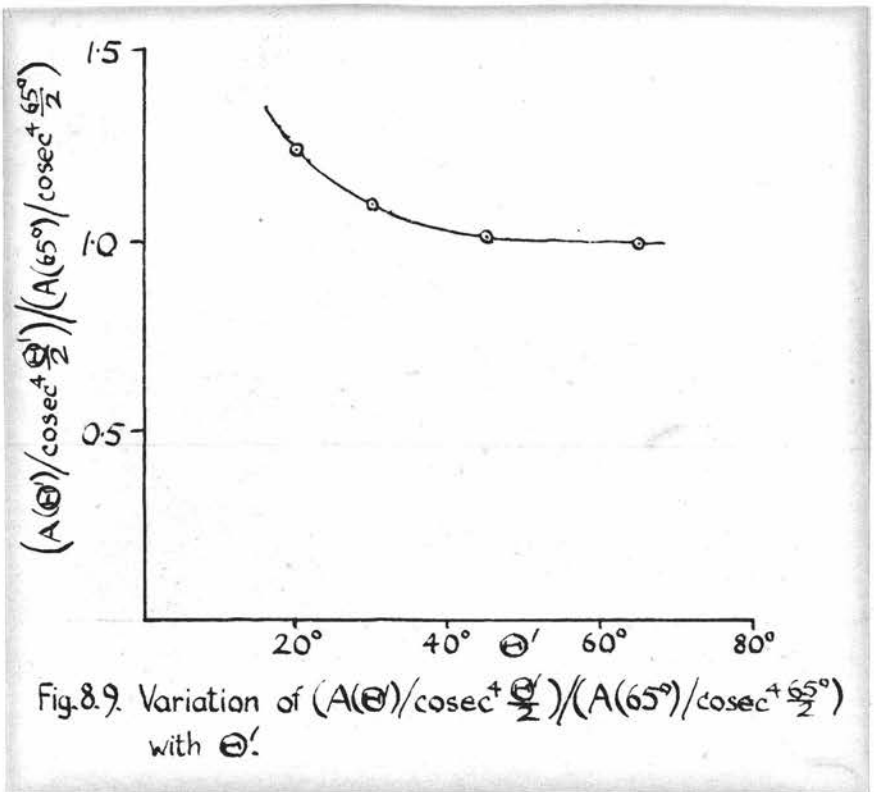

Fig. 8.9. Variation of $(A(\Theta')/\text{cosec}^4 \frac{\Theta'}{2})/(A(65^\circ)/\text{cosec}^4 \frac{65^\circ}{2})$ with Θ'.

was used to "correct" the experimental cross section ratios. The corrected ratios are denoted by crosses in Figs. 8.6 - 8.8. For clarity, the error limits are not repeated on these points.

This correction does not completely account for the rather high value of the 625 keV point in Fig. 8.7. The limiting values of N'_S/τ for 30° and 625 keV (Fig. 8.3) is doubtful (it is probably too high) because of lack of experimental data. An additional point for $1/\tau \sim 4$ would have helped here. As this limiting value is the numerator of the ratio giving the 625 keV point in Fig.

8.7, this last point is also, probably too high.

Conclusions

Because the thinnest gold foils commercially available are too thick, measurements made with them of electron-nuclear (single) scattering cross section ratios were not very precise because of the effects of multiple scattering. At the lower energies and lower scattering angles, where multiple scattering effects were most noticeable, the experimental ratios may very well be too high, even although they are lower than those predicted by theory. The trends suggested by the experimental points do not always agree with the trends given by scattering theory with no screening allowed for. The observed differences, however, agree qualitatively with the predictions of the available theories of screening (see Chapter 2, page 11). The energies at which these differences appear are higher than those suggested by the simpler theoretical approach to the problem of screening, (Mohr and Tassie, 1954) and so give some support to the approach put forward by van der Spuy (van der Spuy, 1959). The results, however, do not support the suggestion (Spiegel et al., 1959) that screening might be important at energies of the order of a few MeV.

Improved experimental measurements would be possible if absolute electron-nuclear cross sections were measured using beams of monoenergetic electrons and employing energy analysis of the scattered electrons.

It is felt, however, that a precise experimental investigation of the effects of screening requires the availability of scattering foils, of known thicknesses, which are much thinner than those available commercially at the moment. Only then can the difficulties produced by multiple scattering be overcome.

APPENDIX 1

THEORETICAL DATA USED IN THE DESIGN OF THE EXPERIMENT

The relativistic classical (or Rutherford) electron-nuclear scattering cross section, $\sigma_R(\Theta, E, Z)$, may be expressed

$$d\sigma_R(\Theta, E, Z) = \sigma_R(\Theta, E, Z)d\Omega = Z^2\left(\frac{e^2}{m_o c^2}\right)^2\left(\frac{1-\beta^2}{\beta^4}\right)\frac{d\Omega}{(1-\cos\Theta)^2} \qquad (A1.1)$$

where e, m_o, βc and E are the electron charge, rest mass, velocity and energy, respectively, Θ is the scattering angle and Z is the atomic number of the scattering material. The corresponding notation for the relativistic quantum mechanical (or Mott) electron-nuclear scattering cross section - with no screening allowed for - is $\sigma_N(\Theta, E, Z)$.

Tables of Mott scattering cross sections have been published by several authors. Those used here were given by Doggett and Spencer (Doggett and Spencer, 1956) and took the form of values of the ratio $\sigma_N(\Theta, E, Z)/\sigma_R(\Theta, E, Z)$ for various incident electron energies E, scattering angles Θ and scatterer atomic numbers Z. The values of these three parameters for which the ratio was calculated were energies of 0.05, 0.1, 0.2, 0.4, 0.7, 1.0, 2.0, 4.0 and 10.0 MeV,

angles between 0° and 180° inclusive at 15 degree intervals and atomic numbers of 6, 13, 29, 50, 82 and 92. An accuracy of 0.5% or better was claimed for the values of the ratio for the lower energies and smaller scattering angles, which are the ones used here.

The relevant values of the ratio $\sigma_N^-(\Theta, E, Z)/\sigma_R(\Theta, E, Z)$ for gold, $Z = 79$, were obtained by interpolating on plots of the tabulated values as a function of Z for energies of 50, 100, 200, 400, 700 and 1,000 keV inclusive and for scattering angles 15°, 30°, 45°, 60°, 75° and 90°. Firstly, for each energy, a group of six curves was plotted - one for each scattering angle - then, for each scattering angle, a group of six curves was plotted - one for each energy. Thus the curve for each of the thirty-six combinations of energy and scattering angle appeared twice and consequently two interpolated values of $\sigma_N^-(\Theta, E, Z)/\sigma_R(\Theta, E, Z)$ were obtained for $Z = 79$.

When these were not the same (due mainly to difficulties in drawing the curves), it was found fairly easy to arrive at a compromise by closer inspection of the curves. The plotted ratios ranged from ~ 1 to ~ 2, and the interpolated values (Table A1.1) were read to the nearest 0.005. Differences (when they occurred) in the interpolated values ranged from $\sim 0.5\%$ to $\sim 1\%$, so that an uncertainty of $\pm 1\%$ in the interpolated values seems reasonable.

Energy (keV) / Θ	50	100	200	400	700	1000
15°	1.020	1.025	1.045	1.080	1.100	1.115
30°	1.000	1.050	1.145	1.240	1.295	1.320
45°	1.040	1.180	1.335	1.475	1.545	1.575
60°	1.140	1.340	1.540	1.690	1.770	1.805
75°	1.280	1.505	1.700	1.830	1.885	1.900
90°	1.430	1.630	1.780	1.840	1.850	1.865

TABLE A1.1. Values of σ_N^- / σ_R for gold (Z = 79) for various values of energy and Θ. Obtained graphically from data calculated by Doggett and Spencer (Doggett and Spencer, 1956) for other Z values.

It had been noticed that the value of the ratio

$$\rho' = \frac{\sigma_N^-(\Theta_1, E, 79)/\sigma_R(\Theta_1, E, 79)}{\sigma_N^-(\Theta_2, E, 79)/\sigma_R(\Theta_2, E, 79)} \qquad (A1.2),$$

where Θ_1 and Θ_2 are scattering angles, E is the incident electron energy and the 79 indicates scattering by gold, atomic number Z = 79, was almost constant for $\Theta_1 = 60°$ and $\Theta_2 = 30°$ as E decreased from 1,000 keV to 200 keV and decreased in a regular manner as E decreased from 200 keV. Therefore all the values of

$\sigma_N^-(\Theta, E, 79)/\ \sigma_R\ (\Theta, E, 79)$ were plotted as a function of scattering angle Θ, and from these curves another series of interpolations yielded values of $\sigma_N^-(\Theta, E, 79)/\ \sigma_R\ (\Theta, E, 79)$ for Θ = 20°, 25°, 35°, 40°, 50°, 55°, 65° and 70°. Values of $\sigma_N^-(\Theta, E, 79)/\ \sigma_R\ (\Theta, E, 79)$ were now known for

Energy (keV) / Θ	50	100	121	200	400	700	1000
15°	1.020	1.025	1.030	1.045	1.080	1.100	1.115
20°	1.015	1.025		1.070	1.125	1.155	1.175
25°	1.005	1.030		1.100	1.175	1.220	1.245
30°	1.000	1.050	1.075	1.145	1.240	1.295	1.320
35°	1.010	1.090		1.205	1.310	1.375	1.405
40°	1.020	1.135		1.270	1.385	1.460	1.495
45°	1.040	1.180	1.220	1.335	1.475	1.545	1.575
50°	1.070	1.235		1.405	1.555	1.630	1.665
55°	1.105	1.290		1.470	1.630	1.705	1.735
60°	1.140	1.340	1.400	1.540	1.690	1.770	1.805
65°	1.185	1.395		1.605	1.750	1.820	1.855
70°	1.230	1.455		1.660	1.795	1.860	1.885
75°	1.280	1.505	1.560	1.700	1.830	1.885	1.900
90°	1.430	1.630	1.675	1.780	1.840	1.850	1.865

TABLE A1.2. Values of $\sigma_N^-/\ \sigma_R$ for gold (Z = 79) for various values of energy and Θ. Obtained graphically from and including data in Table A1.1.

Θ = 15°, 20°, 25°,... 60°, 65°, 70° and 90° (Table A1.2). The ratio ρ' was now calculated for those values of Θ_1 available in the range 45° to 75° inclusive and of Θ_2 available in the range 15° to 45°

45°	50°	55°	60°	65°	70°	75°	Θ_1	45°	50°	55°	60°	65°	70°	75°
50 keV							Θ_2	100 keV						
1.00	1.03	1.065	1.095	1.14	1.185	1.23	45°	1.00	1.045	1.095	1.135	1.18	1.235	1.275
1.02	1.05	1.085	1.12	1.16	1.205	1.255	40°	1.04	1.09	1.135	1.18	1.225	1.28	1.325
1.03	1.06	1.095	1.13	1.175	1.22	1.265	35°	1.085	1.135	1.185	1.23	1.28	1.335	1.38
1.04	1.07	1.105	1.14	1.185	1.23	1.28	30°	1.125	1.175	1.23	1.275	1.33	1.385	1.435
1.035	1.065	1.10	1.135	1.18	1.225	1.275	25°	1.145	1.20	1.25	1.30	1.355	1.415	1.46
1.025	1.055	1.09	1.125	1.17	1.21	1.26	20°	1.15	1.205	1.26	1.305	1.36	1.42	1.465
1.02	1.05	1.085	1.12	1.16	1.205	1.255	15°	1.15	1.205	1.26	1.305	1.36	1.42	1.465
200 keV								400 keV						
1.00	1.05	1.10	1.155	1.20	1.245	1.275	45°	1.00	1.055	1.105	1.145	1.185	1.215	1.24
1.05	1.105	1.16	1.21	1.265	1.31	1.34	40°	1.065	1.125	1.175	1.22	1.26	1.295	1.32
1.11	1.165	1.22	1.28	1.33	1.38	1.41	35°	1.125	1.185	1.245	1.29	1.335	1.37	1.40
1.165	1.225	1.285	1.345	1.40	1.45	1.485	30°	1.19	1.255	1.315	1.365	1.41	1.45	1.475
1.215	1.28	1.335	1.40	1.46	1.51	1.545	25°	1.255	1.325	1.39	1.44	1.49	1.525	1.555
1.25	1.315	1.375	1.44	1.50	1.55	1.59	20°	1.31	1.38	1.45	1.50	1.555	1.595	1.625
1.28	1.345	1.41	1.475	1.535	1.59	1.625	15°	1.365	1.44	1.51	1.565	1.62	1.66	1.695

45°	50°	55°	60°	65°	70°	75°	Θ_1	45°	50°	55°	60°	65°	70°	75°
700 keV							Θ_2	1000 keV						
1.00	1.055	1.105	1.145	1.08	1.205	1.22	45°	1.00	1.06	1.10	1.145	1.18	1.195	1.205
1.06	1.115	1.17	1.21	1.245	1.275	1.29	40°	1.055	1.115	1.16	1.21	1.24	1.26	1.27
1.125	1.185	1.24	1.285	1.325	1.35	1.37	35°	1.12	1.185	1.235	1.285	1.32	1.34	1.355
1.195	1.26	1.32	1.37	1.405	1.435	1.455	30°	1.195	1.26	1.315	1.37	1.405	1.43	1.44
1.265	1.335	1.40	1.45	1.49	1.525	1.545	25°	1.265	1.34	1.395	1.45	1.49	1.515	1.525
1.335	1.41	1.475	1.53	1.575	1.61	1.63	20°	1.34	1.415	1.475	1.535	1.58	1.605	1.615
1.405	1.48	1.55	1.61	1.655	1.69	1.715	15°	1.41	1.495	1.555	1.62	1.665	1.69	1.705

TABLE A.1.3. Values of ρ' for various values of Θ_1, Θ_2 and energy obtained from data in Table A.1.2

inclusive (Table A1.3). It was found, by inspection, that the values of (Θ_1, Θ_2) giving the "best" constancy of ρ' (subject to the above-mentioned energy conditions) are $(70^\circ, 25^\circ)$, $(65^\circ, 30^\circ)$ and $(60^\circ, 35^\circ)$. Curves are reproduced in Figs. A1.1, A1.2 and A1.3.

Now ρ' may be expressed

$$\rho' = \frac{\bar{\sigma_N}(\Theta_1, E, 79)}{\bar{\sigma_N}(\Theta_2, E, 79)} \cdot \frac{\sigma_R(\Theta_2, E, 79)}{\sigma_R(\Theta_1, E, 79)}$$

where the second factor, because of the form of $\sigma_R(\Theta, E, Z)$ - see equation A1.1 - is independent of energy and, for a given Θ_1 and Θ_2, is in fact a dimensionless constant. Consequently, the ratio given by

$$\rho = \frac{\bar{\sigma_N}(\Theta_2, E, 79)}{\bar{\sigma_N}(\Theta_1, E, 79)} = \frac{1}{\rho'} \frac{\sigma_R(\Theta_2, E, 79)}{\sigma_R(\Theta_1, E, 79)} \qquad \text{(A1.3)}$$

is also energy independent, subject to the energy conditions on ρ' mentioned earlier, as is the quantity

$$\sum_E \rho = \sum_E \frac{\bar{\sigma_N}(\Theta_2, E, 79)}{\bar{\sigma_N}(\Theta_1, E, 79)} \qquad \text{(A1.4)}$$

where the summation is made over all energies in any range within the limits $\sim$200 keV to $\sim$1,000 keV.

It will be observed that the values of ρ' in Table A1.3 were found by at least one, usually two interpolations. A check of the accuracy of computation

Fig. A1.1. Variation of $\varepsilon' = \frac{\sigma_N^-(\Theta, E, 79)}{\sigma_N^-(25°, E, 79)} \cdot \frac{\sigma_R(25°, E, 79)}{\sigma_R(\Theta, E, 79)} = \frac{1}{\varepsilon} \frac{\sigma_R(25°, E, 79)}{\sigma_R(\Theta, E, 79)}$ with energy E for various scattering angles Θ indicated.

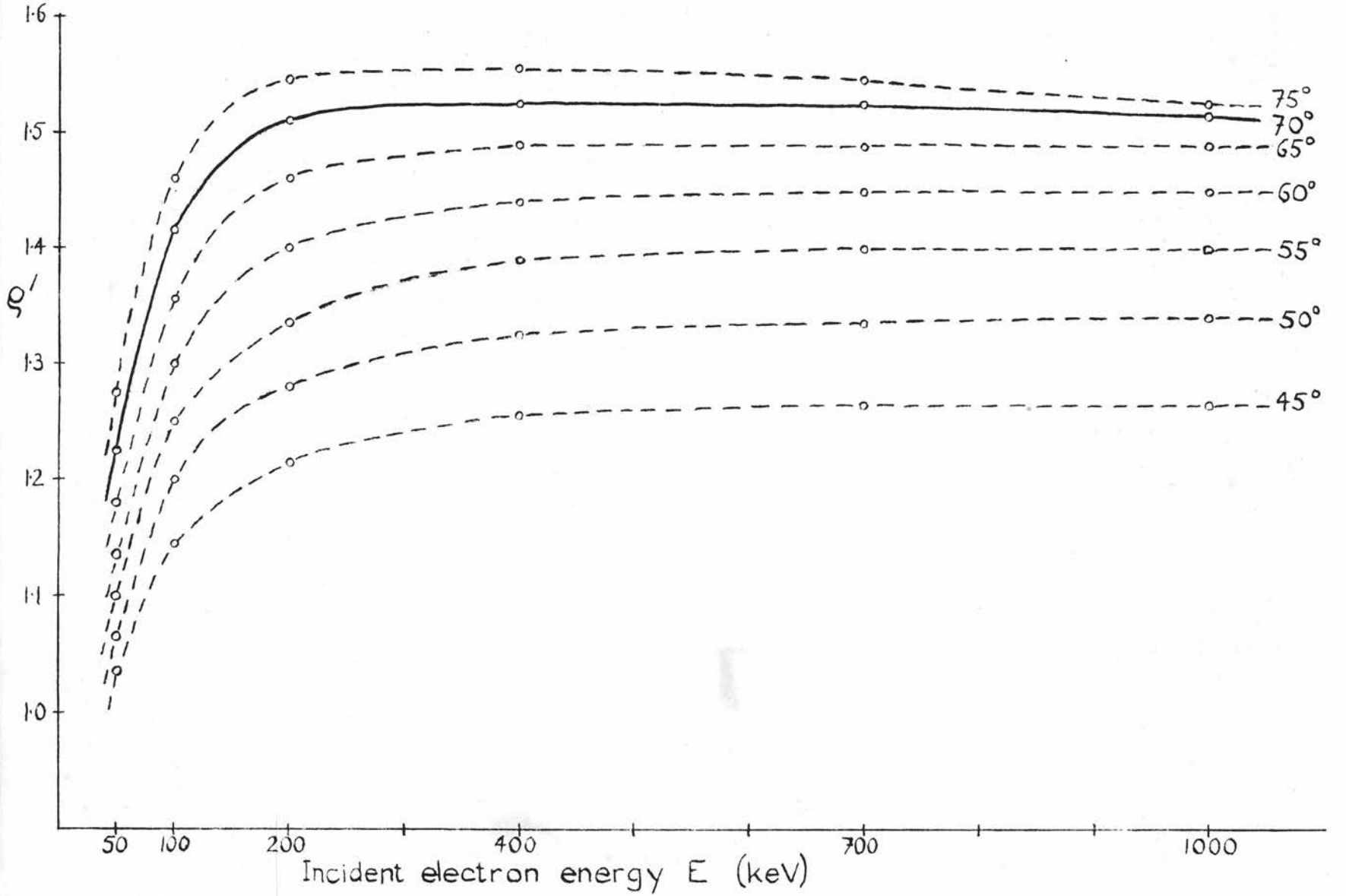

Fig.A1.2. Variation of $\varrho' = \frac{\sigma_N^{\sim}(\Theta, E, 79)}{\sigma_N^{\sim}(30°, E, 79)} \cdot \frac{\sigma_R(30°, E, 79)}{\sigma_R(\Theta, E, 79)} = \frac{1}{\varrho} \frac{\sigma_R(30°, E, 79)}{\sigma_R(\Theta, E, 79)}$ with energy E for various scattering angles Θ indicated.

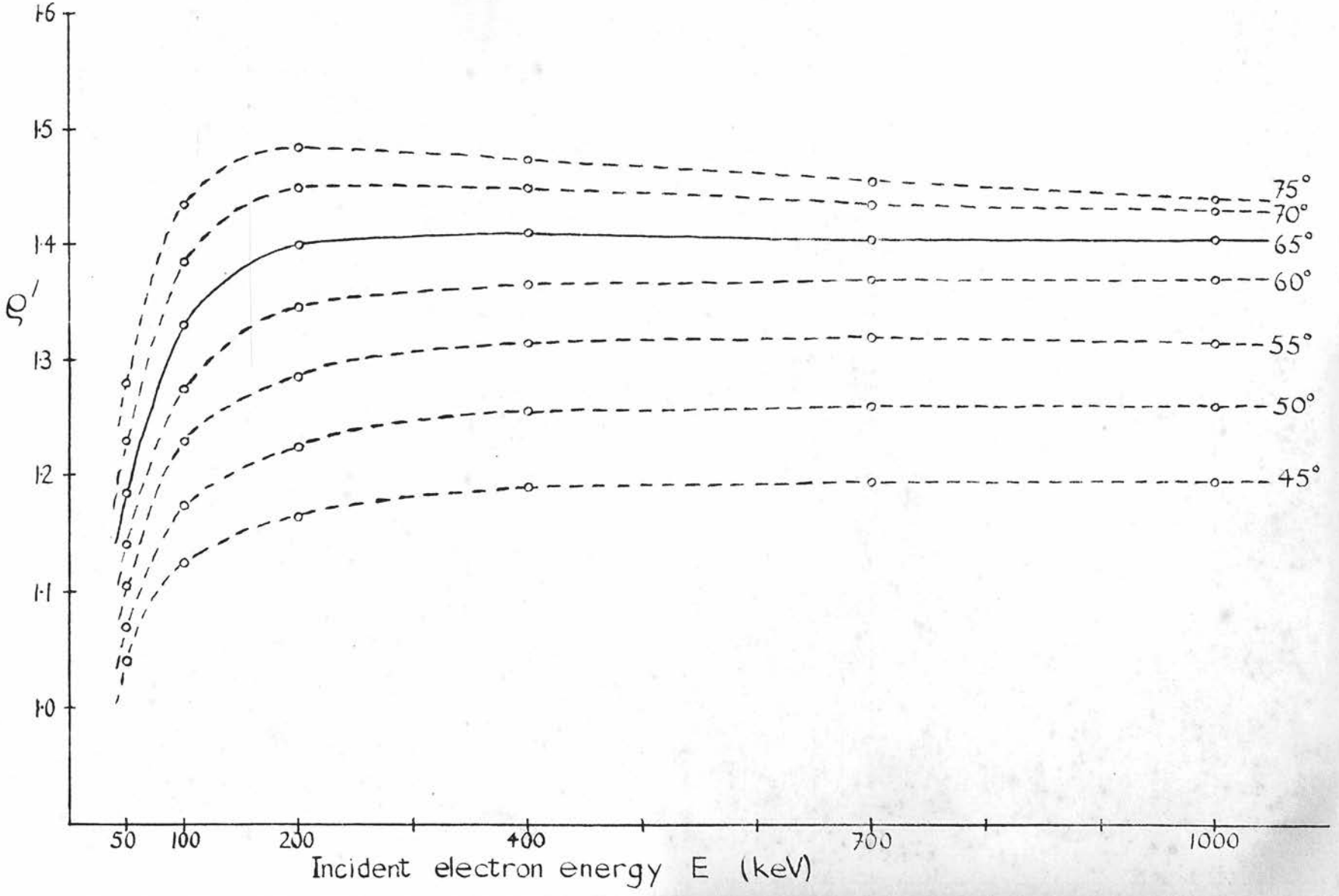

Fig.A1.3. Variation of $\rho' = \frac{\bar{\sigma_N}(\Theta, E, 79)}{\bar{\sigma_N}(35°, E, 79)} \cdot \frac{\sigma_R(35°, E, 79)}{\sigma_R(\Theta, E, 79)} = \frac{1}{\rho} \frac{\sigma_R(35°, E, 79)}{\sigma_R(\Theta, E, 79)}$ with energy E for various scattering angles Θ indicated.

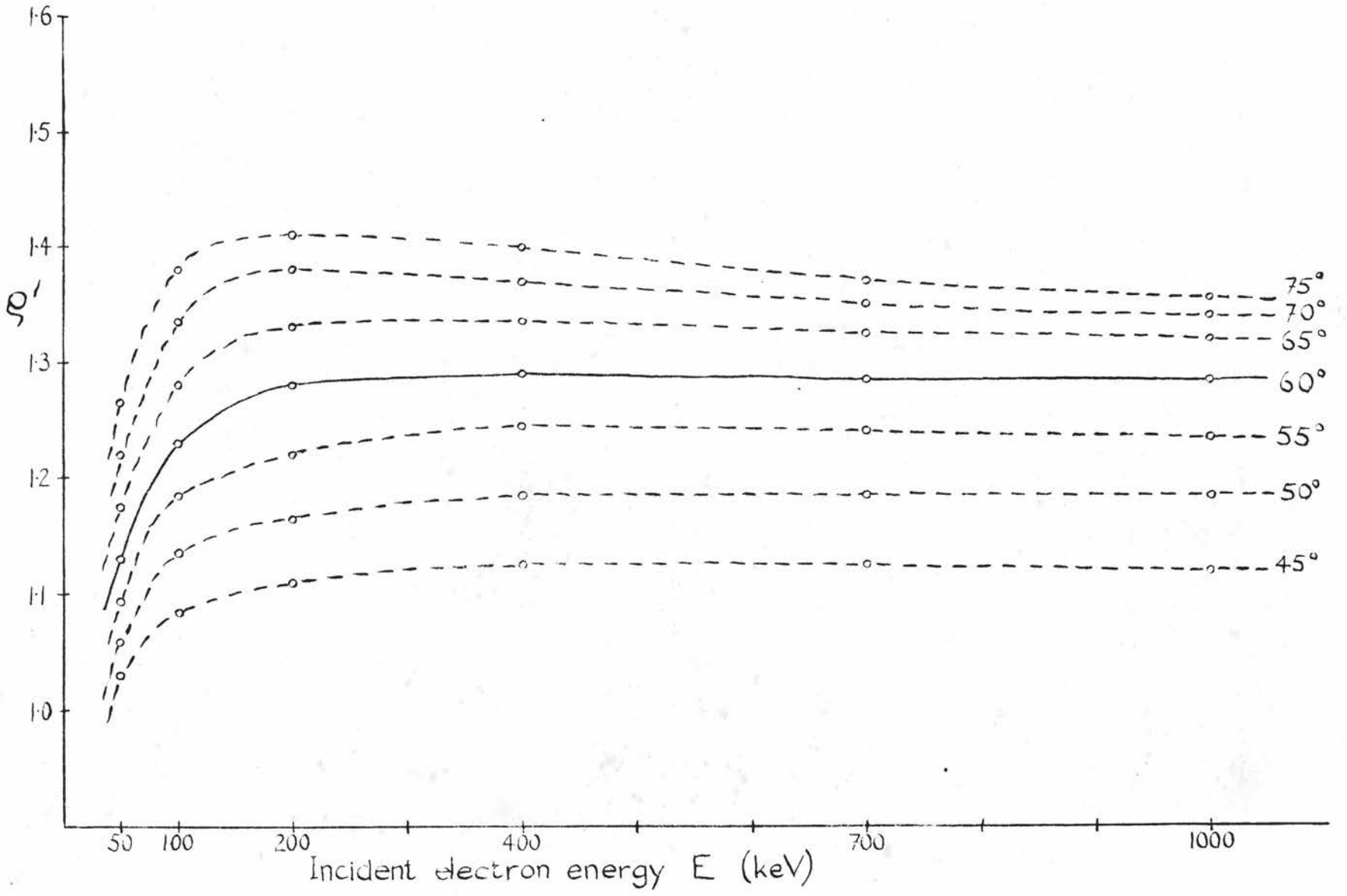

of the values of ρ' was made in the following way. $\sigma_R(\Theta, E, 79)$ was calculated to an accuracy of better than 1% for $\Theta = 30^\circ$, 45°, 60° and 75° and $E = 121$ keV ($\beta = 0.59$). The ratios $\sigma_R(30^\circ, 121, 79)/\sigma_R(\Theta, 121, 79)$ for $\Theta = 45^\circ$, 60° and 75° were divided by the corresponding values for ρ' obtained by yet another interpolation from the curves in Fig. A1.2. The results were values for the ratio $\rho = \bar{\sigma}_N(30^\circ, 121, 79)/\bar{\sigma}_N(\Theta, 121, 79)$. Now values of $\bar{\sigma}_N(\Theta, 121, 79)$ are given in a paper by Sherman and Nelson (Sherman and Nelson, 1959) from which accurate values of $\bar{\sigma}_N(30^\circ, 121, 79)/(\bar{\sigma}_N(\Theta, 121, 79)$ were calculated and compared with those obtained, as explained

Θ	$\sigma_R \times 10^{-4}$	$\frac{\sigma_R(30^\circ)}{\sigma_R(\Theta)}$	ρ'	ρ	Sherman & Nelson	
					$\bar{\sigma}_N \times 10^{-4}$	$\frac{\bar{\sigma}_N(30^\circ)}{\bar{\sigma}_N(\Theta)}$
30°	14.85	1.0	1.0	1.0	16.00	1.0
45°	3.11	4.775	1.14	4.19	3.790	4.22
60°	1.065	13.94	1.30	10.7	1.494	10.7
75°	0.485	30.62	1.455	21.0	0.7591	21.1

TABLE A1.4. Check of accuracy of interpolation procedure. The data in columns 5 and 7 are independent computations of $\bar{\sigma}_N(30^\circ, E, Z)/\bar{\sigma}_N(\Theta, E, Z)$ for energy $E = 121$ keV ($\beta = 0.59$) and atomic number $Z = 79$. Cross sections are expressed in barns/sterad.

above, after several interpolations. From columns 5 and 7 of Table A1.4 it is clear that there is agreement

to better than 1% which may therefore be taken as a measure of the accuracy of the values of ρ' , and hence of ρ .

APPENDIX 2

THE PROBLEM OF BEAM INTENSITY IN ELECTRON-NUCLEAR SCATTERING

Consider an electron scattering experiment carried out with an apparatus characterised by Fig. A2.1. Then

No. of electrons incident on foil per second

$$= N_e \times \frac{\Omega_1}{4\pi}$$

where N_e is the total number of electrons emitted per second by the radioactive "point" source. Suppose that the source is a pure β-emitter, i.e. each disintegration corresponds to the emission of one electron. A source strength of 1 millicurie would then produce $\sim 4 \times 10^7$ electrons per second. Let N mc. be the strength of the source being considered. Then $N_e = N \times 4 \times 10^7$ per second. Suppose, further, that at some stage in the experiment energy selection occurs. It is necessary to consider only the fraction, F, of the electrons whose energies are in the range selected. For the purposes of the experiment, therefore,

Incident intensity

$$= N_i = N_e \times F \times \frac{\Omega_1}{4\pi} = N \times F \times \Omega_1 \times \frac{10^7}{\pi}$$

per second.

Let the area of the foil be A_1 and the number of scattering centres per unit area be n (for Mott

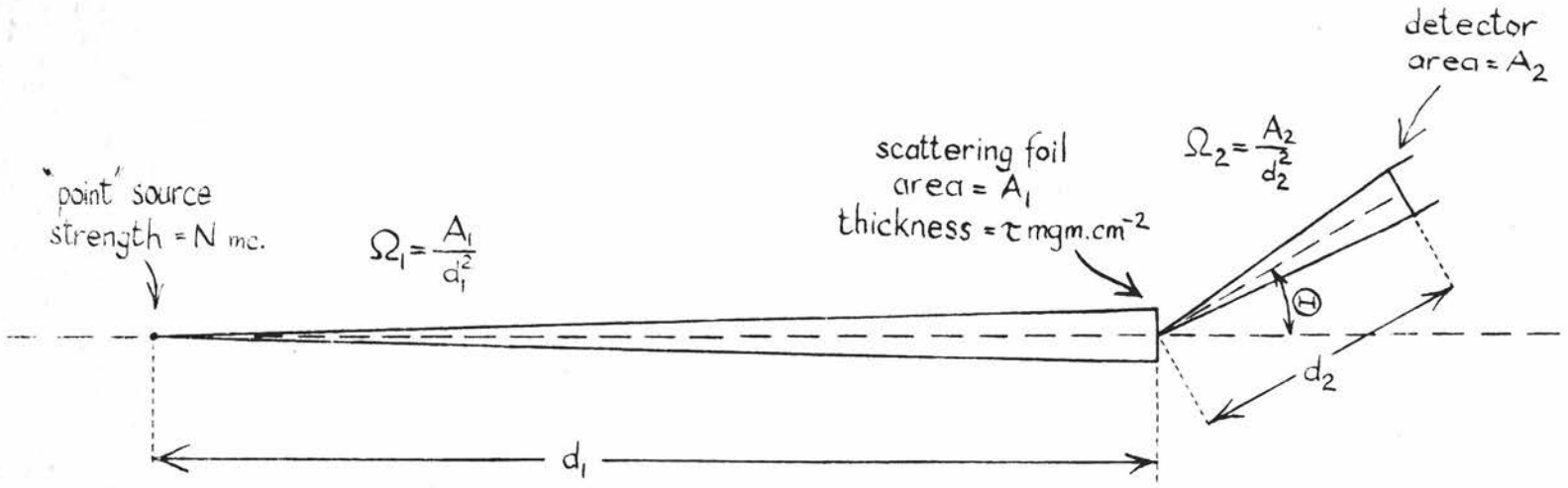

Fig. A2.1. Notation used in discussion of "ideal" scattering experiment.

scattering, this is the number of nuclei per unit area). It follows that

No. of scattering centres = $A_1 \times n$.

Let the scattering cross section for an angle Θ, i.e. the probability of an incident electron being deflected through an angle between Θ and $\Theta + d\Theta$ as a result of a collision with one scattering centre, be $\sigma d\Omega$. The solid angle $d\Omega$ is defined in Fig. A2.2. σ may be called the "cross section per unit solid angle".

Finally, let the solid angle subtended by the detector at the centre of the scattering foil (Fig. A2.1) be Ω_2.

In the hypothetical experiment being considered, the number of electrons detected per second can be expressed

$$\begin{pmatrix}\text{no. of electrons}\\ \text{detected per sec.}\end{pmatrix} = \begin{pmatrix}\text{incident}\\ \text{intensity}\end{pmatrix} \times \begin{pmatrix}\text{no. of scatter-}\\ \text{ing centres}\end{pmatrix} \times \begin{pmatrix}\text{cross section}\\ \text{per unit solid}\\ \text{angle}\end{pmatrix} \times \begin{pmatrix}\text{actual solid}\\ \text{angle}\end{pmatrix}$$

$$\text{or} \quad N_S = N_i \times A_1 n \times \sigma \times \Omega_2$$

$$= (NF\Omega_1 \times \frac{10^7}{\pi}) \times (A_1 n) \times \sigma \times \Omega_2 \qquad \text{(A2.1)}$$

Now for Mott scattering,

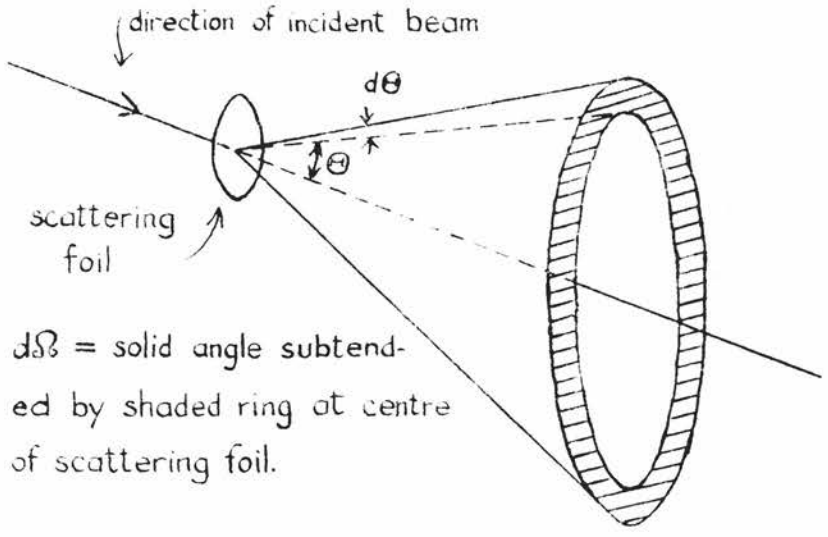

Fig. A2.2. Definition of solid angle dΩ.

n = no. of nuclei per $cm.^2$ of scattering foil

$$= \frac{\text{thickness (in gm. cm.}^{-2})}{\text{gram molecular mass}} \times \text{Avogadro's Number}$$

$$\frac{\tau \times 10^{-3}}{197} \times 6 \times 10^{23} \qquad \text{(A2.2)}$$

for a gold scattering foil, where τ is the thickness expressed in mgm. $cm.^{-2}$. Substituting into (A2.1) gives

$$N_S = NF\Omega_1 A_1 \tau \bar{\sigma}_N \Omega_2 \times 10^{25} \text{ per second} \qquad \text{(A2.3)}$$

where $\sigma = \bar{\sigma}_N$ is the Mott scattering cross section.

Some idea of the size of N_S can be found by substituting "reasonable" values for N, F, etc. in (A2.3). Consider firstly the geometrical factors Ω_1, Ω_2 and A_1. Let $A_1 = 1$ $cm.^2$ and $\Omega_1 = A_1/d_1^2 = 1/50^2$, i.e. let the source-to-foil distance (Fig. A2.1) be 50 cm. Assuming a detector area $A_2 = 1$ $cm.^2$ at a distance $d_2 = 10$ cm. from the centre of the scattering foil gives $\Omega_2 = 1/10^2$. Thus $\Omega_1 A_1 \Omega_2 = (1/50^2) \times 1 \times (1/10^2) = (1/25) \times 10^{-4} = 4 \times 10^{-6}$. Equation (A2.3) may now be written

$$N_S = 4NF \tau \bar{\sigma}_N \times 10^{19} \text{ per second} \qquad \text{(A2.4)}$$

The four factors N, F, τ and $\bar{\sigma}_N$ should be made as large as possible to make N_S as large as possible and so the statistical error in N_S as small as possible. Once the scattering angles and mean incident electron energy have been decided, the range of values of $\bar{\sigma}_N$ is

fixed. Assuming energies in the range 100 keV to 1,000 keV and scattering angles ranging from 30° to 75° leads to: maximum value of $\bar{\sigma_N} \sim 10^{-18}$ cm.^{2} for 100 keV and 30°; minimum value of $\bar{\sigma_N} \sim 10^{-21}$ cm.^{2} for 1,000 keV and 75°.

The upper limit to the value of N is determined, in the first instance, by expense and safety. For the measurements to be reported here, an upper limit of N was arrived at such that the source preparation was as simple and safe as possible. For Cs^{137}, the maximum value of N was 10.

The maximum value of F is more difficult to arrive at at this stage. Assuming that some kind of pulse-height analysis provides the energy selection, a value of 10^{-2} is not unreasonable.

The maximum value of τ is very much dependent on the energy of the electrons being scattered, for it is an assumption of the theory that each scattered electron makes only one collision on its way through the scattering foil. For 100 keV electrons a value of $\tau \sim 0.1$ is probably reasonable; for 1,000 keV electrons, τ should not be greater than 1.0. For these values of energy and foil thickness, plural and multiple scattering should be almost negligible compared with single scattering.

To get some idea of N_S, therefore, suppose that $N = 10$, $F = 10^{-2}$, $\tau = 1$ and $\sigma_N = 10^{-18}$ cm. It

follows that $N_S \sim 4$ per second, from equation (A2.4), for the "best" case of lowest energy and lowest scattering angle. For the "worst" case - highest energy and highest scattering angle - $N_S \sim 4 \times 10^{-3}$ per second. The corresponding counting times, for a statistical error of $\sim 1\%$ are, respectively, 40 minutes and 700 hours, approximately.

It was clear that one way of increasing counting rates and so decreasing counting times was to accept more of the available electrons from the source than those in the solid angle Ω_1 (Fig. A2.1). A focussing device to increase the incident intensity by two orders of magnitude at least was required.

APPENDIX 3

THE DESIGN OF MAGNETIC LENS SHIELDING

On the basis of the design of and the measurements of the properties of a large number of iron-shielded magnetic lenses, Dunandeau and Fert (Durandeau and Fert, 1957) produced a set of equations and curves which prove useful in the design of short-focus, iron-shielded magnetic lenses. The quantities which must be determined are shown in Fig. A3.1.

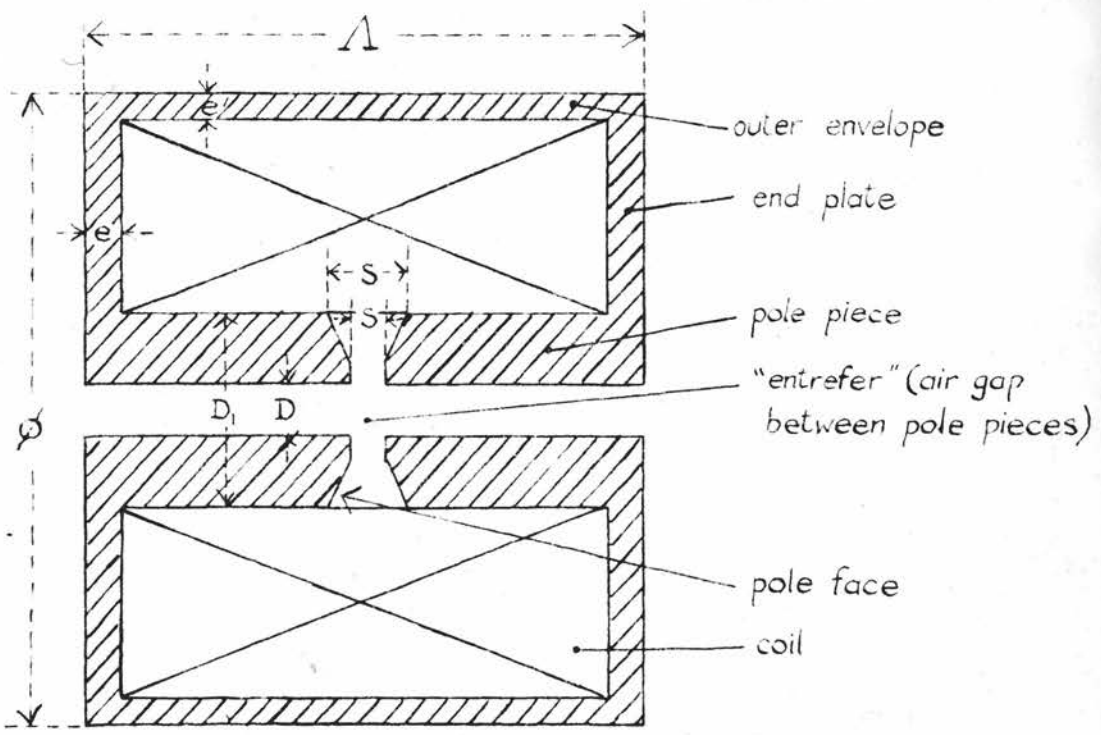

Fig. A3.1. Notation used in description of magnetic lens shielding. (Based on Fig.1, p.206, of original paper by Durandeau and Fert.).

The general shape of the pole faces is governed by S, S_1 and the diameters D and D_1 of the cylindrical pole pieces. They are chosen so that the effects of saturation of the pole pieces are either minimised or eliminated completely. e and e' can also be chosen to satisfy this condition, but more often than not they are decided upon by the condition that the structure be mechanically rigid. When this second condition is satisfied, then the first is almost always satisfied also. Λ and ϕ are determined broadly by the number of turns of the coil, N, and the current through the coil, I. The number of amp.-turns NI depends on the energy of the electrons to be focussed by the lens.

The problem of saturation is two-fold and applies mainly to the pole pieces which are supposed to produce a magnetic field in the entrefer only. It is found that the magnetic flux increases from the entrefer to the end plate. If the flux is large enough, the iron saturates and an additional magnetic field is established on the axis of the lens away from the entrefer. If large fluxes are anticipated, therefore, it is advisable to increase D_1 from the entrefer to the end plate, so making the pole pieces conical rather than cylindrical. By doing so, the flux density in the pole pieces becomes nowhere sufficiently great to saturate the iron. The second way in which the effects of saturation appear is in the extent of the magnetic field in the entrefer. It

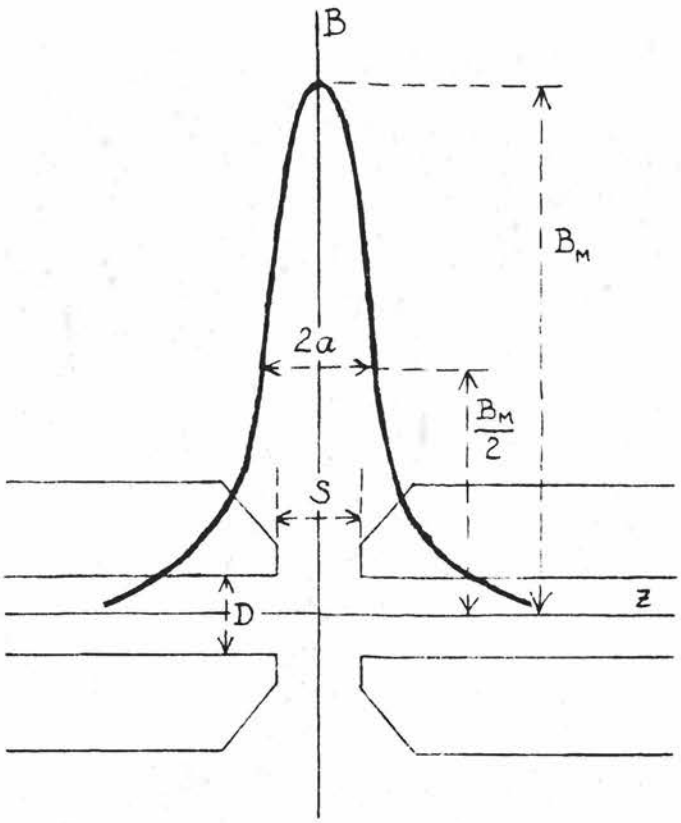

Fig. A3.2. Shape of magnetic field on z-axis in region of entrefer.
(Based on Fig. 2, p. 207, of original paper).

is found that for a given S and D, the shape of the magnetic field (Fig. A3.2) is, to a good approximation, independent of the shape of the pole faces, provided no saturation occurs (i.e. provided NI is less than some critical value). As NI increases, however, it is found

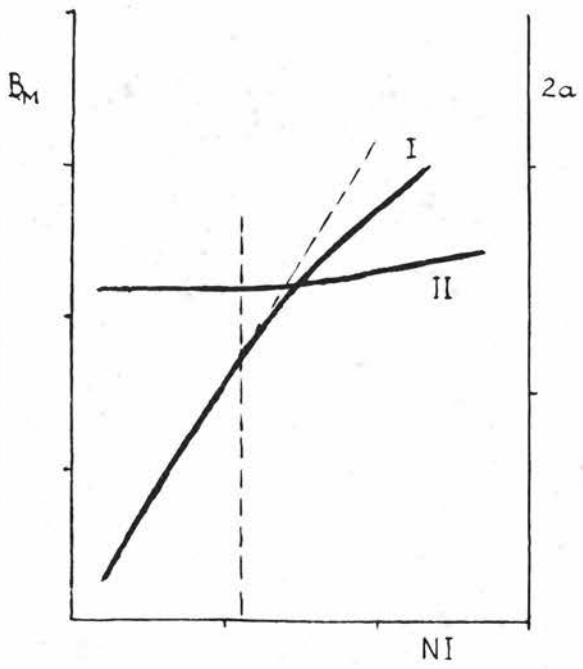

Fig.A3.3. Variation of B_M and 2a with NI. All units arbitrary.

curve I : B_M

curve II : 2a

(Based on Fig.5, p.211, of original paper).

(Fig. A3.3) that the magnetic field extends axially (i.e. 2a increases) and B_M increases more slowly with NI. Pole pieces of the type shown in Fig. A3.4 appear

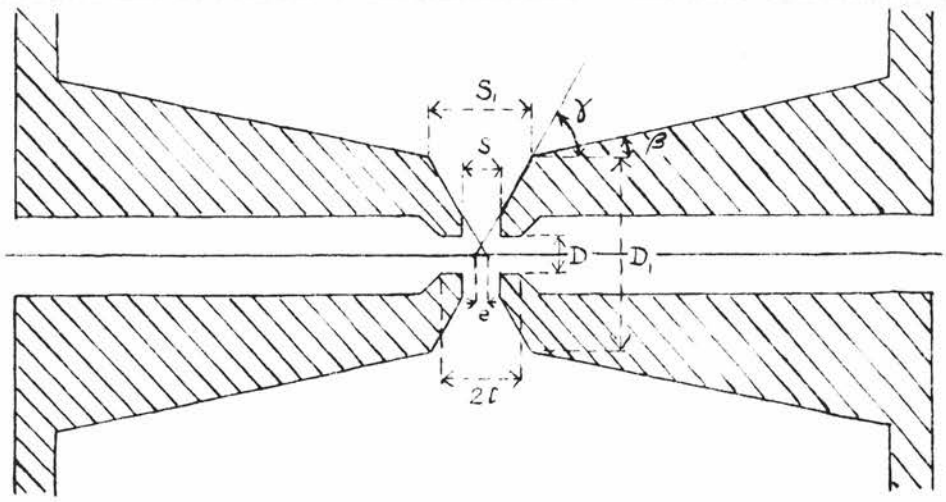

Fig.A3.4. Typical pole pieces for optimum focussing properties.

(Based on Fig.7, p.212, of original paper).

to minimise the distortions of the field in the entrefer due to saturation.

To find the number of amp.-turns NI necessary to focus electrons of energy V eV, the path of the electrons through the lens must be considered (see Fig. A3.5). Assuming that the source of electrons is a point radioactive source, then if the magnetic lens is to be used in the manner of an objective lens in an electron microscope, a source at the position F_o' (Fig. A3.5)

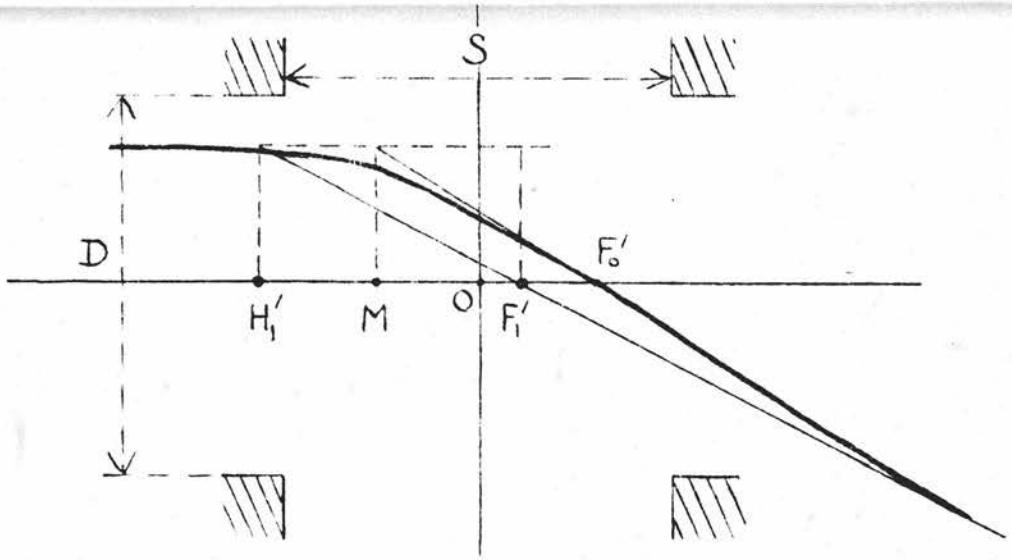

Fig. A3.5. Definition of electron-optical parameters.

Objective lens : $f_o = MF_o'$, $z_o = OF_o'$

Projection lens : $f_1 = H_1'F_1'$, $z_1 = OF_1'$

(Based on Fig. 9, p. 214, of original paper).

ought to produce a parallel beam of electrons moving to the left. Durandeau and Fert found that for D/S in the range 0.5 to 2, the distance $H_1'F_1' = f_1$ had a

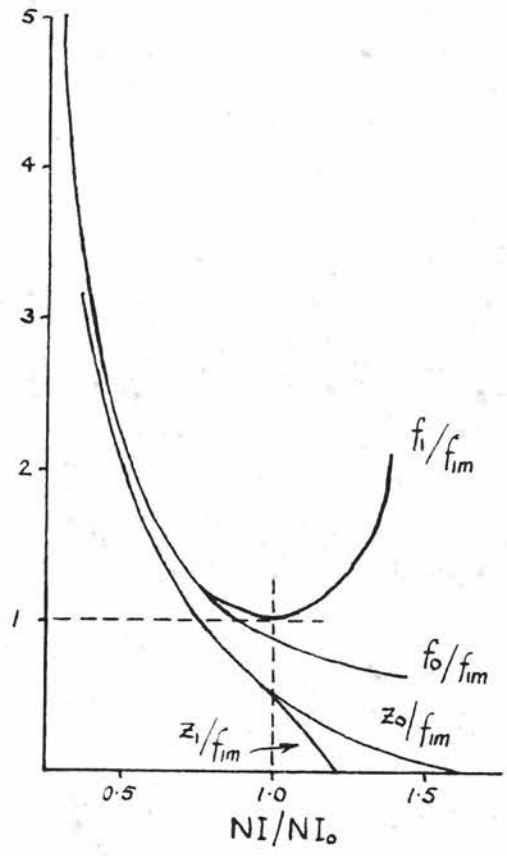

Fig. A3.6. Universal reduced curves.

(Based on Fig. 11, p. 216, of original paper).

which saturation effects begin to appear, was 1000S where S is measured in mm. Supose that, using mild steel, it turns out that $NI_o > 1000S$. Then the effective values of S, D and a (S', D' and a', say - see Fig. A3.2) can be found from

$$\frac{S' - S}{S} = \frac{D' - D}{D} = \frac{a' - a}{a} = m \frac{NI_o - 1000S}{1000S}$$

where $m \simeq 0.14$ for mild steel. From S' and D', the effective value of f_{1m}, say f'_{1m}, can be readily found. NI/NI_o can then be found from the ratio z_o/f'_{1m} as explained in the previous paragraph, and hence the appropriate number of amp.-turns NI.

The Determination of the Number of Turns N in the Final Focussing System

This value of N was estimated by following the steps (i) to (v) listed above:

(i) $S = D = \frac{1}{2}$ in. $\simeq$ 12.5 mm.

(ii) $f_{1m} = 0.5 \times 12.5 \times \sqrt{1.45} \simeq 7.5$ mm.

(iii) $z_o = 10$ mm. (an "order of magnitude" value).

(iv) $z_o/f_{1m} \sim 1.3$; $NI/NI_o = x \sim 0.65$.

(v) $NI \sim 13.5 \times \sqrt{V^*} \times 0.65$.

For electrons of energy $V \sim 500$ keV,

$V^* = V(1 + 0.98 \times 10^{-6} V) \sim 500(1 + 0.5) \sim 750$ keV.

Hence $NI \sim 13.5 \times \sqrt{0.75} \times 10^3 \times 0.65 \sim 7.5 \times 10^3$.

Assuming I to be a few amps. led to $N \sim 2 \times 10^3$ turns.

minimum value at $NI/\sqrt{V^*} = NI_o/\sqrt{V^*} \simeq 13.5$, where $V^* = V(1 + 0.98 \times 10^{-6}V)$. This minimum value of f_1 could be expressed $f_{1m} = 0.5\sqrt{S^2 + 0.45D^2}$. They then produced a set of "universal reduced curves" by plotting f_1/f_{1m}, f_o/f_{1m}, z_1/f_{1m} and z_o/f_{1m} as functions of NI/NI_o (Fig. A3.6).

To find the number of amp-turns NI to produce a parallel beam of electrons of energy V eV the following procedure can be used:

(i) Choose S and D so that they are approximately the same.

(ii) calculate $f_{1m} = 0.5\sqrt{S^2 + 0.45D^2}$ where S and D are in mm.

(iii) decide on the source position F_o'; this immediately gives $z_o = OF_o'$,

(iv) calculate z_o/f_{1m} and find the corresponding value of NI/NI_o from Fig. A3.6. Call this ratio x.

(v) from $NI_o = 13.5\sqrt{V^*}$, it follows that

$$NI = 13.5\sqrt{V^*}\,x$$

so that the variation of NI with V is known to a good approximation.

The previous paragraph assumes that no saturation has occurred. Whether or not it will depends on the magnetic properties of the material that the pole pieces are made from. Durandeau and Fert considered only ordinary mild steel ("fer doux courant") and found (Fig. A3.3) that the critical value of NI, i.e. the value at

The lenses which were eventually constructed (as explained in Chapter 3) each had 23 layers of approximately 100 turns, giving a total of 2.3×10^3 turns.

To check whether or not saturation effects were likely, NI_o was found from the empirical equation $NI_o = 13.5\sqrt{V} = 13.5 \times \sqrt{0.75} \times 10^3 \sim 1.2 \times 10^4$. This is essentially equal to the (empirical) maximum value for no saturation: $1000S = 1.25 \times 10^4$. Consequently, no serious saturation effects were anticipated.

APPENDIX 4

SUPPLY AND CONTROL OF MAGNETIC LENS CURRENTS

The current for the magnetic lenses was obtained from rectified three-phase supply. The current control circuit is given in Fig. A4.1.

The variable resistance RM provided a course control for the current through the load. R1 and R2 provided fine controls for the currents I1 and I2 through L1 and L2 respectively, these currents being read from the ammeters A1 and A2.

A 1000 μF smoothing capacitor was included in the circuit in parallel with the load.

The transistorised part of the circuit was a current stabiliser based on circuits discussed by Wenham (Wenham, 1959 and 1961). It functions briefly as follows. The current through the load flows through a liberally rated variable resistor RT, providing a "test voltage". This voltage is one of the inputs to a difference amplifier. The other input is obtained from a reference circuit consisting of a Zener diode (SX56) and voltage divider. Any difference in the input voltages is amplified and appears across the 3.3 kΩ resistor. Thus if the test voltage increases due to an increase in the supply voltage, the voltage across the 3.3 kΩ resistor increases. This tends (a) to increase the voltage between base and collector of the GET 116 transistor of the series

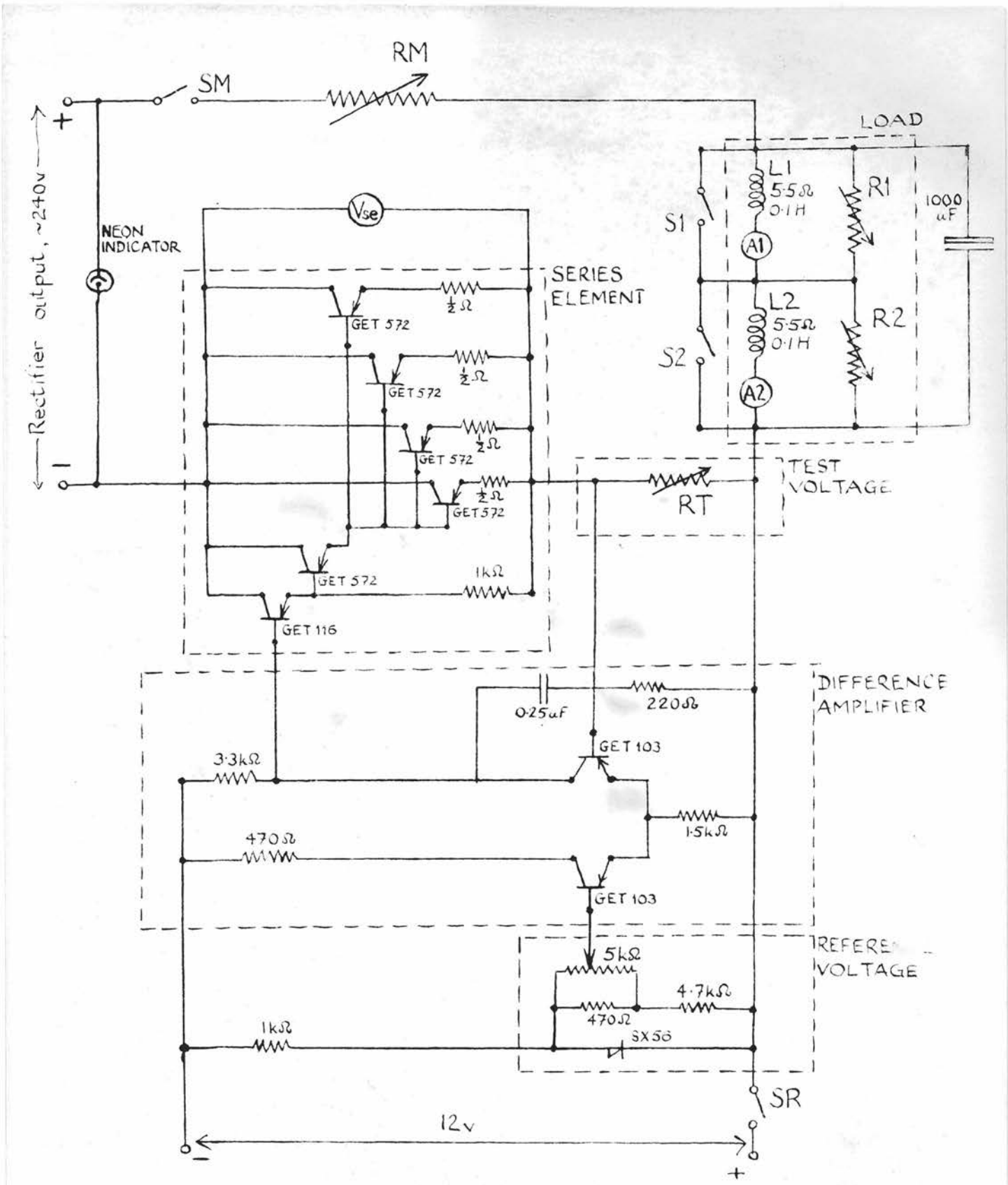

Fig. A4.1. Details of current supply and control circuit.

element and (b) to decrease the emitter to base voltage of the same transistor. (b) results in a decrease in current through all the transistors in the series element, and so counteracts the increase in current (and test voltage) caused by the increase in the supply voltage. (a) results in an increased voltage drop V_{se} across the series element. In this way, changes in supply voltage (due, say, to fluctuations in the mains supply to the rectifier) result in changes in V_{se} but not in the current flowing through the load.

The stabiliser was checked by varying the input voltage to the rectifier by means of a three phase "Variac" transformer. The resulting variations in the rectifier output voltage, V, caused V_{se} and the current through the load to change. As the value of the current increased, the degree of stabilisation decreased. Fig. A4.2 shows how Il and V_{se} varied with V for an intermediate value of Il $\sim$ 2 amps. For the central part of the range of V, 234 to 244 volts, the increase in V of 4% leads to an increase in Il of 1%. As stated in Chapter 7, for most counting rate measurements the mains supply voltage was sufficiently stable for the fluctuations in V to be much less than the 10 volts mentioned in the previous sentence. This implies that the variations in current were less than $\pm \frac{1}{2}$%.

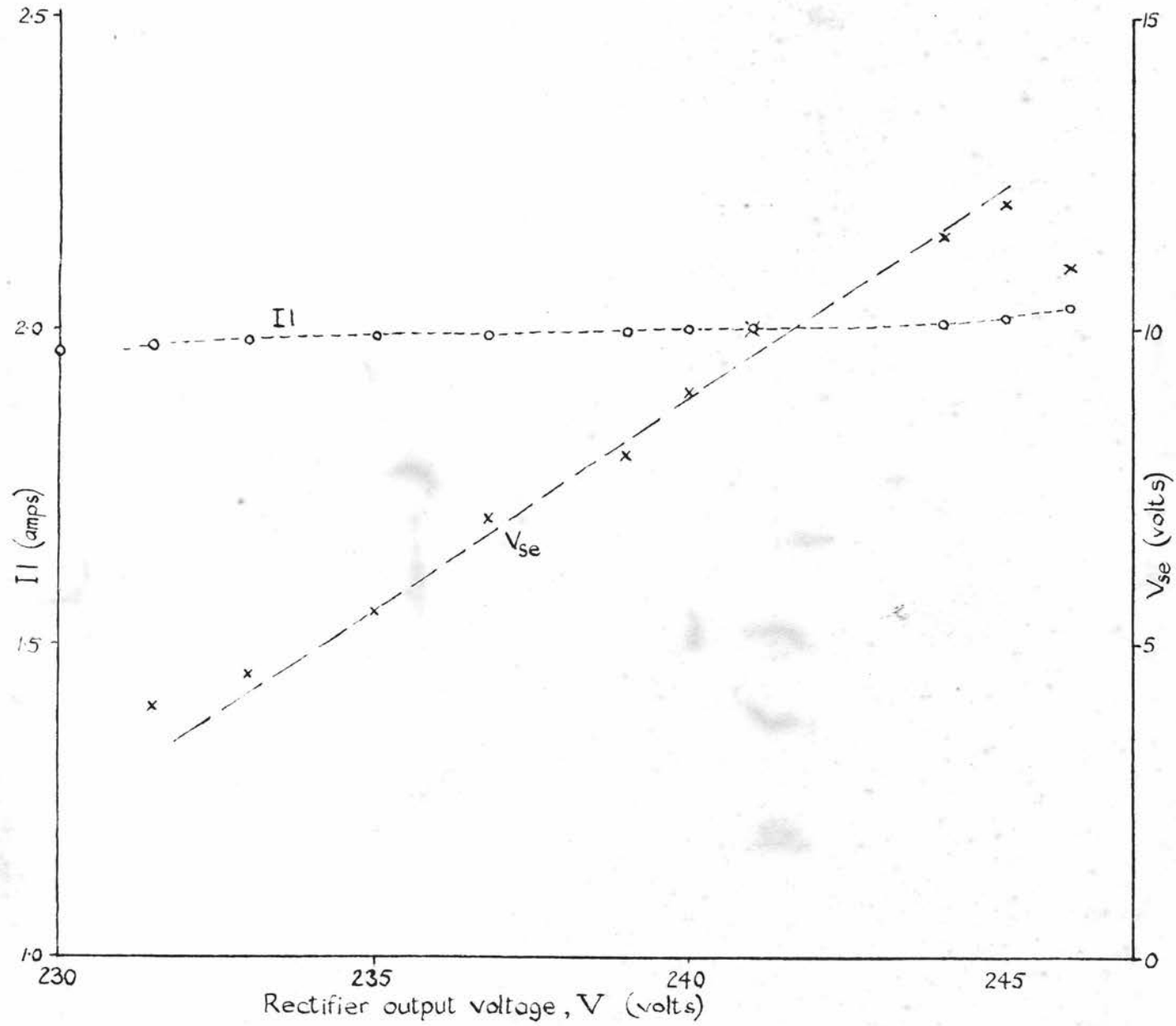

Fig.A4.2. Variation of I1 and V_{se} with rectifier voltage **V** for I1 ~ 2amps.

ACKNOWLEDGEMENTS

I offer my sincere thanks to Professor N. Feather, F.R.S., for giving me the opportunity of carrying out this research. I am very grateful to Dr. P.S. Farago for his skilful and considerate supervision of the work.

The co-operation of Mr. Headridge and his staff in the construction and the maintenance of the apparatus is greatly appreciated.

I am indebted to three former members of the research group, Dr. J. Muir, Dr. A.G.A. Rae and Dr. R.B. Gardiner, for their assistance at various stages of the project.

REFERENCES

Bienlein, Felsner, Günther, v. Issendorff and Wegener, 1959 Zeit. Physik 154, 376.

Chase and Cox, 1940 Phys. Rev. 58, 243.

Doggett and Spencer, 1956 Phys. Rev. 103, 1597.

Durandeau and Fert, 1957 Rev. d'Opt. 36, 205.

Dymond, 1934 Proc. Roy. Soc. A145, 657.

Greenberg, Malone, Gluckstern and Hughes, 1960 Phys. Rev. 120, 1393.

Grodzins, 1959 Prog. Nuclear Phys. 7, 163.

Kepes, Waldman and Miller, 1959 Ann. Physics (New York) 6, 90.

Kulchitsky and Latyshev, 1942 Phys. Rev. 61, 254.

Lee and Yang, 1956 Phys. Rev. 104, 254.

Lee and Yang, 1957 Phys. Rev. 105, 1671.

Massey and Mohr, 1941 Proc. Roy. Soc. A177, 341.

Mohr, 1943 Proc. Roy. Soc. A182, 189.

Mohr and Tassie, 1954 Proc. Phys. Soc. A67, 711.

Møller, 1932 Ann Physik 14, 531.

Mott, 1929 Proc. Roy. Soc. A124, 425.

Mott, 1932 Proc. Roy. Soc. A135, 429.

Murray, 1960 Ph.D. Thesis, University of Edinburgh.

Nelson and Pidd, 1959 Phys. Rev. 114, 728.

Page, 1959 Rev. Mod. Phys. 31, 759.

Page, 1962 Ann. Rev. Nuclear Science 12, 43.

Richter, 1937 Ann. Physik 28, 533.

Ryu, Hashimoto and Nonaka, 1953 J. Phys. Soc. Japan 8, 575.

REFERENCES (Contd.)

Sherman, 1956 Phys. Rev. 103, 1601.

Sherman and Nelson, 1959 Phys. Rev. 114, 1541.

Shull, 1942 Phys. Rev. 61, 198.

Spiegel, Miller and Waldman, 1959 Ann. Physics (New York) 6, 86.

Spiegel, Ruane, Anthony, Waldman and Miller, 1959 Ann. Physics (New York) 6, 70.

Sternheimer, 1959 Adv. Electronics and Electron Phys. 11, 31.

Tolhoek, 1956 Rev. Mod. Phys. 28, 277.

Van der Spuy, 1959 Nucl. Phys. 10, 53.

Wenham, 1959 Proc. Inst. Elect. Engin. B106, 1384.

Wenham, 1961 Private Communication.

Williams, 1939 Proc. Roy. Soc. A169, 531.

Williams, 1940 Phys. Rev. 58, 292.